PHYSICAL MODELLING OF THE SALT TECTONICS OF ALLOCHTHONOUS CANOPY AND NAPPE SYSTEMS AT DEEPWATER CONTINENTAL MARGINS:

APPLICATIONS TO THE ABENAKI AND SABLE SUB-BASINS, SCOTIAN MARGIN

Clarke T. Campbell

Submitted in Partial Fulfillment of the Requirements
for the Degree of Bachelor of Science, Honours
Department of Earth Sciences
Dalhousie University, Halifax, Nova Scotia
March 2007

DALHOUSIE UNIVERSITY
Inspiring Minds

Department of Earth Sciences
Halifax, Nova Scotia
Canada B3H 4J1
(902) 494-2358
FAX (902) 494-6889

DATE: April 27/07

AUTHOR: Clarke T. Campbell

TITLE: Physical Modelling of the Salt Tectonics of Allochthonous Canopy and Nappe Systems at Deepwater Continental Margins: Applications to the Abenaki and Sable sub-basins, Scotian Margin

Degree: B. Sc Convocation: May 28 Year: 2007

Permission is herewith granted to Dalhousie University to circulate and to have copied for non-commercial purposes, at its discretion, the above title upon the request of individuals or institutions.

Signature of Author

ABSTRACT

Now that hydrocarbon exploration is moving into the deepwater Scotian Slope, specifically the areas basinward of the Sable and Abenaki sub-basins, a better understanding of the evolution and controlling factors of the complex allochthonous salt nappe systems of the deepwater Scotian Slope is needed. A lack of exploration wells and seismic imaging problems associated with the complex salt bodies hinder structural interpretation in these areas. Through scaled physical modelling of salt tectonics and sedimentation processes in rift basins with different basement morphologies, expected in the Scotian Basin, new structural and mechanical concepts have been developed to support seismic interpretation in this area. These concepts include: 1) Downbuilding of sediments as the dominant mechanism of initial salt movement in the landward part of the rift basins with thick salt (2 km). 2) The salt thickness due to the basement floor morphology, rather than the geometry of the basinward rift shoulder, is the controlling factor for how efficiently landward downbuilding inflates the basinward autochthon salt, and later evacuates salt into the allochthon canopy and nappe systems. 3) The timing and rate of the allochthonous nappe advancement into the deepwater basin is dependant on the efficiency of early salt evacuation and mid-stage progradation of sediments over the inflated autochthon basinward salt complex. These concepts derived from the physical experiments can be applied for the interpretation of complex salt structures observed in seismic lines along the deewater Scotian Margin and can help to correlate and interpret the observed salt structures and their depositional environment in terms of initial rift basin geometry and related salt thickness. Both parameters are difficult to observe directly in the geophysical data but are essential for the interpretation of the deepwater slope setting.

Key words: Salt tectonics, allochthonous salt nappe systems, Scotian Margin, analogue modelling.

Table of Contents

Table of Figures

Table of Tables

ACKNOWLEDGEMENTS

I would first like to thank my parents for making this possible; their support has brought me to where I am today. I would like extend a special thanks to Dr. Juergen Adam for taking me on in this project and for providing me knowledge, guidance and showing great patience during this undertaking. A special acknowledgement goes out to Dr. Csaba Krezsek, a geology guru of sorts who could make the greatest of tasks seem easy. I'd like to thank Dr. Grant Wach for his support and help during my days at Dalhousie. I would like to thank my partner in crime on this project, Cody MacDonald, we started this project as naïve students and have both come a long way in a short time. I have to thank Shell Canada for their funding which has allowed me to work on such a rewarding project. I would like to thank my great roommates, Michael Giles, Bryan Rae and Alana Haysom. Despite us all working on our own theses, we all managed to stay sane throughout the whole ordeal. My girlfriend Livia Goodbrand deserves to be acknowledged for her impeccable proof reading skills and managing to put up with my stubborn nature, she's a great inspiration. I must acknowledge all my friends and family, all great people that I am lucky to be acquainted with. I have most likely omitted some people that have made great contributions, thank you very much for your help.

CHAPTER ONE: INTRODUCTION

1.1 Geological Problem

The latest phase of hydrocarbon exploration on the Scotian Margin has yielded unfavourable result due to lack of understanding of the margin's geological complexity (Enachescu and Wach, 2005). The Scotian Shelf has been well explored and documented (Wade and MacLean, 1990; Shimeld, 2004) but the feedback between sedimentation and salt tectonics affecting the area make slope and deepwater interpretation difficult. This depositional system complexity has lead to the failure so far to find reservoir rocks in recent wells in deep water exploration.

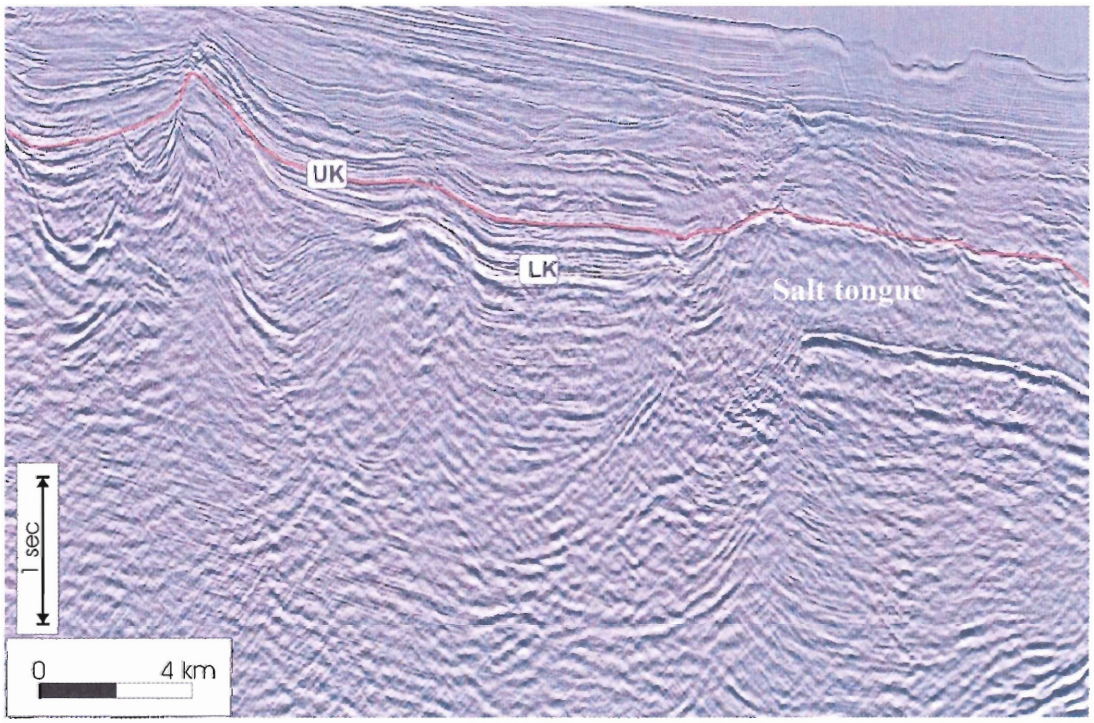

Figure 1.1. Seismic line with strong reflections at the top and base of a salt –tongue canopy. Imaging below the tongue is poor due to the acoustic shadowing caused by the salt structure. Horizon UK is a near top Cretaceous marker; Horizon LK is a Late Cretaceous marker (After Shimeld, 2004).

One problem with understanding the geology in the slope and deep water is the lack of expensive deep exploration wells that would be able to provide detailed stratigraphic information. Seismic imaging problems caused by complex salt bodies and overpressure in the substratum hinder the interpretation of basement and sedimentary architecture (Figure 1.1). Problems associated with interpreting these complex salt bodies in seismic sections is not limited to the Scotian Margin (Figure 1.2; Figure 1.3) however, using interpretation concepts from other passive margins that have proved successful are not easily transferable to the Scotian Margin because of its unique tectonic and stratigraphic history.

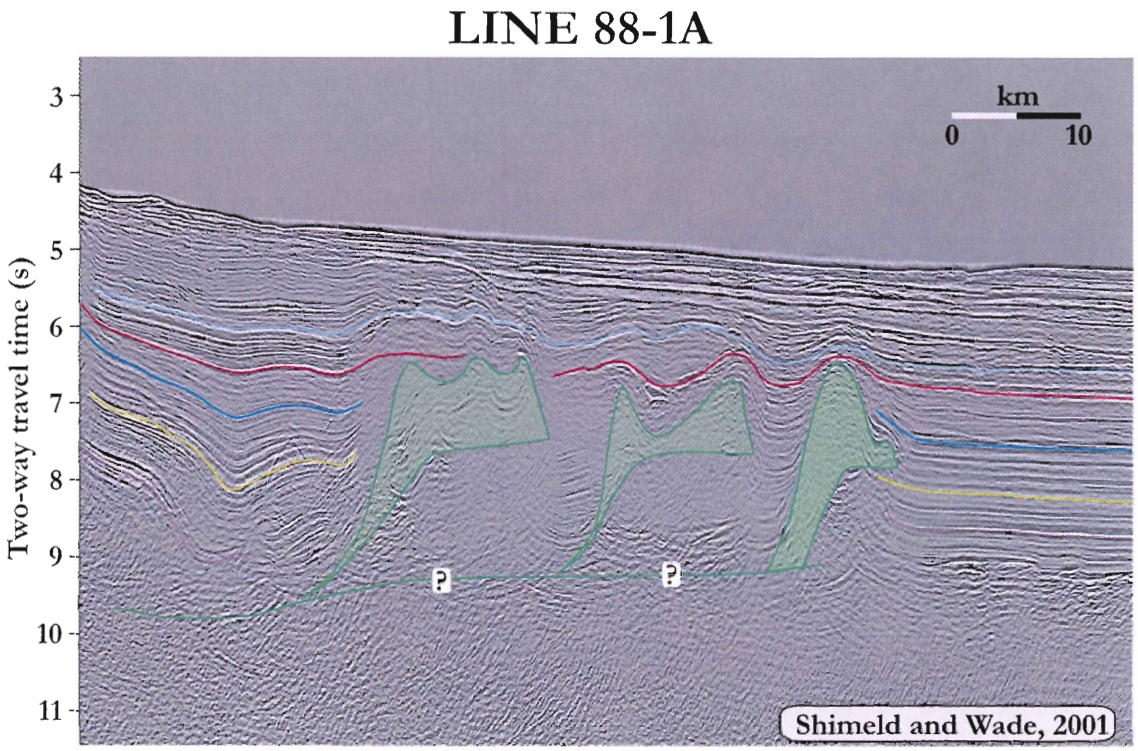

Figure 1.2. Possible interpretation of subsurface allochthonous salt nappes on the Scotian Margin, offshore Nova Scotia. (Shimeld and Wade, 2001)

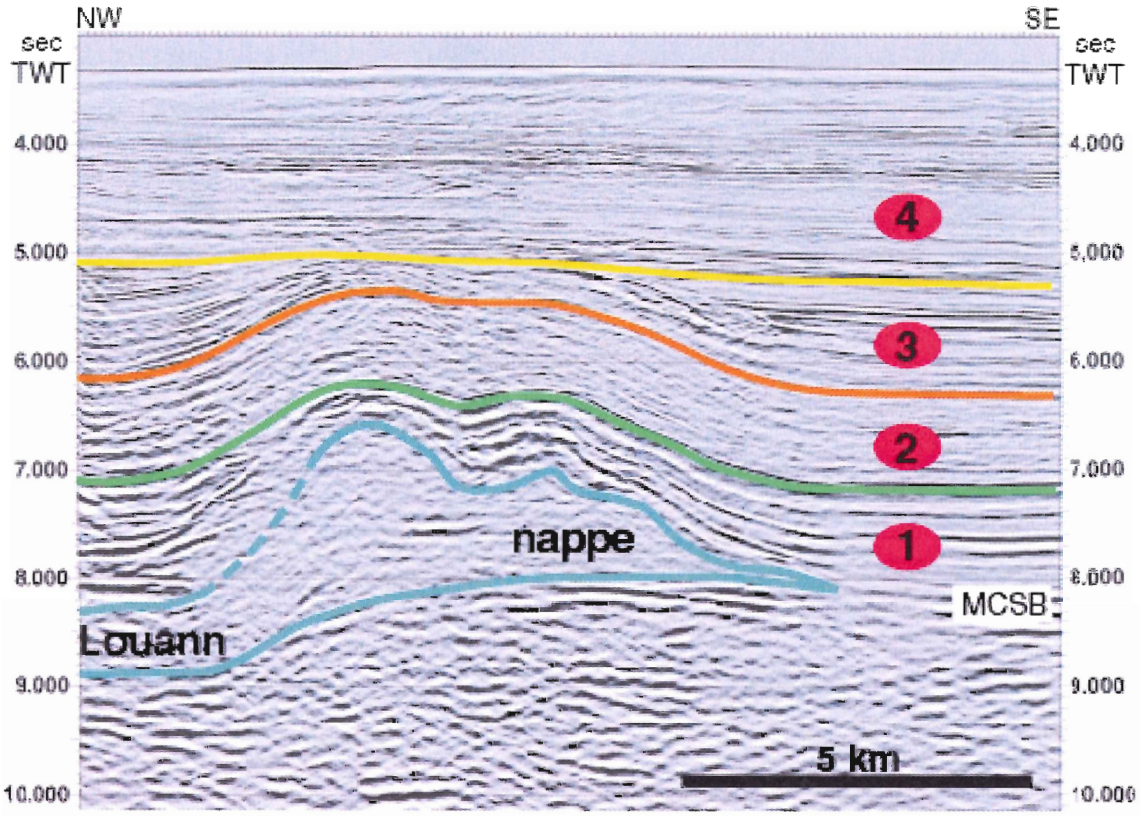

Figure 1.3. Interpretation of subsurface salt nappe in the Gulf of Mexico (Rowan, 2005)

1.2 Objectives

The purpose of this work is to use analogue modeling to better understand the interaction of tectonics and deposition with specific application to passive margin, sedimentary basins affected by thin skinned extension and controlled by salt mobilization. The physical experiments simulate the evolution of the Scotian Basin in the Abenaki and Sable Subbasin areas which are parts of the basin that have been deeply influenced by salt tectonics. The experiments represent the evolution of the basin from the Jurassic to the Early Cretaceous, covering the main phase of salt tectonics in the development of the Scotian basin. On the basis of pilot experiments and published seismic data, likely basement morphologies are used to simulate the first-order features of salt tectonics and depositional systems in the North-Central Scotian Margin.

Physical modeling of the tectonic evolution of passive margin sedimentary basins detached on salt quantitatively improves the understanding of fault mechanics, interaction between tectonic and depositional processes in a clearly constrained lab system. Deduced from open problems and the geological framework of the North-Central Scotian Margin, this thesis systematically evaluates the tectonic relationship between low sedimentation rates combined with a thick salt basin in passive margin settings affected by gravity spreading on the salt substratum (Adam et al. 2006). The Analogue experiments are dynamically scaled and use brittle and ductile model materials to interpret the evolution of the basin. Particle Imaging Velocimetry (PIV) is used to analyze 3D surface deformation (Figure1.4), and then sets of 2D cross sections, cut shelf to slope, are made to give a quantitative analysis of the structural, kinematic, and dynamic evolution of the Scotian Basin. The results from these analogue experiments can then used, combined with available seismic data, to better understand how salt mobilization has affected the Scotian Margin.

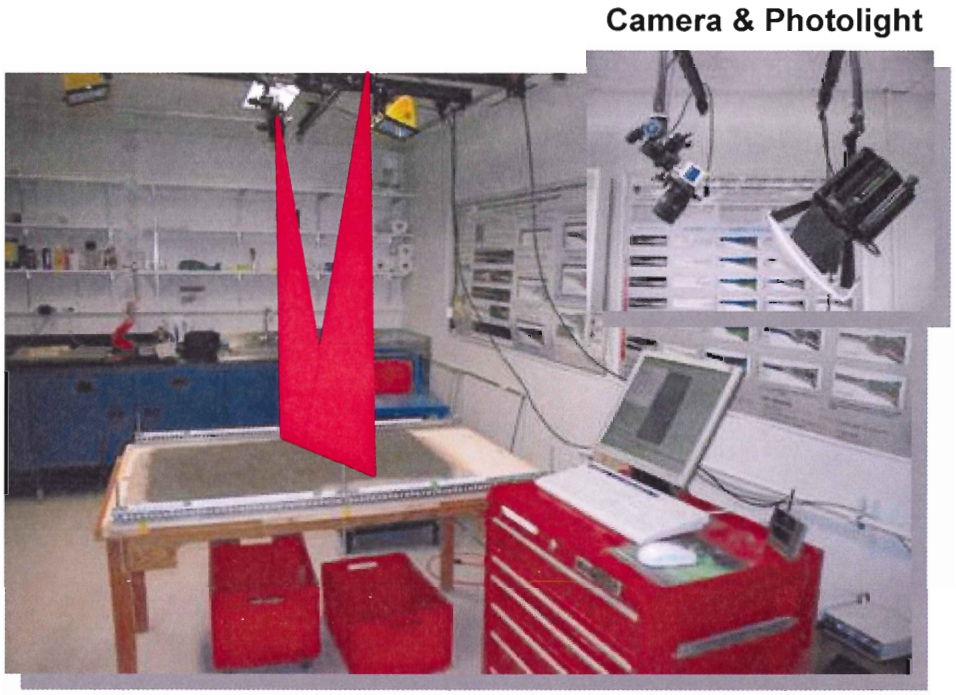

Figure 1.4 General view of PIV setup of analogue experiment. Cameras and lights setup above experiment for monitoring of surfical deformation. Red triangles indicate the viewing direction of the stereoscopic cameras.

CHAPTER TWO: SALT TECTONICS ON PASSIVE MARGINS AND GEOLOGY OF SCOTIAN BASIN

2.1 Advances in the understanding of salt tectonics

Advances in the study of salt tectonics have been divided into 3 major eras, defined by advances in the understanding of mechanisms controlling salt tectonics as outlined by Jackson (1995). The eras include the pioneering era, fluid era and the brittle era. Early salt tectonics studies began in ~1856 and the present day salt tectonics concepts applied in this thesis are mainly developed in the modern brittle era of salt tectonics research.

2.1.1 Pioneering Era

The *pioneering era* (1856-1933) in salt tectonics was driven by the wish to understand salt diapirism. In this era, debate eventually focused on the effects of buoyancy versus orogeny after data from oil exploration eliminated speculation of more erroneous notions (igneous activity, residual islands, etc.). Other important advances in this era included the discovery of salt glaciers, and proposals of downbuilding and differential loading as diapiric mechanisms.

2.1.2 Fluid Era

The *fluid era* (1933-~1989) focused on the belief that salt tectonics resulted from Rayleigh-Taylor instabilities in which the dense fluid overburden with negligible yield strength sinks into the less dense fluid salt layer, causing upward displacement. In this era, density contrasts, viscosity contrasts, and dominant wavelengths were emphasized

while strength and faulting of the overburden were ignored. This era led to the discovery of structures such as turtle structures, recognition of allochthonous salt sheets, subtle traps, salt canopies, and mushroom canopies, all of which will be explained later in this thesis.

2.1.3 Brittle Era

The origin of the *brittle era* (1989-present) exists in the 1947 discovery that a diapir will stop rising when its overburden becomes too thick. Through simulation by sandbox experiments and computerized simulations of Gulf Coast diapirs and surrounding faults, the brittle era generated explanations for regional detachments, salt welds and fault welds along vanished salt allochthons and raft tectonics, etc. Rules were developed for structural balancing for salt tectonics in this era. This era also revealed ideas of reactive as a diapirism resulting from differential loading, thin-skinned extension and influence of sedimentation rates on the geometry of passive diapirs and extrusions.

2.2 Structures in Salt tectonics

Structures associated with salt tectonics can give insight into the structural evolution of salt basins in relation to sedimentation rates and original salt thickness since certain structures can only be produced under conditions. These structures can play an important role in petroleum exploration, by creating traps and seals within the system. Structures that are related to salt tectonics include basinward listric growth faults, landward listric growth faults, fault rollovers, expulsion rollovers, keystone grabens, diapirs, salt rollers, canopies, nappes and allochthonous sheets.

2.2.1 Salt Structures

Salt diapirs comprise a mass of salt that has flowed in a ductile manner and appears to have discordantly pierced or intruded the overburden (Jackson & Talbot, 1994; Mrazec, 1907). This piercing appearance led to the early idea that density contrast alone was responsible for the initiation of diapirs (Rowan, 2005). Newer concepts, mainly derived from the seismic data aquired for petroleum exploration, interpret the formation of diapirs through emplacement by downbuilding or by faulting of the prekinematic overburden (Jackson & Talbot, 1994). Diapirs may be initiated during extension, as overburden is stretched and thinned, or by contraction, as shortening occurs and the overburden is uplifted in growing detachment folds, faulted and eroded enough for salt to break through (Rowan, 2005).

There are 3 stages in the evolution of a diapir which are the reactive, active and passive stages (Figure 2.1). Reactive stage diapirs are the first to occur in diapir evolution and occur as overburden becomes thin and stretched creating faults and graben in the brittle overburden and an *inverse graben* where the salt meets the overburden (Rowan, 2005). Through differential pressure, the salt will react by infilling the space created by the inverse graben creating a triangular, reactive diapir (Rowan, 2005). Active diapirism, occurs after the diapir is tall enough and overburden is thin enough that the diapir can pierce through the overburden due to buoyancy forces and reach the surface as a passive diapir (Rowan, 2005).

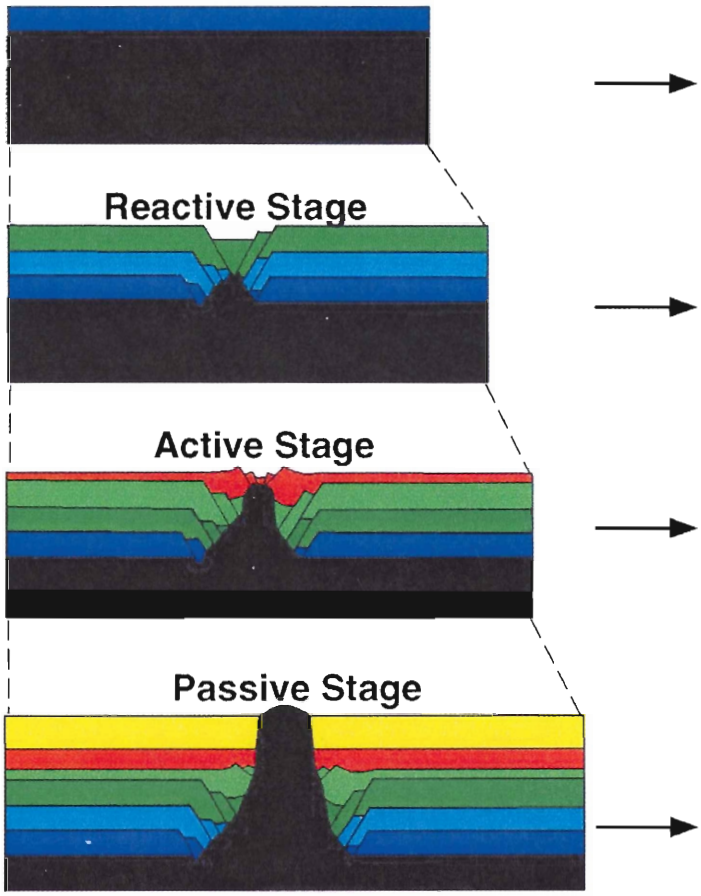

Figure 2.1 Diapir initiation and growth through the reactive, active and passive stages in an extensional setting (Vendeville & Jackson, 1992)

Salt rollers are low-amplitude, asymmetric salt structures (reactive diapirs) that comprise a gently dipping flank in conformable stratigraphic contact with overburden and a more steeply dipping flank in normal-faulted contact with the overburden (Jackson & Talbot, 1994; Bally, 1981) (Figure 2.2). The presence of salt rollers in a system indicates thin skinned extension perpendicular to the strike of the rollers.

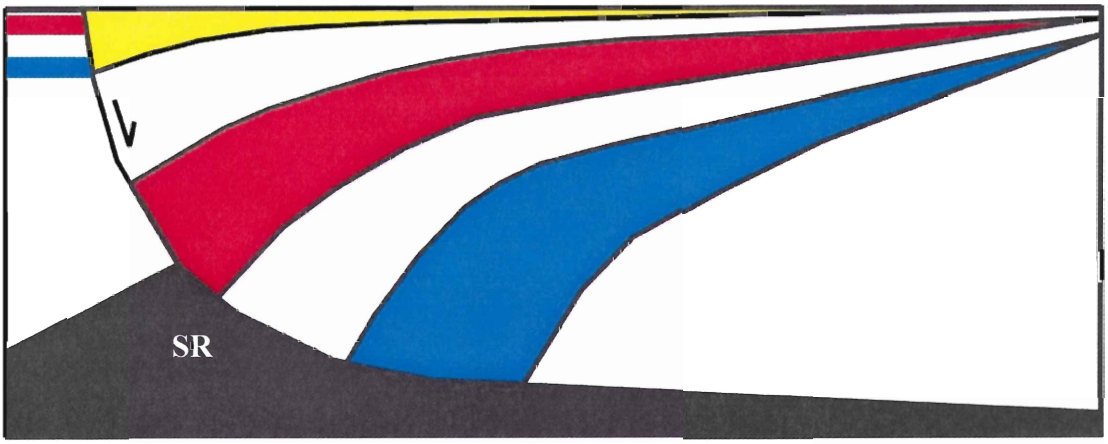

Figure 2.2 Diagram showing triangle shaped salt rollers (SR) occurring as extension and growth faulting takes place. Salt represented by black layer.

Salt welds occur after complete withdrawal of salt causing strata to come in contact where salt had previously been in place (Figure 2.3). Salt welds can form along the autochthonous salt layer when the subsiding overburden comes in contact with the subsalt strata (primary weld; Rowan, 2005). They can form on an incline due to evacuation above a dipping base salt or vertical if a salt wall or diapir is squeezed closed due to contraction (secondary weld; Rowan, 2005). They can also form in combination of vertical and horizontal welds (tertiary weld) (Rowan, 2005).

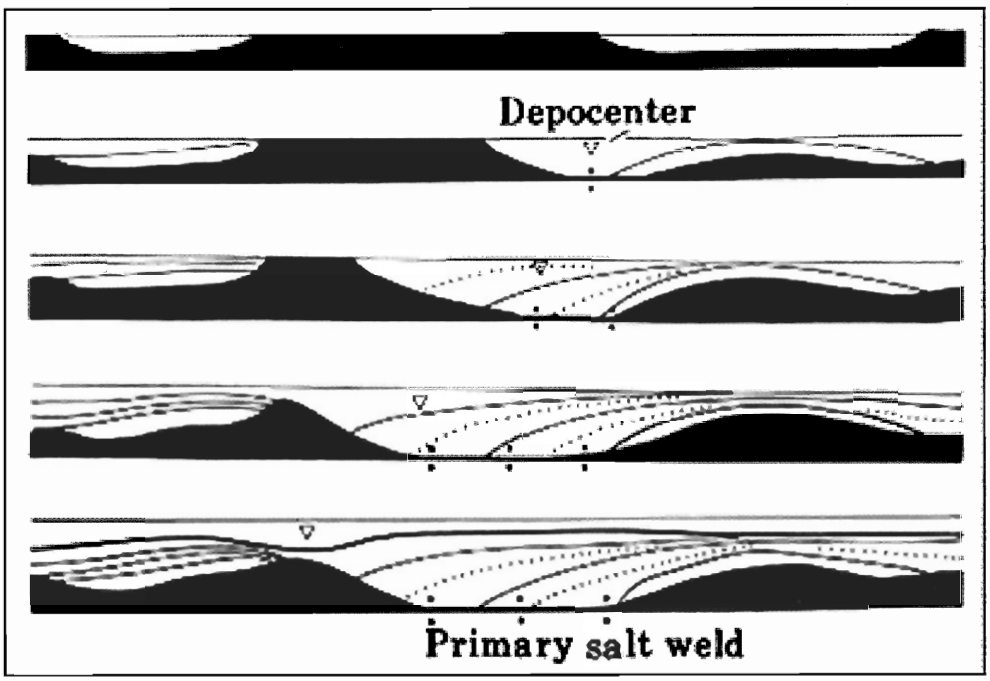

Figure 2.3 The formation of a primary weld as salt evacuates out of the basin (Jackson & Cramez, 1989).

Salt canopies are diapiric structures formed by partial or complete coalescence of diapir overhangs or salt sheets (Jackson et al. 1987). Salt canopies can be classified by their components as salt-stock canopies, salt-wall canopies, and tongue canopies (Figure 2.4) from the coalescence of each of these structures (Jackson & Talbot, 1994). Salt stocks refer to plug like salt diapirs that form a bulb like platform as salt is extruded radially from the feeder (Figure 2.5). Salt walls refer to elongated upwellings of diapiric salt that form sinuous, parallel rows. Salt tongues refer to passive diapers that move like a glacier along the sea floor while still being attached by a feeder (Figure 2.5). Salt sutures are junctions between salt structures that have coalesced laterally to form a canopy (Jackson & Talbot, 1994).

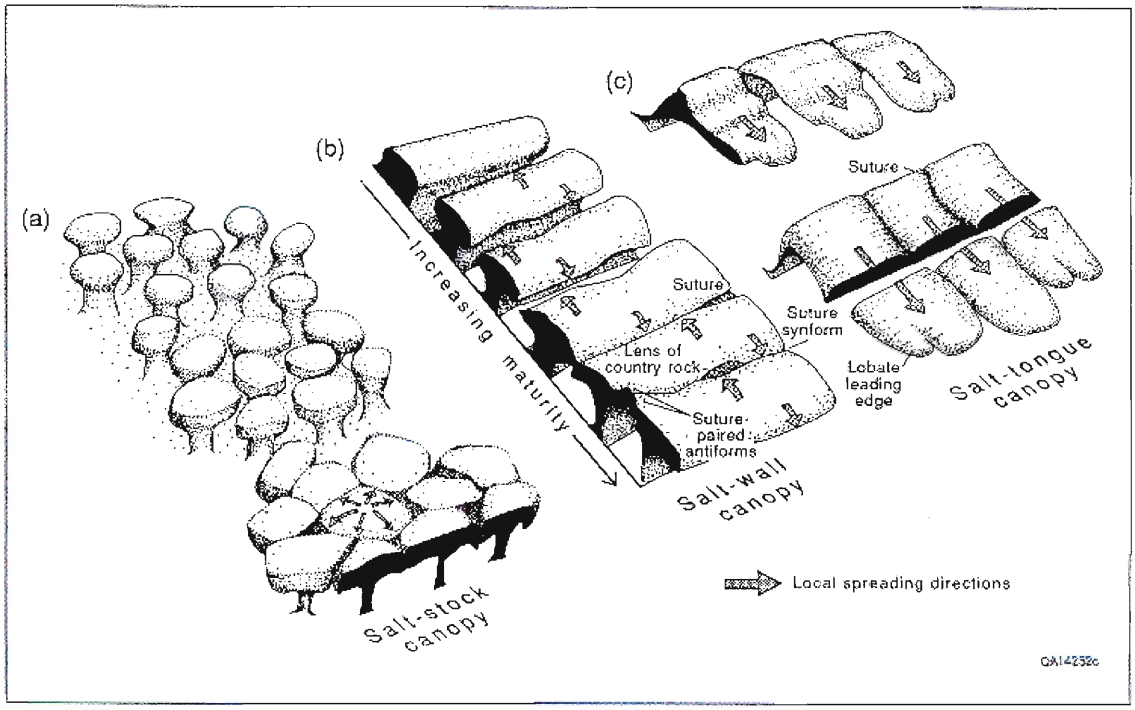

Figure 2.4 Salt-tongue Canopy created by the merging of 2 or more salt stocks, walls or tongues (Jackson and Talbot, 1991).

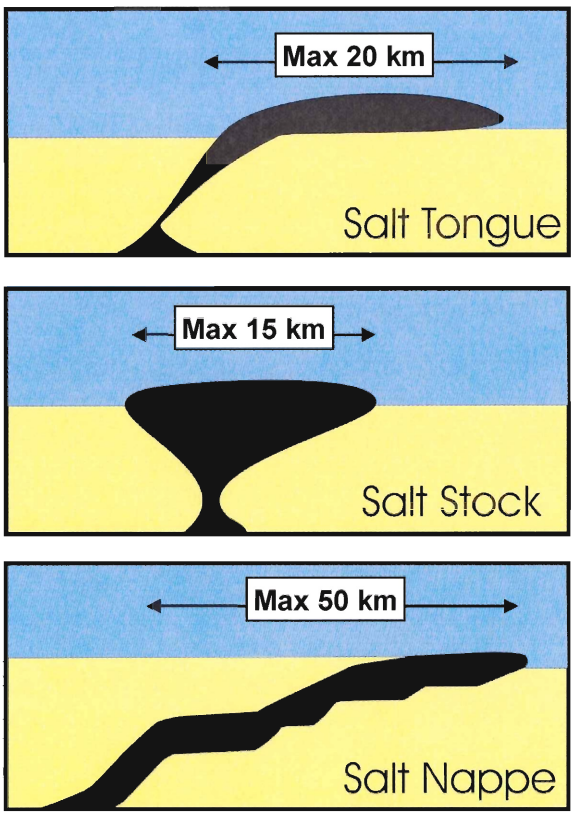

Figure 2.5 Contrasting shapes and extents of salt tongues, salt stocks and salt nappes (After Rowan, 2005).

Salt nappes are larger than individual salt tongues or stocks (Rowan, 2005). Salt nappes are similar to salt canopies however they are distinguished by a lack of local feeders (Rowan, 2005). Nappe emplacement is driven by 3 main overlapping processes (Table 2.1.). Salt nappes can be recognised by their characteristic, by their step like pattern associated with salt climbing up ramped sediments (Figure 2.5).

Overlapping Processes driving Nappe Emplacement	
Process 1	Depositional loading of deep, landward sources.
Process 2	Basinward translation of the overburden on the source layer.
Process 3	Depositional loading and translation of the older, landward portions of the nappe.

Table 2.1 Table showing the overlapping processes driving the emplacement of nappes. (From Rowan, 2005).

Allochthonous salt refers to sheet like bodies that have migrated to stratigraphic levels above the autochthonous layer (Figure 2.6) in which it was deposited (Jackson & Talbot, 1994). It lies on top of younger strata and underlying strata are usually truncated by the base salt while overlying strata are generally parallel (Rowan, 2005). The salt can be driven out of its autochthonous zone by a decrease in sedimentation which could result in lateral flow if diapirs are still being fed by the source in existing basins (Rowan, 2005). It could also be driven out by an increase in sedimentation which would create an associated load that may drive out the salt more rapidly and create lateral extrusion (Rowan, 2005). Finally, increased rates of gravity gliding and spreading can squeeze existing diapers and drive extrusion (Rowan, 2005).

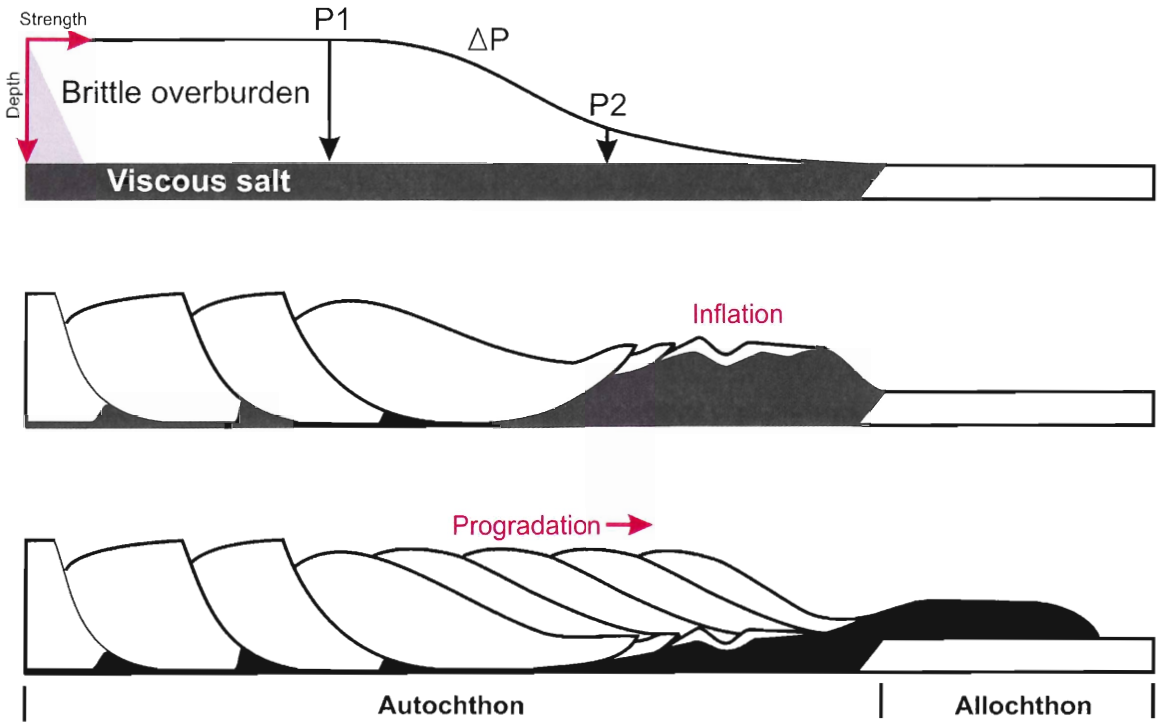

Figure 2.6 Stages of deformation of an initial sedimentary wedge of brittle sediments over viscous salt pushing salt out of depositional domain into the allochthon.

2.2.2 Salt-related Fault Structures

Basinward listric growth fault rollover systems are created by a relatively high sedimentation rate coupled with a relatively low salt thickness (Figures 2.7 and 2.8). The listric shape is attributed to changes in rock rheology at depth or though asymmetrical extension. Landward listric faults develop from a basinward listric fault system as sedimentation overrides the fault system and the listric faulting of the overburden switches from basinward to landward (Figure 2.7 and 2.8). This can be due to high sedimentation rates or a relatively thin underlying salt layer beneath the hanging wall rollover.

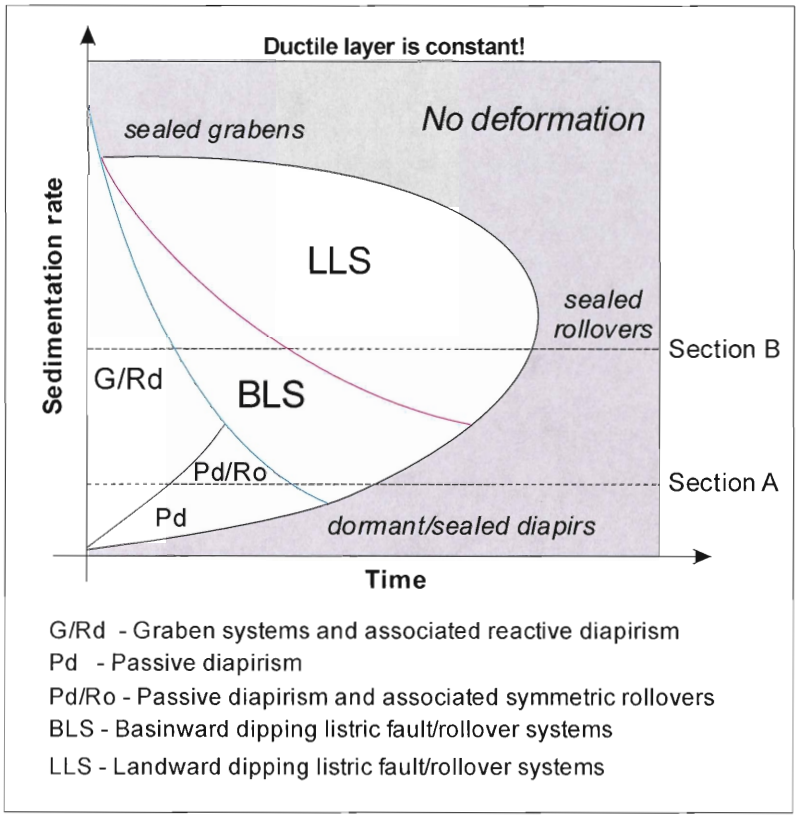

Figure 2.7 Evolution of fault structures in relation to sedimentation rate (Krezsek, 2006).

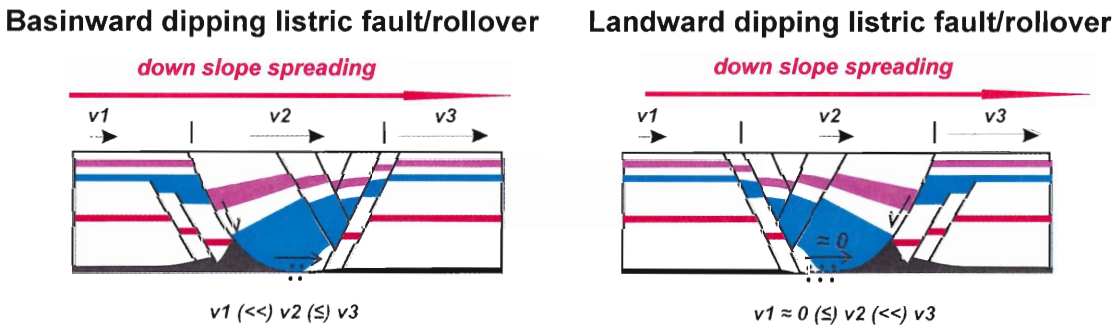

Figure 2.8 Basinward dipping listric faulting vs. landward listric faulting as extension occurs and varied velocities of spreading strata represented by v1, v2, and v3. Colored layers represent marker horizons of sedimentation intervals (Krezsek, 2006).

Growth fault rollovers are related to listric faulting and form as sedimentation occupies available accommodation space created during extension. Growth strata can be identified by thickening of the sedimentary layers towards the fault which are active during deposition. This makes fault rollovers different than expulsion rollovers which

are caused by the evacuation of underlying salt causing subsidence and thickening of sediments towards the salt where the greatest accommodation space is created (Figure 2.9).

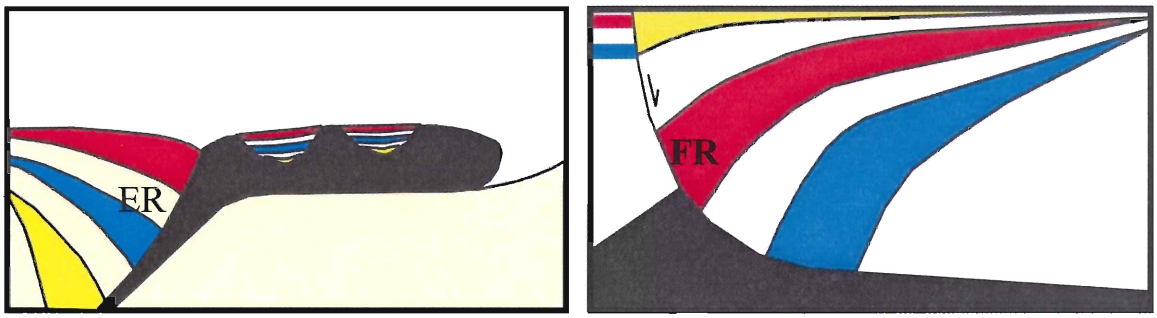

Figure 2.9 Comparison between expulsion rollovers (ER) and fault rollover (FR) structures.

Keystone grabens refer to extensional fault structures that form due to bending of the brittle overburden in rollovers (Figure 2.10). The bending causes a succession of faulting creating grabens with fault steps. The succession of faulting associated with keystone grabens begins on the edges with the order of faults getting younger to the center.

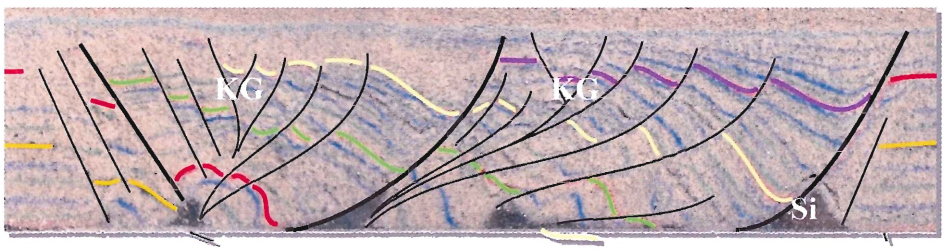

Figure 2.10 Cross-section showing keystone graben (KG) structure formed as silicone (Si) evacuated out of the system. Faults in each complex young towards the center. (Adam, 2006).

2.3 Salt Deformation Mechanics

The behavior of salt is controlled by two factors that make it a different from other typical sedimentary rocks. The first factor is that salt is weaker than other lithologies under compression and tension. Salt acts like a viscous material that flows in a combination of Poiseuille flow due to overburden loading and Couette flow due to translation of overburden (Rowan, 2005). Poiseuille flow refers to a channel flow where the fluid flows faster in the center where there is less drag and is caused by downbuilding of overburden sediments (b in Figure 2.11). Couette is a flow is caused by shearing of overburden in which velocity vector is greatest at translating overburden (c; Figure 2.11). The strength of salt will remain constant with depth whereas the strength of the sediment overburden is increasing linearly with depth which makes salt a detachment surface (Figure 2.12) into which faults sole (Rowan, 2005).

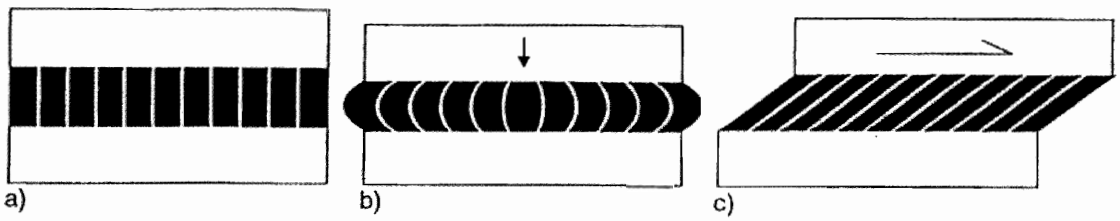

Figure 2.11 Flow of viscous material: (a) undeformed; (b) Poseuille flow; (c) Couette flow (After Rowan,2006).

The second factor that dictates the behaviour of salt is that salt has a constant density of 2.2 g/cm^3 that, unlike most sedimentary strata, will actually decrease with depth due to thermal expansion (Rowan, 2005). This makes salt denser than surrounding strata at the surface but at depths between 1000 – 1500m will become less dense (Rowan, 2005). The low density of salt is the reason that it was believed that salt punched through

the denser overburden until reaching neutral buoyancy. This scenario is true only as a secondary effect when there is only a thin weak overburden present but thick overburden behaves as a brittle material, not a viscous one (Figure 2.12). Vendeville and Jackson (1992) have documented the factors needed for salt flow to occur (Table 2.2).

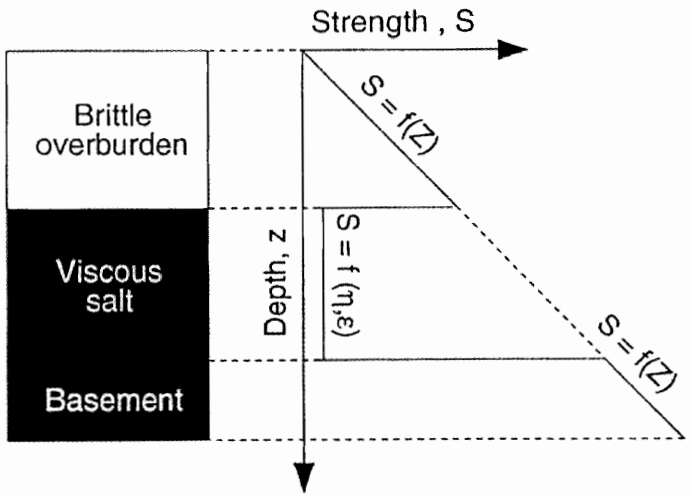

Figure 2.12 A 3-layer model of the crust with a weak, constant strength, salt layer between 2 brittle layers whose strength increases with depth (Vendeville & Jackson, 1993).

	Concepts for salt flow
Factor 1	Must be open path to near-surface salt body.
Factor 2	Overburden must be thin and weak enough for differential fluid pressure to overcome its strength, which will deform thin overburden.
Factor 3	Salt does not drive salt tectonics, it only reacts passively to external forces.

Table 2.2. Factors needed to understand salt flow (From Vendeville & Jackson, 1992).

2.4 Evolution of passive margins affected by salt tectonics

Salt basins can occur in rift basins and along passive margins or in deformation settings such as in the Alpine/Himalayan system (Rowan, 2005). Salt basins mainly form during the late syn-rift to early postrift phase, such as offshore Brazil and the Gulf Coast,

or during rifting, such as the Scotian Basin (Jackson & Vendeville, 1994). Salt deposition in rift basins occurs as extension occurs in the continental crust, which leads to graben development. As rift grabens form initial deposition includes non-marine clastics due to syn-rift uplift caused by high heat flow (Rowan, 2005). Graben subsidence from heat and loading leads to a transition from terrestrial deposition to marine incursion. This transition is where deposition of evaporates occur (Rowan, 2005). Our experiments simulate various basement architectures (grabens, half-grabens etc.) that occur in rift basins and are infilled with evaporates and sediments (Figure 2.13).

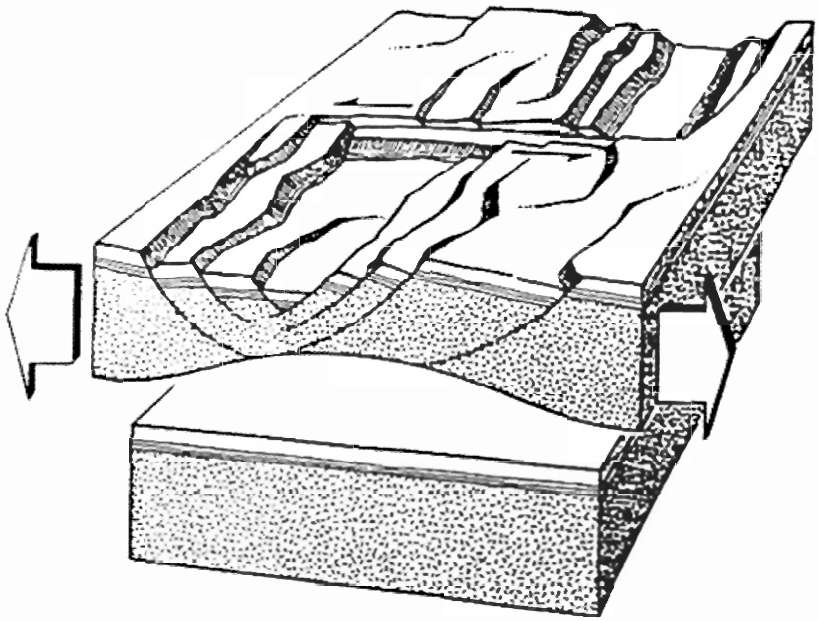

Figure 2.13 Graben formation through extension and subsidence creating rift basin. (Stonely, 1981)

Salt deposited in these rift basins will behave like a viscous material under sediment loading over geological time. It will begin to move immediately under a differential load which occurs in passive margin settings because most sedimentation will take place closer to the shelf, causing basinward flow of salt and subsequential brittle

deformation on overburden (Figure 2.14). In the presence of proper buttresses located in seaward limit of the basin, the landward extension in the landward limit of the basin will be balanced by basinward compression and salt inflation in the deepwater region before the salt is pushed out of the basin as an allochthonous sheet. The interaction of gravity driven deformation, syntectonic sedimentation and salt mobilization will result in complex salt structures and evolution of the basin (Adam et al. 2006).

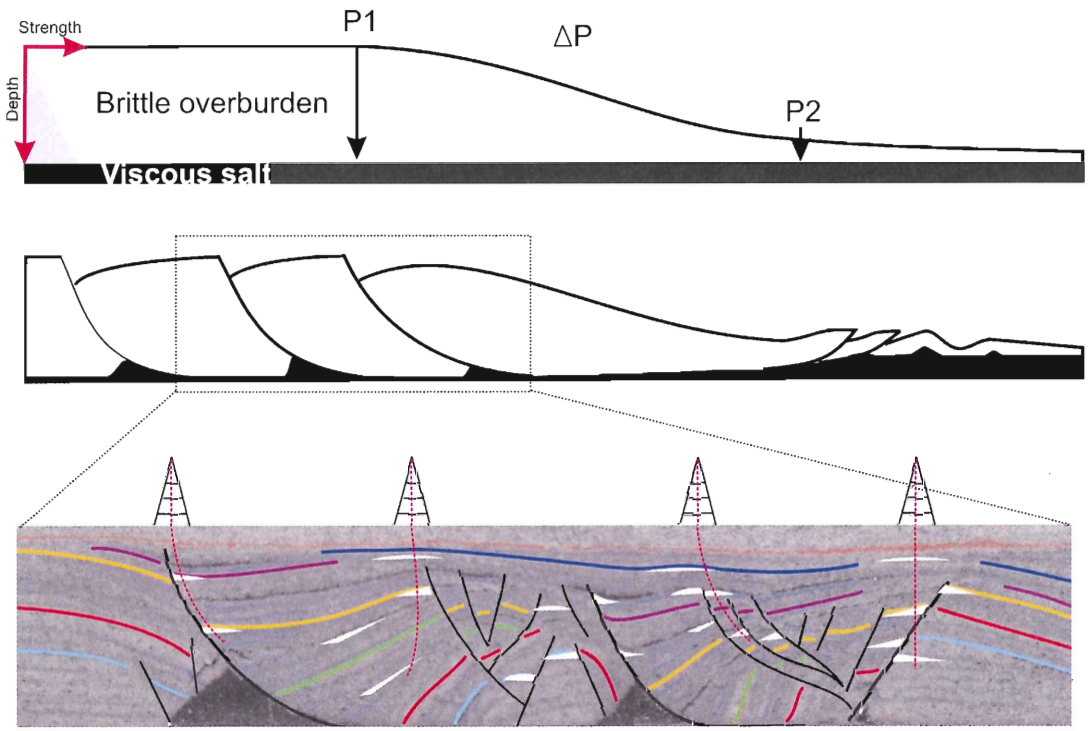

Figure 2.14 Deformation of brittle sediments over viscous salt due to a change in pressures exhibited by the sedimentary wedge (Kreszek et al. 2006).

2.5 Geology of Scotian Basin

The Scotian Basin is located offshore Nova Scotia and extends 1,200 km from the eastern part of Georges Bank in the southwest and the southwestern Grand Banks in the northeast (Jansa & Wade, 1975). The basin encompases the continental slopes and rises

of these areas (Jansa & Wade, 1975). The Scotian Basin is divided into 8 sub-basins defined by syn-rift basement topography, and formation of different syn-rift depocenters (Figure 2.15). The experiments conducted for this thesis focus on the area encompassing the Sable and Abenaki sub-basins based on favourable sedimentation rates in its depositional history for reservoir potential and because of the recent focus of these sub-basins in the latest exploration cycle.

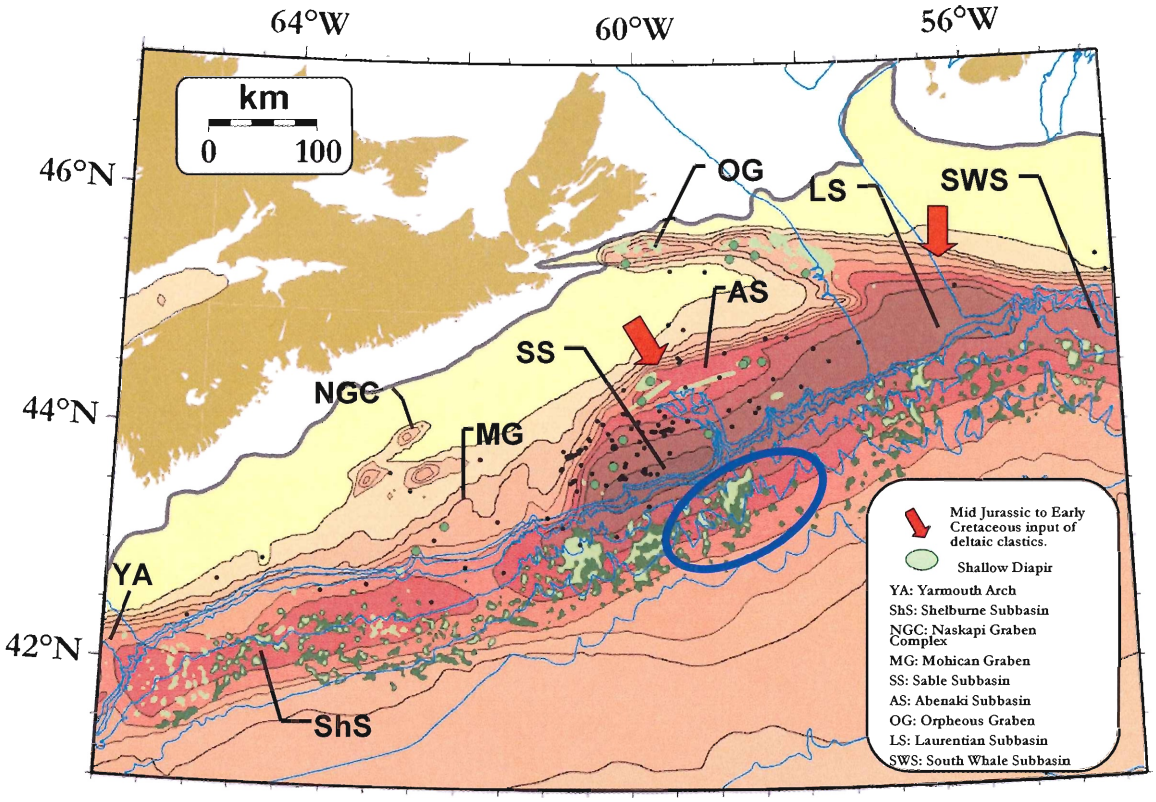

Figure 2.15 Map of Scotian Basin showing all sub-basins and extent of observed salt structures. Study area is indicated by blue circle (After Shimeld, 2004).

The northern and northwestern limits of the Sable Sub-basin are located at the North Sable high and the basement hinge zone (Figure 2.16). The southern boundary of this basin is not well defined in seismic data due the thickness of sediment and abundance of salt overlying the basement (Jansa & Wade, 1975). The Sable sub-basin is believed to have accumulated up of approximately 10 – 12 km of sediments (Jansa & Wade, 1975).

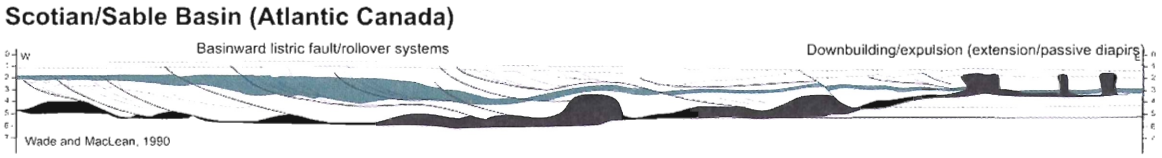

Figure 2.16 Cross Section of the Sable Sub-basin showing salt in black and deformed., brittle sediments (Modified from Wade & MacLean, 1990).

The Abenaki Sub-basin is located south of the Canso Ridge, an elevated horst block that separates it from the Orpheus graben in the northern shelf, and may contain as much as 11 km of sediments (Jansa & Wade, 1975). The northern limit of the sub-basin is marked by basement faults which controlled the basin morphology that influenced deposition of Upper Triassic-Lower Jurassic red beds and the overlying Argo Salt (Jansa & Wade, 1975). Like the Sable Sub-basin the southern boundary of the Abenaki is not well defined due to the thick sediment succession overlying the basin floor and southern margin.

The salt sediments present in the Scotian Basin are known as the Argo Formation (Figure 2.17). This formation was deposited in the late syn-rift stage between the Middle to Late Triassic and has strongly influenced the evolution of the Scotian Margin. The Argo unit was deposited together with other fluvial-lacustrine sediments until the early Jurassic when marine flooding occurred. In the basinward slope area of the Scotian Basin, uninterrupted sedimentation occurred from the Jurassic to the Cretaceous. On the landward shelf area of the basin, the deposition of the Abenaki Formation, a carbonate bank, was interrupted by a regression, which occurred from the Late Jurassic to the Early Cretaceous. This is believed to be related to tectonic uplift and caused strong progradation of deltaic sediments of the Mississauga Formation in the basin Jansa & Wade, 1975).

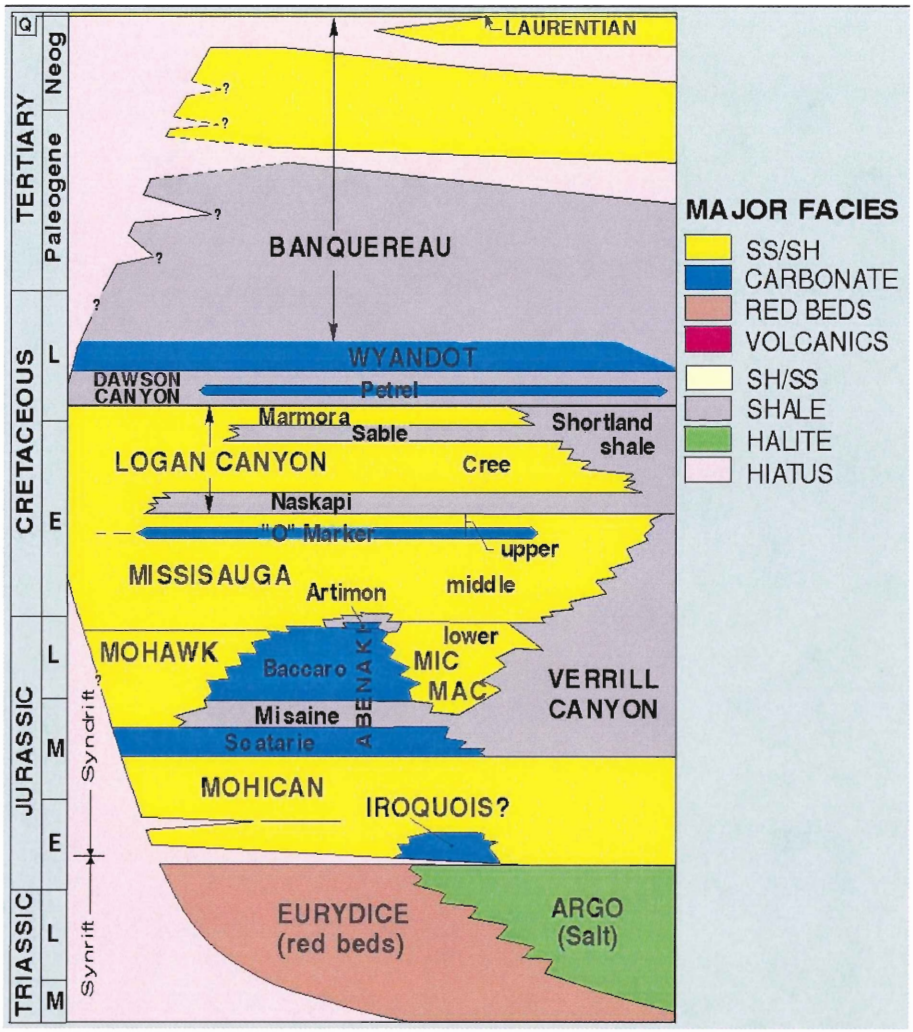

Figure 2.17 Generalized lithostratigraphy chart of the Scotian Shelf (Wade, 1990).

2.6 Salt tectonic sub-provinces

The salt tectonic sub-provinces have been defined in modern seismic data of the slope area based on distinctive salt deformation styles and depositional environments by Shimeld (2004). It is proposed that the particular salt tectonic styles in the different provinces are controlled by basement morphology and variations in sedimentation history (Shimeld, 2004). Based on the structural variations, the Scotian Basin can be differentiated into 5 salt tectonic sub-provinces (Figure 2.18; Table 2.3). The focus of

this thesis is of the allochthonous salt nappe and canopy systems within Subprovince III and IV within the salt tectonic sub-provinces (Figure 2.18).

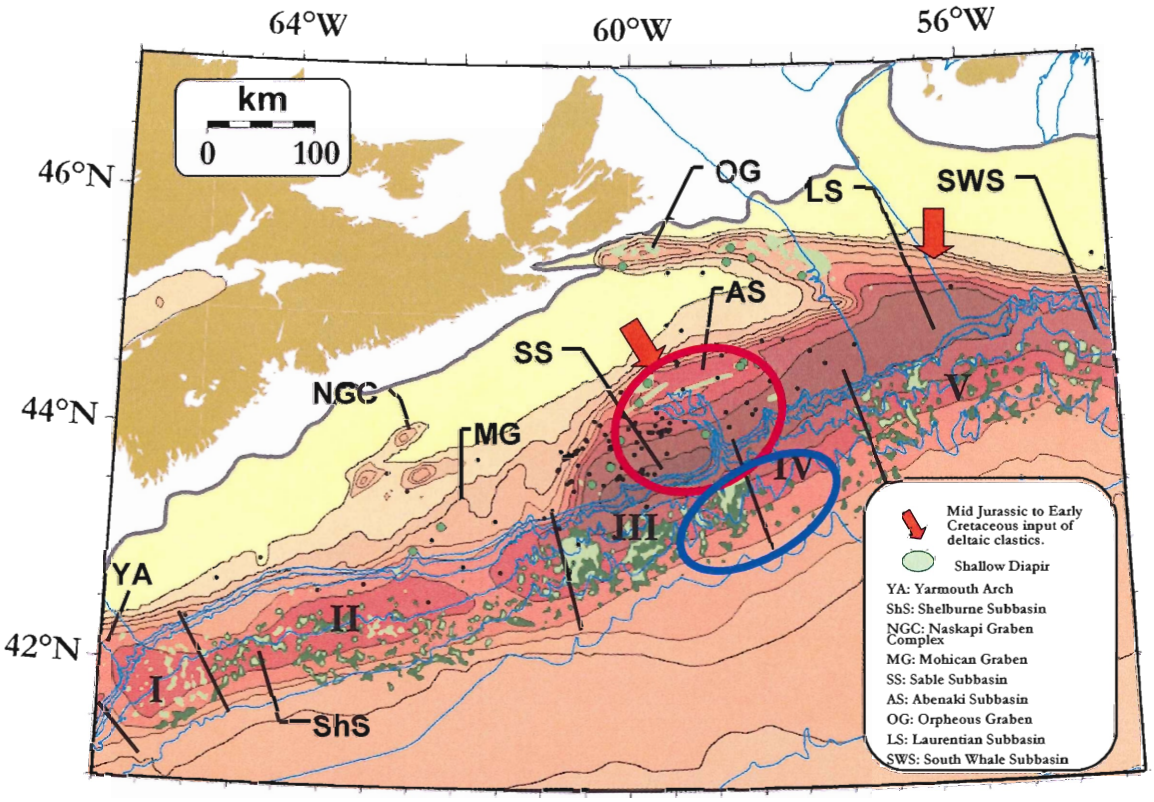

Figure 2.18 Map of Scotian Basin Salt Subprovinces with study area marked by blue circle and original salt basin marked by red circle (modified after Shimeld, 2004).

Overview of Scotian Basin Sub-provinces	
Subprovince I	Diapirs in form of elongated walls, seaward tongue canopy system. Passive diapirs flanked by marginal synclines.
Subprovince II	Linear salt walls (aligned with edge of Abenaki carbonate platform. In east, vertical diapirs, seaward nappes. In west, mushroom to tongue shaped diapirs.
Subprovince III	Salt nappes, extensional synkinematic structures associated with overburden on nappes.
Subprovince IV	Lack of diapirs, salt nappes with basinward listric rollover system associated with overburden.
Subprovince V	Complex 3D morphology. Complex extensional and contractional structures. Diapirs in slope under thin cover.

Table 2.3. Table showing variations in salt structures characterizing Salt provinces in Scotian Basin (After Shimeld, 2004).

Subprovince III (Figure 2.12; Table 2.3), in which the Sable subprovince is located, is characterized by extensive salt nappes of Cretaceous age that have moved 80 to 100 km basinward and have associated overburden sediments showing a variety of extensional syn-kinematic structures. Subprovince IV (Figure 2.12; Table 2.3), in which the Abenaki Sub-basin is located, is characterized by a lack of diapirism in the shelf area and virtually no diapirs beneath the shelf break. The upper slope of the modern margin is defined by salt nappes with basinward listric rollover systems developed in the sediment overburden (Shimeld, 2004).

CHAPTER 3: RESEARCH APPROACH

3.1 Concept of Analogue Modelling

Analogue Modeling has proven to be an effective tool in the testing and understanding of 3D brittle/ductile deformation systems under variable geological boundary conditions (Vendeville & Jackson. 1992). In these experiments, brittle sediments are simulated with sand while ductile materials are represented by silicone rubbers or putties. Results and interpretations for this thesis use analogue modeling with high-resolution strain monitoring techniques coupled with structural modeling and seismic interpretation. The integration of experimental concepts in interpretation of seismic data is useful to gain a better understanding of passive margin, sedimentary basin evolution, structural evolution of the salt tectonic structures and the depositional system present in the deepwater Scotian Basin.

3.2 Materials

For the conduction of these experiments, brittle and viscous analog materials are used to simulate brittle sediments and ductile salt respectively. Sifted silica sand is used to represent the brittle sediments while ductile salt is represented by silicone rubber. In order to better understand the mechanics of the analogue models and to calculate the scaling factors, specific parameters of the materials are measured (Table 3.1).

Property	Sifted Silica Sand	Silicone Rubber
Grain Size	0.02 – 0.45	
Density (g/cm^3)	1.6	0.99
Viscosity (Pas)		$6*10^4$
Angle of internal friction (°)	34	

Table 3.1 Table showing material properties of sieved silica sand and silicone rubber used in experiments.

3.3 Scaling

All experiments are dynamically scaled by the material parameters to simulate nature; thus all parameters of the experiments, including geometries, kinematics and stresses are comparable to nature quantitatively (Costa & Vendeville 2002 from Hubert 1937, Weijermars et al. 1993). With a time scaling factor of $1.4 * 10^{-14}$, experiments run for approximately 10 days depending on how salt is flowing in the system to simulate the basin evolution . This time frame simulates the Late Jurassic to Early Cretaceous basin evolution in nature. The geometric scaling factor is derived from similarities in cohesion, density of sand and sedimentary rocks, and gravitational acceleration. From these calculations the geometric scaling factor is given with 10^{-5} and 1 cm in the experiment equals 1 km in nature (Table 3.2). The time scaling factor is derived from the viscosity ratios of silicone and salt as well as the density ratios of the overburden sand and sediments. With the time scale factor of $1.4 * 10^{-14}$, 1 hr in the experiment equals approximately 150 000 years in nature (Table 3.2).

Scaling Parameters	Experiment	Nature	Scaling Factor
Time	1 hr	150 000 yrs	$1.4 * 10^{-14}$
Geometry	1 cm	1 km	$1*10^{-5}$

Table 3.2 Conversion of experimental parameters to time and geometry in nature based on scaling factors.

3.4 Setup

All experiments are completed in two different setups for this project. The setup for the small-scaled, pilot experiments (Figure 3.1) consists of a glass-sided tank with a horizontal rigid base and one on an incline (Exp 5-4), all with dimensions of 80 cm

length * 30 cm width (Table 3.3). The only variation in the setup of each experiment is the basement morphology which represents possible basement architecture expected for the North-Central Scotian Basin (Figure 3.2). The purpose of the experiment series with different basement morphologies is to better understand how basement architectures influence salt mobilization and deformation in a passive margin setting. The basement geometries are setup using a sand border of a vertical thickness of 2 cm for all experiments.

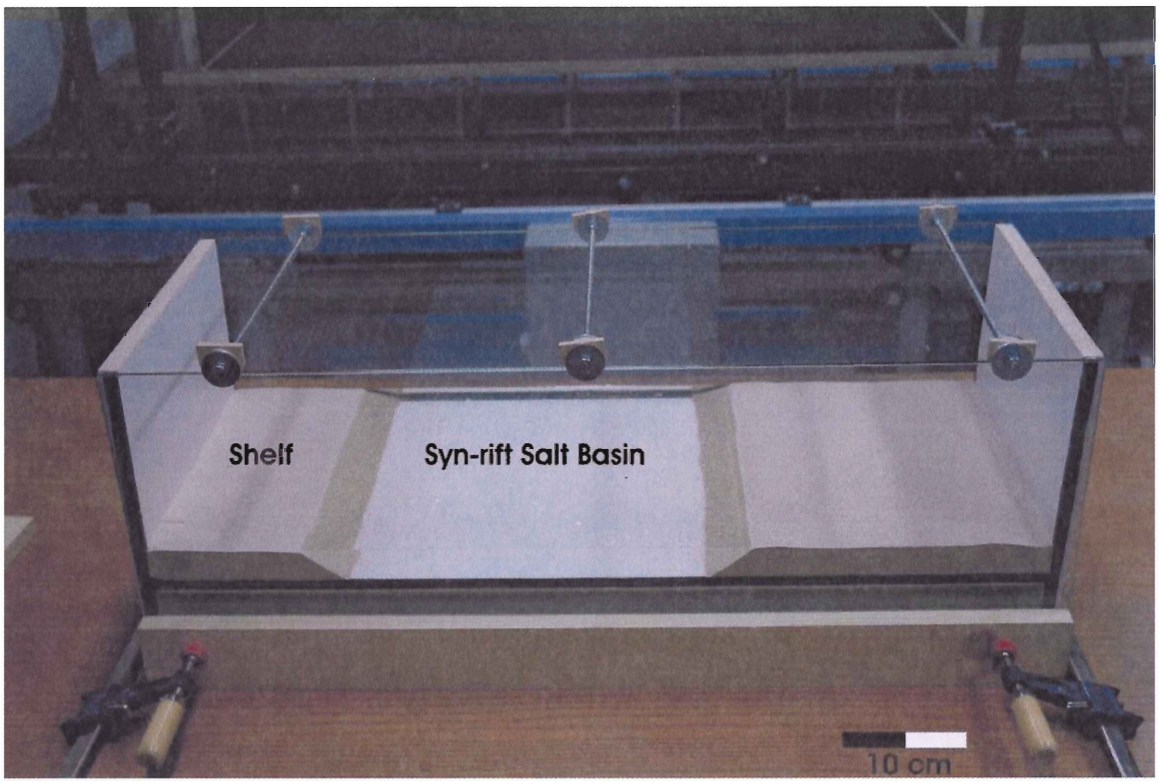

Figure 3.1 Initial setup of the small-scalled, pilot experiments with 2 cm thick silicone basin. Image shows the intial setup for Exp 5-2, a symmetric graben configuration.

Pilot Experiment Setups							
Experiment	**Setup**	**Basin Geometry**	**Shelf Buildup**	**Sedimentation rate (const. vol.)**	**Modelled sediment input: km^3/km of margin in 150 000 yr**	**Sieve Intervals**	**Duration**
5-1	Symmetric Graben	Full graben 35 cm length 2cm salt	4.0 cm	0.25 cm/2 hr	3.13	2 hr	240 hr
5-2	Symmetric Graben	Full graben 35 cm length 2 cm salt	4.0 cm	0.25 cm/2 hr	1.57	2 hr	240 hr
5-3	Wedge	Half graben wedge 35 cm length 2 cm salt	4.0 cm	0.25 cm/2 hr	1.57	2 hr	234 hr
5-4	Compressional Reactivation/tilt	Full silicone basement 1 cm salt	4.0 cm	0.25 cm/2 hr	1.57	2 hr	336 hr
5-5	Basement step	Half graben step 35 cm length 2 cm salt	4.0 cm	0.25 cm/2 hr	1.57	2 hr	290 hr
5-6	Intemediate Horst	Full graben with intermediate horst 35 cm length 2 cm salt	4.0 cm	0.25 cm/2 hr	1.57	2 hr	260 hr

Table 3.3. The setups for each of the pilot experiments including basin geometry, sedimentation rates, sieve intervals and durations.

Large-scaled Experiment Setups							
Experiment	**Setup**	**Basin Geometry**	**Shelf Buildup**	**Sedimentation rate (const. vol.)**	**Modelled sediment input: km^3/km of margin in 150 000 yr**	**Sieve Intervals**	**Duration**
5-7	Symmetric graben	Full graben 60 cm length 2 cm salt	4.0 cm	0.25 cm/4 hr	1.95	4 hr	224 hr
5-8	Wedge	Half graben 60 cm length 2 cm salt	4.0 cm	0.25 cm/4 hr	1.82	4 hr	176 hr
5-9	Basement Step	Half graben step 60 cm length 2 cm salt	4.0 cm	0.25 cm/4 hr	1.82	4 hr	188 hr

Table 3.4. The setups for each of the large-scaled experiments including basin geometry, sedimentation rates, sieve intervals and durations.

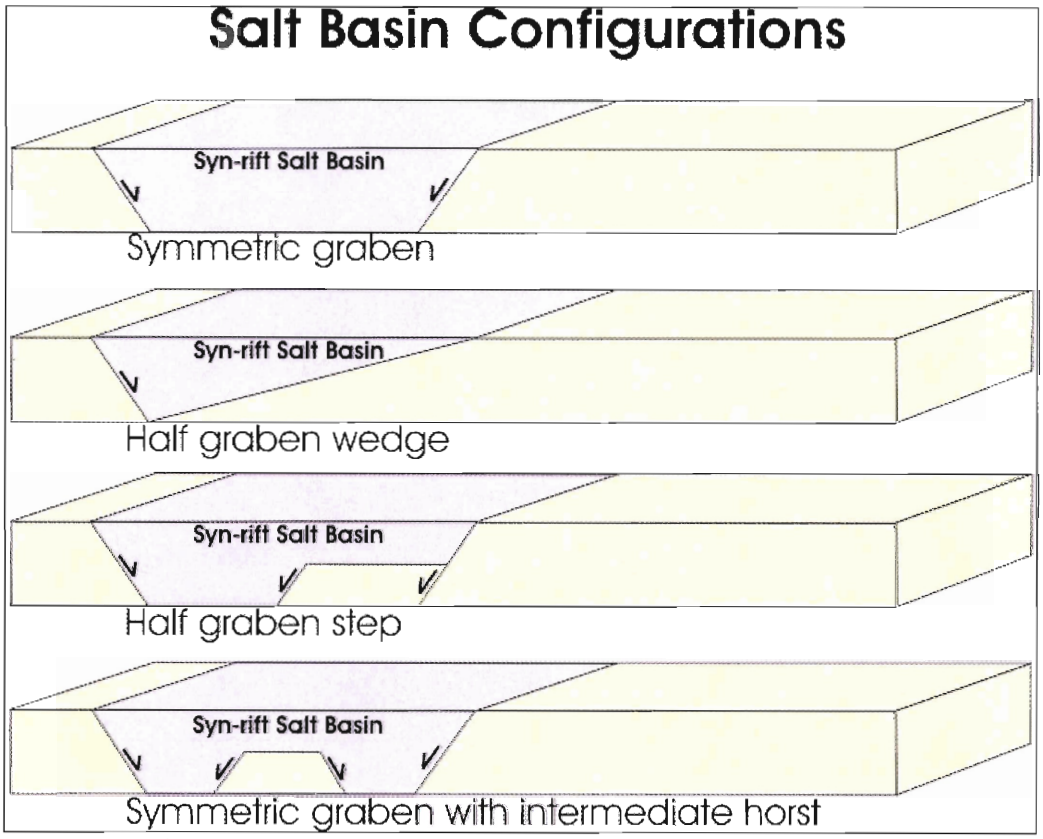

Figure 3.2. The various basement morphologies represented in the analogue experiment series. Landward side of experiment is on the left, basinward is on the right. Dimensions represent an 80 km x 30 km x 2 km total basin.

Once the pilot experiments are completed and a better understanding of the interaction between salt deformation and basement variation, the large-scaled experiments are completed to obtain a larger, more concise data set. The experiments are completed on a horizontal rigid base with dimensions of 120 cm length * 90 cm width (Figure 3.3; Table 3.4). A rail system and guide is used for accurate sieving of sand layers for measuring sedimentation intervals and the experiments are monitored with Particle Imaging Velocimetry (PIV) technology to obtain high resolution incremental 3D strain data of surface deformation and structures evolving in the basin (Adam et al. 2005).

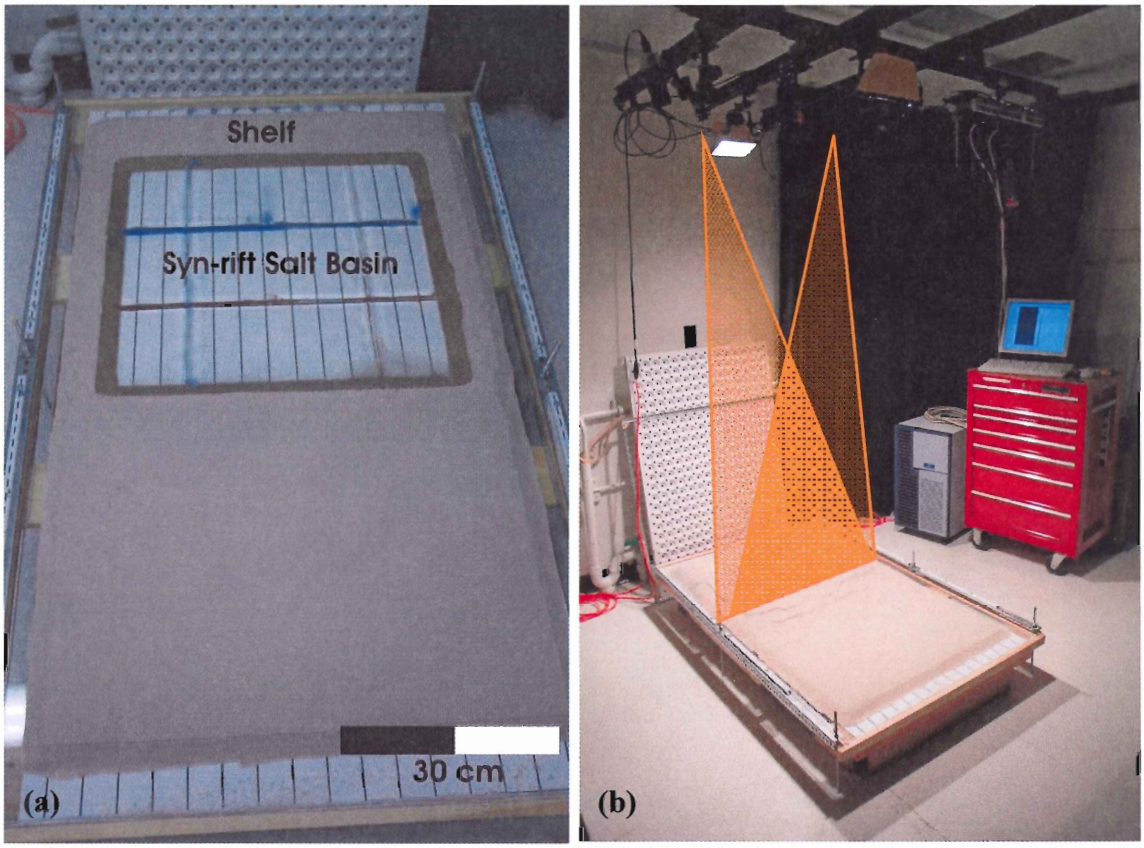

Figure 3.3 Initial setup of the large scaled experiments with a 2 cm thick silicone basin. Image (a) shows initial setup of Exp_5-7, a symmetric graben configuration. Image (b) shows PIV cameras with stereoscopic setup for 3D strain monitoring evolution of the experiment.

3.5 Monitoring Techniques

3.5.1 Imaging of pilot experiments

Small-scale, pilot experiments are monitored with a high resolution digital camera. The camera is positioned to the side, at an oblique angle to the experiments in order to monitor cross-section and oblique surface evolution. The pictures, which show a basinward to landward view of the experiment (left to right), are taken every 2 hours before each new sedimentation interval to show the surface structures. Detailed pictures are taken when structures of interest are observed during basin evolution (Figure 3.4).

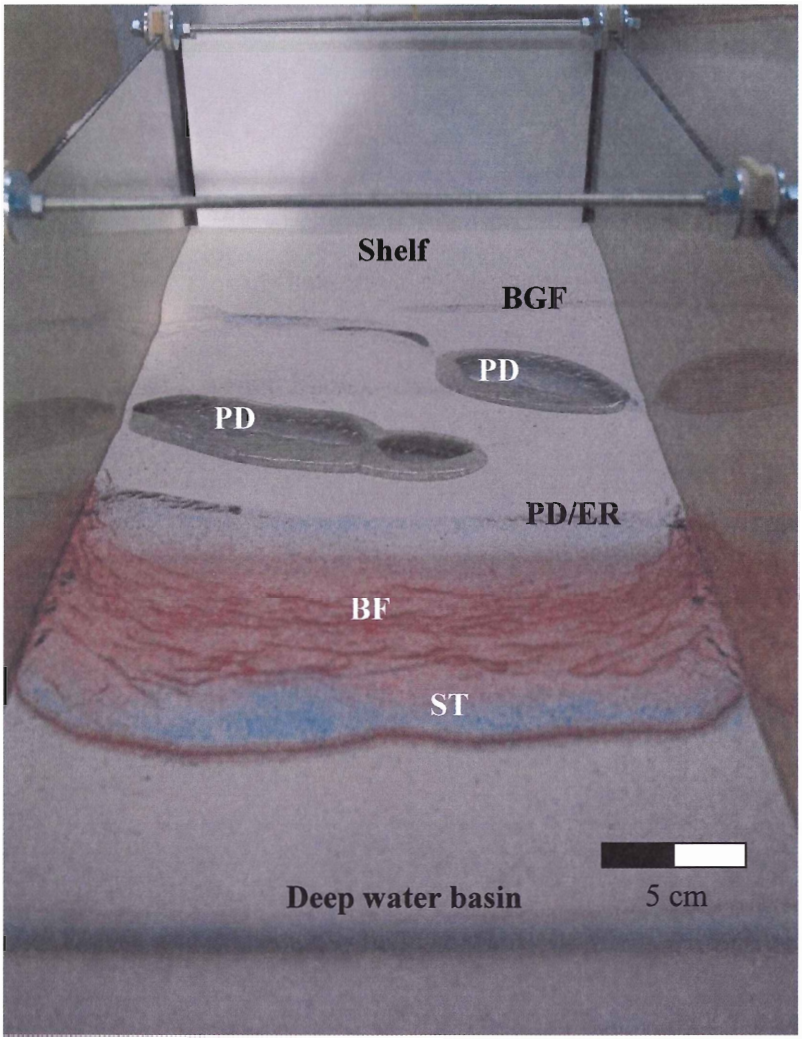

Figure 3.4 Detailed Image of Experiment 5-2 (54 hours) showing growth faulting (BGF), passive diapirs (PD) with seaward leaning silicone canopies, passive diapirs with expulsion rollovers (PD/ER) and buckle folding (BF) on inflated silicone and an allochthonous salt tongue (ST).

3.5.2 PIV Monitoring/Digital imaging

The large-scaled experiments are all monitored using Particle Imaging Velocimetry, which is a high resolution, optical 3D technique used to monitor surface flow and deformation. The system involves 2 high-resolution digital cameras with stereoscopic setup that monitors the 3D surface deformation and evolution by calculating the incremental displacement field with image correlation of time-series images of the

model surface (Adam et al. 2005). Once the displacement field data is calculated, additional displacement and strain components can be derived which include for example subsidence (dz) and horizontal strain (exx) (Figure 3.5). Finite deformation can also be calculated by summing up the incremental vector data to quantify the space and time evolution of structures and depositional systems (Adam et al. 2005).

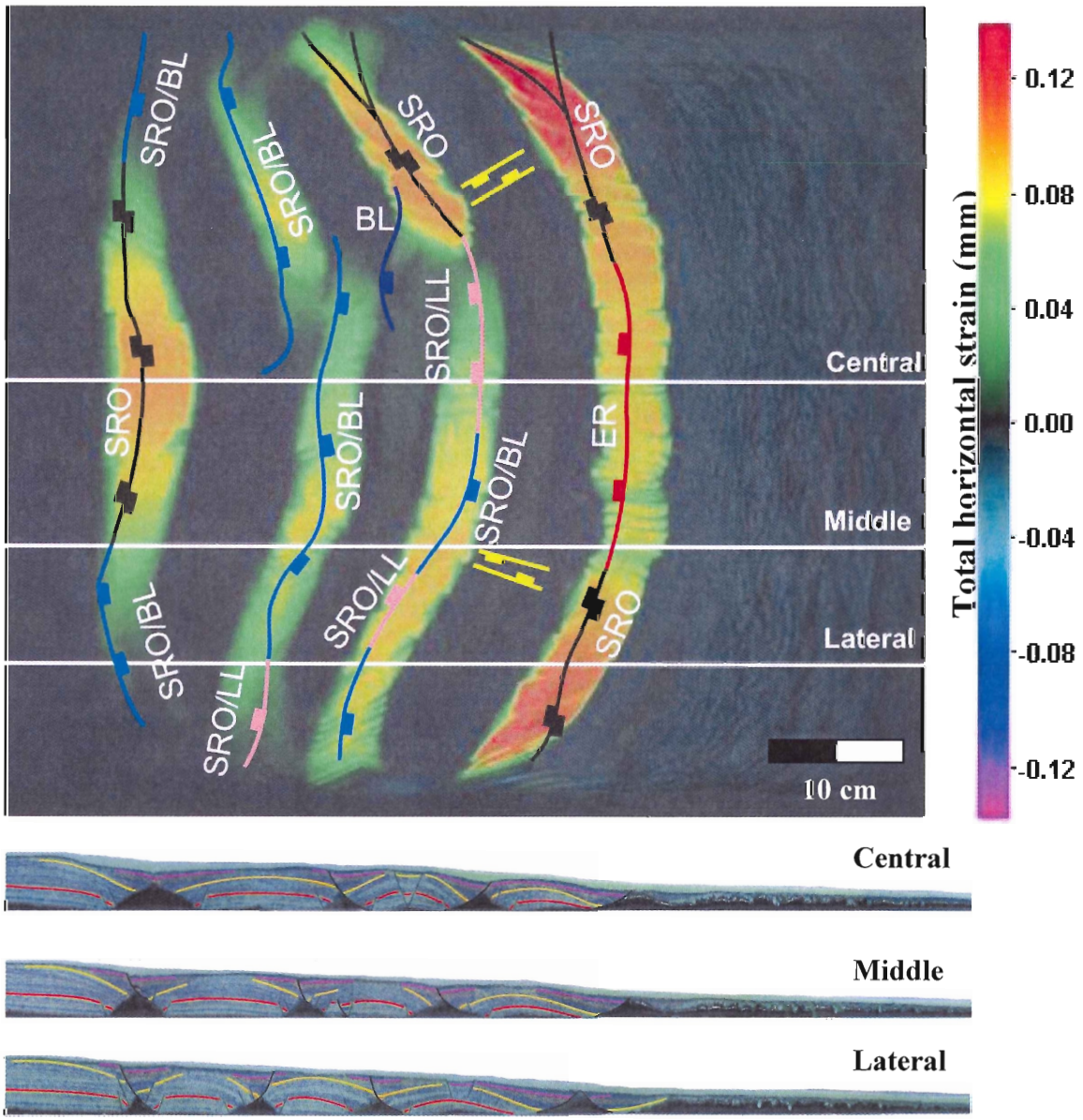

Figure 3.5 Surface image of experiment using incremental displacement vector data and derived total horizontal stain (exx) to visualize development of symmetric rollover systems (SRO), basinward listric faulting (BL) and expulsion rollovers (ER). Interpreted cross-sections overlying surface data show how structures look at subsurface (Krezsek et al. 2006).

3.5.3 Sedimentation Procedure in Experiments

In all experiments, sedimentation is simulated by sieving silica sand with specific material parameters and a given sieving procedure. The sand is sieved on experiments with plastic cups while a guide is in place to ensure the equal distribution for increment sedimentation layers with 0.25 cm thickness. To simulate sediment delivery by rivers from the coast (in nature), areas in the landward part of the model including structural lows are always filled first before sedimentation progradates into the deeper basin (Figure 3.6).

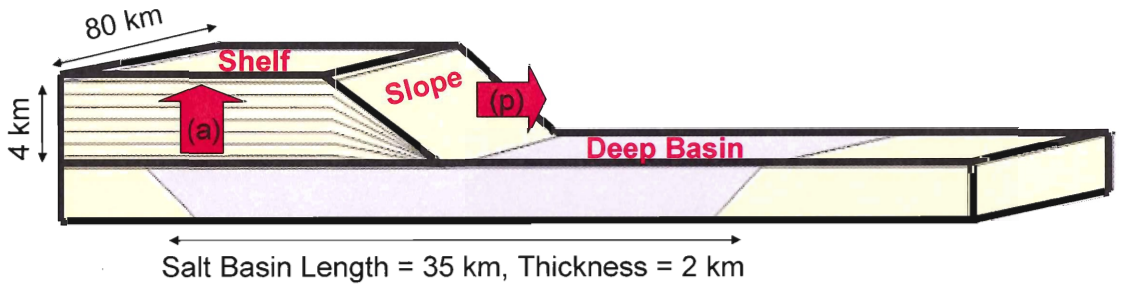

Figure 3.6 Sedimentation pattern implemented for experiments based on the depositional history of the Scotian Basin divided into aggradation (a) during the initial shelf build-up and late progradation (p) once the shelf is build-up to 4 km is reached.

For the first setup of the small-scale, pilot experiments, 250 g of sand is sieved onto the models in 2 hour intervals as 0.25 cm thick layers. The thickness was calculated from described cores from the Scotian Basin scaled to the model and the mass was calculated was based on the thickness and area over which sand is sieved and density of sand. Sedimentation is focused close to shelf on the experiments to match sedimentation patterns of the Scotian Basin. Once the aggradation of the landward shelf area reaches a height of 4 cm (base level of margin), sediment progradation begins with a new constant sieving rate of 175 g every 2 hours. This number is again based on rates observed from described cores.

For the large-scaled experiments, 800 g of sediments, which changed to 700 g for later experiments, is sieved at 4 hour intervals to simulate the sedimentation rate of the Scotian Margin, which experiences relatively low sedimentation. Like the small-scaled experiments, the amount of sand was calculated based on area over which sand is sieved and density of the sand.

3.5.4 Sectioning

Upon completion of each experiment, the model is covered with sand and sprayed with water to seal the system and essentially freeze it from further movement. The experiments are cut into cross sections at 1.25 to 2.5 cm spacing for the pilot experiments and at 5 cm spacing for the large scaled experiments. The cross sections are cut from shelf to slope of each experiment (Figure3.7). Each section is photographed using a high resolution, digital camera and cross sections are structurally interpreted and restored using balancing techniques.

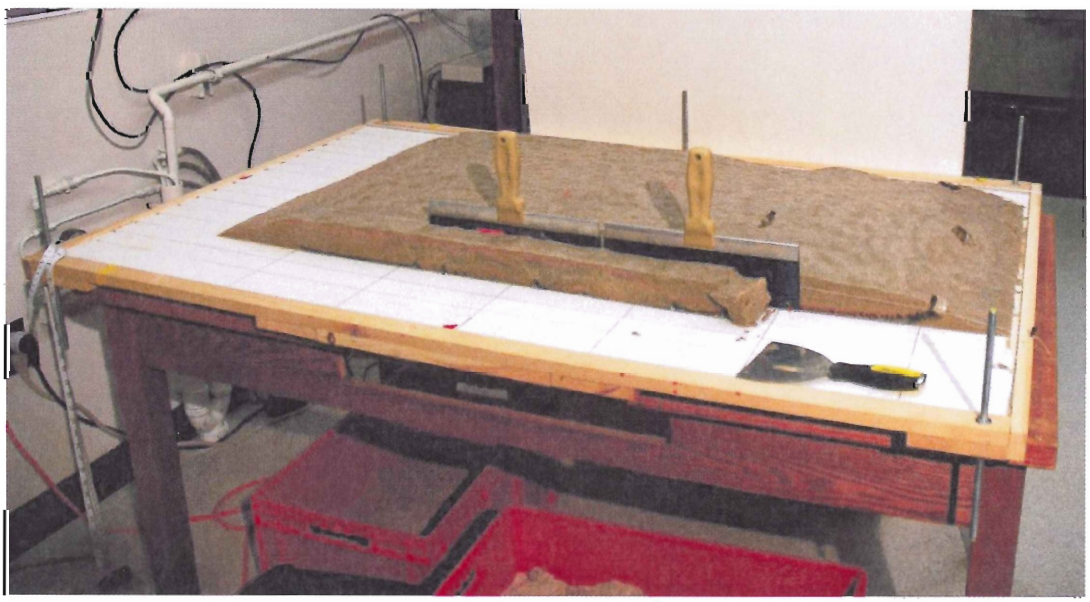

Figure 3.7 The sectioning of a large scaled experiment in order to acquire cross-section images of the completed experiment.

CHAPTER 4: RESULTS

4.1 Experiment Overview

The early stage evolution in each of the experiments began with the initiation of a basinward dipping growth fault (BGF) in the landward area of the basin that continued until the hanging wall block welded to the basement floor (Fig. 4.1). Buckle folding also occurred in all the experiments in the basinward area of the salt basin as shortening and thickening took place while silicone was being pushed basinward from the deforming sediment wedge. In both the half graben wedge and half graben step experiments, there were expulsion rollovers (ER) with associated reactive diapirs (D) that became passive diapirs (PD) with overhangs during sedimentation breaks (Fig. 4.1).

The mid-stage evolution occurred in all experiments as sediments began to weld to the basement floor. The mid-stage evolution of each of the experiments differed slightly between the symmetric graben and half graben experiments. Salt advancement into the allochthonous system began earlier in the symmetric graben experiments. Structures observed in some experiments were the presence of the passive diapirs that experienced multiple landward and basinward oriented overhangs at different times as overburden deformation took place (PD; "Christmas tree shape" diapirs). Rafted blocks, which are caused by fault blocks that become completely separated from their associated package as silicone occupies the space were also common in some of the experiments. These blocks welded to the basement and later welded with younger strata as salt moved out of the system (D; Figure 4.1).

In the late stage of all experiments, defined by major evacuation of the silicone into the allochthon, basinward allochthonous salt sheets climbed up the basin strata over

time and moved like a glacier. Structures associated with the allochthonous silicone ranged from a simple tongue with no sediment deposition on top of the tongue (Symmetric Graben; Figure 4.1), to a large nappe with listric growth faulting occurring in the sediments which were progradated over the nappe as silicone moved basinward (Half Graben Wedge; Figure 4.1). The rate and extent of silicone movement in the allochthonous regions ranged in the experiments. Experiment 5-5 and Experiment 5-6 show a steady outflow of silicone into the allochthous zones with the greatest extent. Experiment 5-2 and Experiment 5-5 show less silicone flowing into the allochthonous zones. In the half graben experiments, an allochthonous nappe formation started as sediments progradated over the mid basin silicone inflation. This occurred quickly in the Half Graben Wedge experiment as evidenced by the listric growth faulting occurring in the sediments (Half Graben Wedge; Fig. 4.1) and slower in the Half Graben Step experiment as evidenced by the subsided raft and diapirs (Half Graben Step; Fig. 4.1).

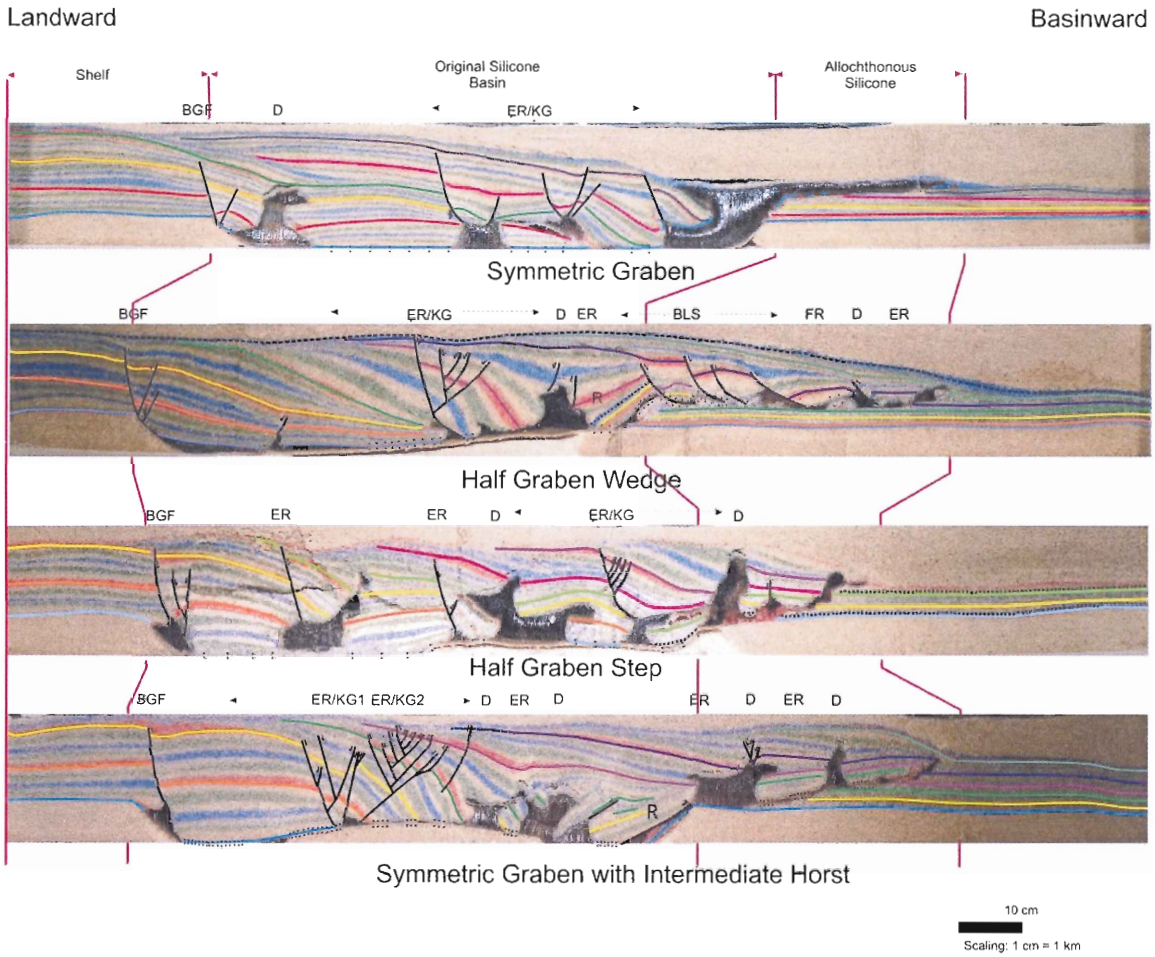

Figure 4.1. Overview of the center sections from the pilot experiments. All experiments are labelled with main structures including diapirs (D), basinward dipping growth faults (BGF), keystone grabens (KG), and expulsion rollovers (ER) as well as shelf, original silicone basin (autochthon) and extent of allochthonous silicone nappes.

4.2 Pilot Experiment Interpretations

Upon completion of the experiments, interpretations of the sectioned experiments were completed by my colleague Cody MacDonald and me for our Honours Projects (Table 4.1). These interpretations were then used by both of us for our respected topics. Interpretations were done with standard graphical software packages to analyze the structural evolution of the experiments. The experiments all represented possible basement configurations that may have occurred in the Abenaki and Sable Subbasins in

the Scotian Margin. All other variables throughout the experiments, including sedimentation rates, basin width, length and thickness were kept the same.

Experiment	Setup	Basin Geometry	Interpreter
5 - 1	Full Graben	Full Graben; 35 cm length. 2 cm of salt	Training
5 - 2	Full Graben	Full Graben; 35 cm length. 2 cm of salt	Clarke Campbell
5 - 3	Wedge	Half Graben Wedge; 35 length. 2 cm of salt	Cody MacDonald
5 - 4	Compressional Reactivational/ Tilt	Full Silicon Basement; 1 cm of salt	Test
5 - 5	Basement Steps	Half Graben Steps; 35 cm length. 2 cm of salt with no step. 1 cm of salt with step	Clarke Campbell
5 - 6	Intermediate Horst	Full Graben with Intermediate Horst; 35 cm length. 2 cm of salt with no horst. 1 cm of salt with horst	Cody MacDonald
5 - 7	Full Graben	Full Graben; 60 cm length. 2 cm salt	TBA
5 - 8	Wedge	Half Graben Wedge; 60 length. 2 cm of salt	TBA
5 - 9	Basement Steps	Half Graben Steps; 60 cm length. 2 cm of salt with no step. 1 cm of salt with step	TBA

Table 4.1. List of experiments and interpreters.

4.2.1 Allochthonous System for Experiment 5-2

Represented by a symmetric graben basement morphology, Exp_5-2 exhibited a very unique allochthonous system compared to the other experiments (Appendix 1). This experiment succeeded in efficiently evacuating salt out of the autochthonous initial salt basin (Figure 4.2). Sediments sieved early on the experiment subsided vertically with little translation along the basinward growth normal fault (BGF; Figure 4.2) and initiated salt mobilization which moved the salt into the basinward area of the salt basin causing buckle folding and inflation of the salt. Since downbuilding was the main mechanism for salt mobilization, only minor extensional structures occurred in the forms of keystone grabens (KG; Figure 4.2) associated with expulsion rollovers (ER; Figure 4.2) that formed as silicone evacuated out of the basin.

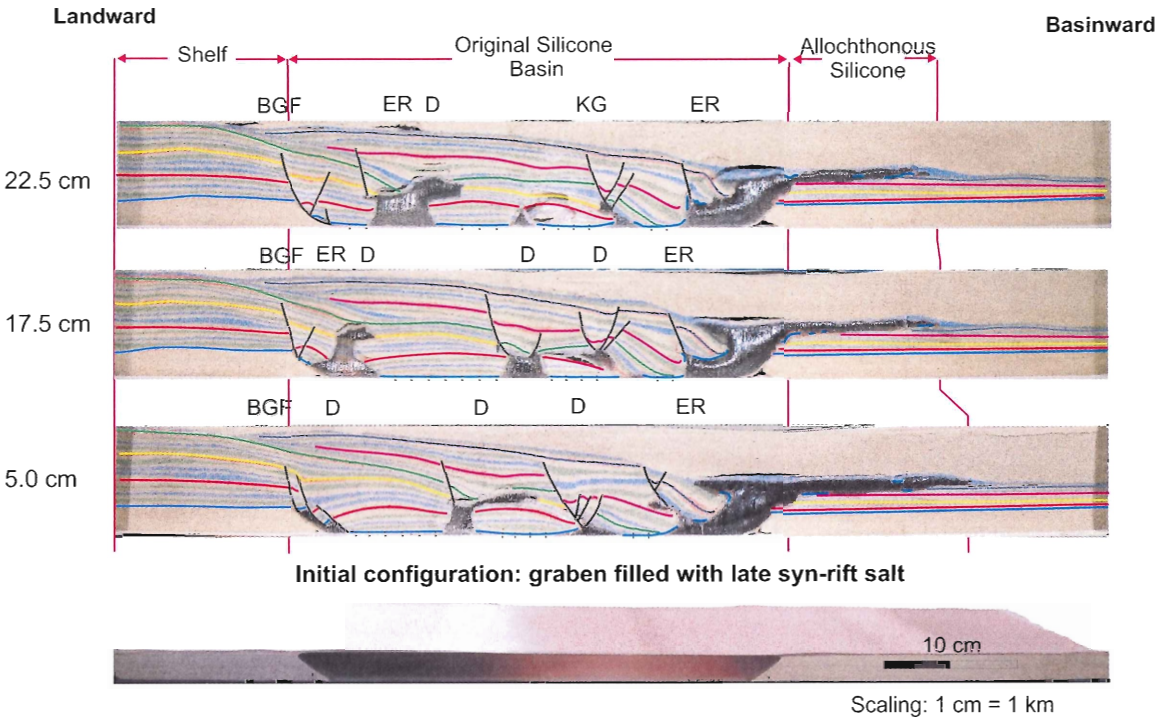

Figure 4.2 Cross-sections of the completed symmetric graben experiment (Exp_5-2) showing main structures including basinward dipping growth faults (BGF), keystone grabens (KG), expulsion rollovers (ER), diapirs (D) and extent of allochthonous tongue system.

As progradation occurred, the allochthonous system for this experiment evolved as a large salt tongue system (Figure 4.3). The steady evacuation of silicone out of the initial silicone basin allowed for continuous accommodation space to be created and a constant depocenter within the initial salt basin. With no sediments able to make it on top of the allochthonous system, the large tongue flowed like a glacier towards the basinward direction of the experiment about 15 km in the late stage (15 cm in the experiment).

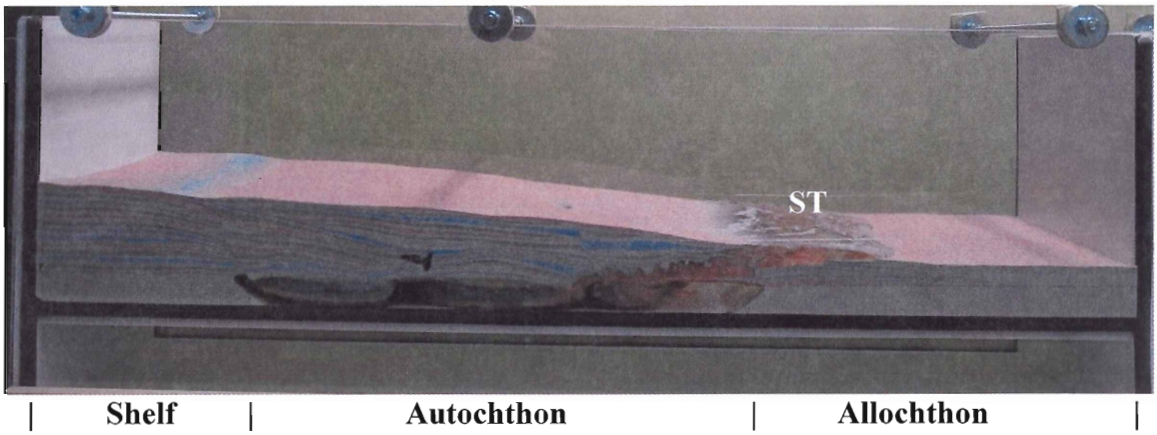

Figure 4.3. Oblique angle view of Experiment 5-2 showing the large silicone tongue (ST) extruding into the allochthonous zone. Length of tank is 80 cm.

4.2.2 Allochthonous System for Experiment 5-3

Represented by a half graben wedge morphology, Exp_5-3 showed an allochthonous silicone system that evolved in the late stages, but when extruded into the allochthonous zone, moved very quickly outboard (Figure 4.4). The half graben wedge morphology, which despite having no pronounced buttress at the basinward limit to hinder salt flow, evolved into the allochthonous zone latter than the symmetric graben setup. A basinward dipping growth fault (BGF) occurred at the landward limit of the basin which initiated downbuilding of sediments overlying the silicone. Thinning of the silicone layer caused basinward folding and inflation in the mid-basin area resulting in the large passive diapir viewed in the cross sections (D; Figure 4.5).

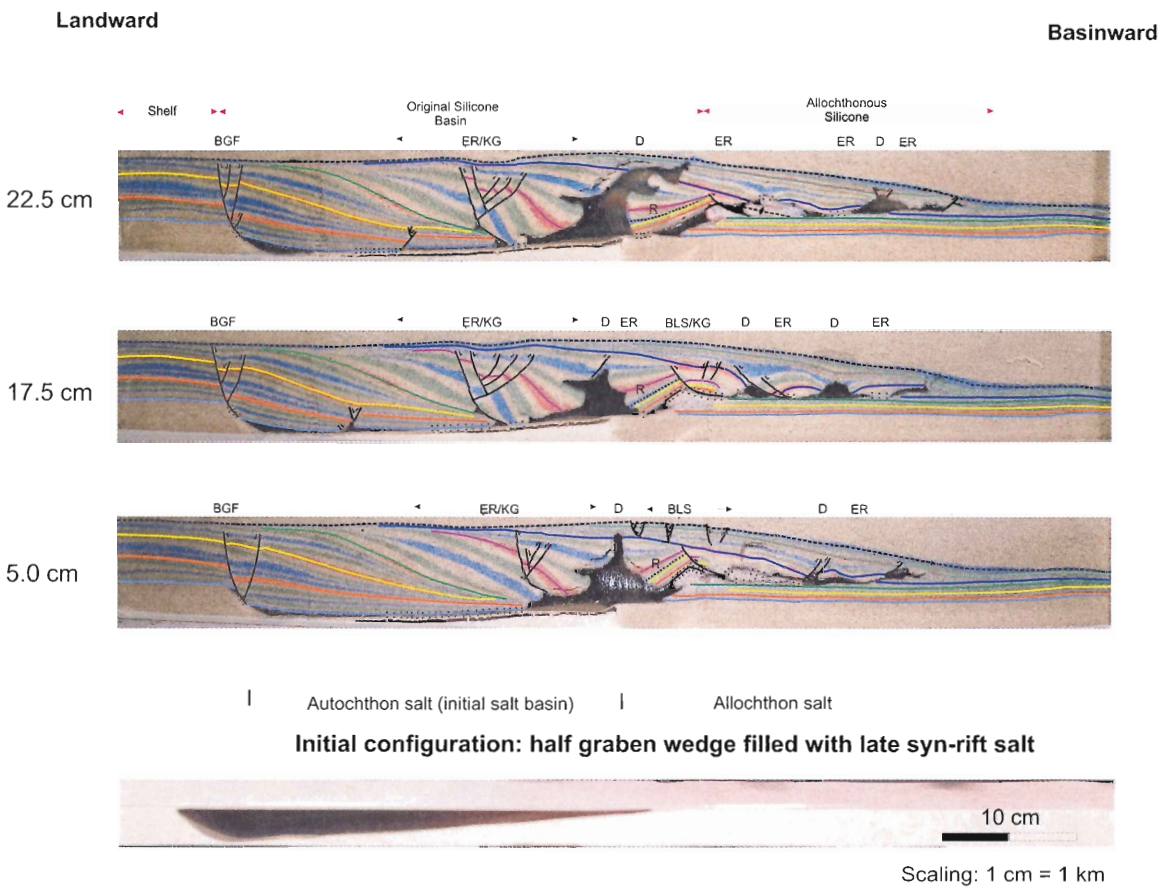

Figure 4.4 Cross-sections of the completed half graben wedge experiment (Exp_5-3) showing main structures and extent of allochthonous nappe system.

Progradation of sediments in the later stage caused formation of symmetrical expulsion rollovers and extrusion of silicone as an allochthonous silicone nappe (N; Figure 4.5). The silicone moved quickly into the allochthonous system and the overburden deformed as basinward listric growth faulting (BLS) occurred in the overburden sediments to keep up with the fast moving silicone. This silicone extruded outward approximately 24 km (24 cm in experiment) despite having half the silicone basin volume as the symmetric graben Exp_5-2.

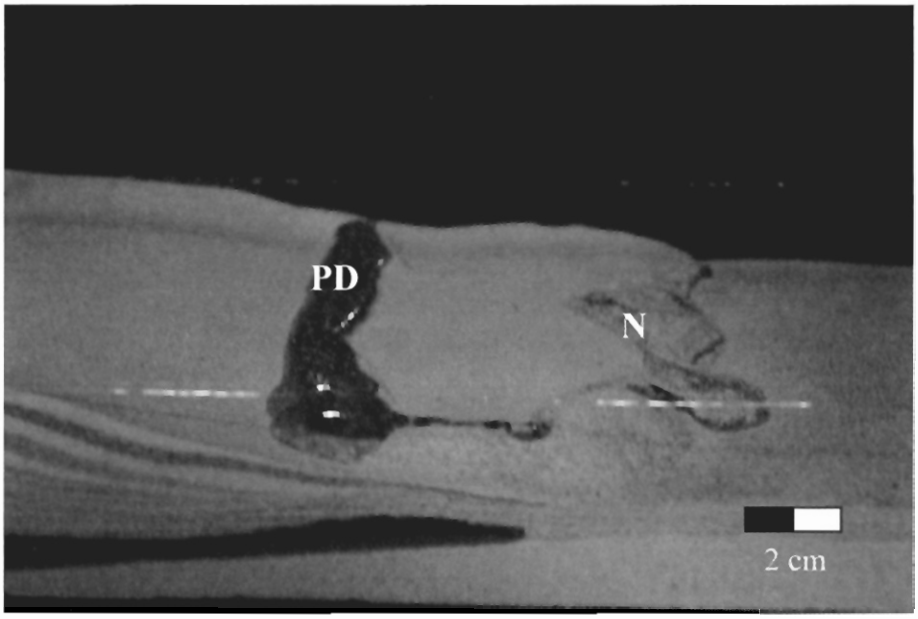

Figure 4.5 Passive diaper (PD) and a silicone nappe (N) in the allochthonous zone after 150 hours. Basinward is left in image.

4.2.3 Allochthonous System for Experiment 5-5

Exp_5-5 represented a half graben with basement step. Deformation began in the shallow basin with basinward growth faulting (Figure 4.6). Compressional buckle folding and inflation began above the step and then migrated further basinward as the silicone flowed out of the initial salt basin into the allochthonous nappe. Due to the buttress created by the basement step, much of the silicone was accumulated in this position in the early stage of the experiment evolution.

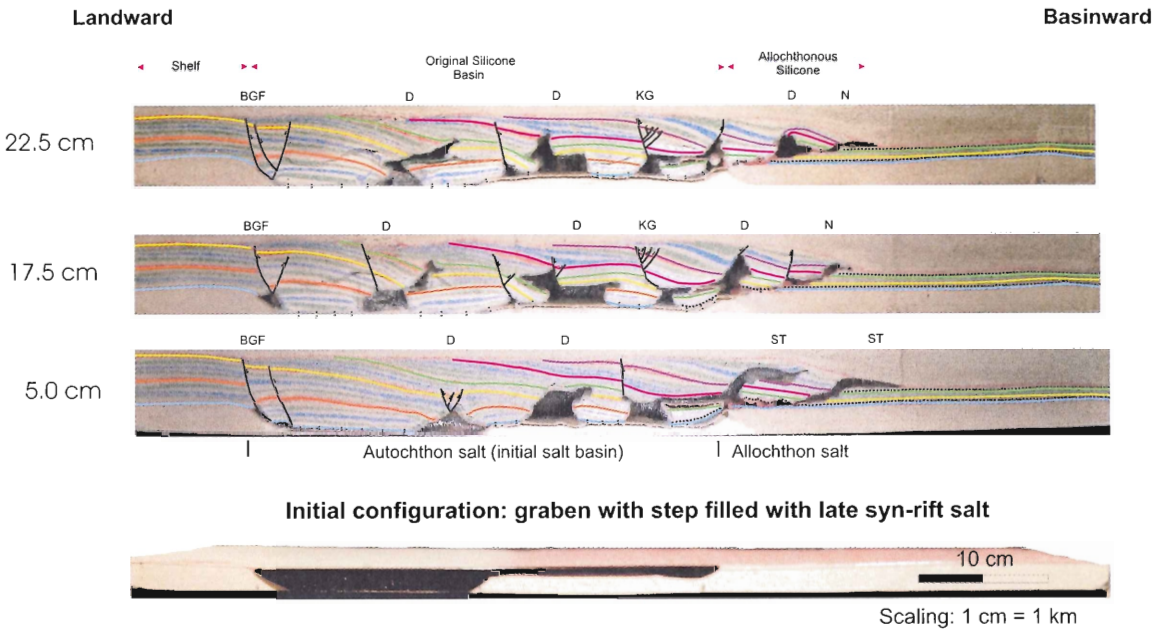

Figure 4.6 Cross-sections of the completed half graben with step experiment (Exp_5-5) showing main structures and extent of allochthonous nappe system.

The progradation of sediments over the inflated salt lead to the silicone being overrun and trapped in the autochthonous basin and less silicone was left to advance into the allochthonous system (Figure 4.6). The silicone that advanced into the allochthonous zone, created an allochthonous nappe system (N; Figure 4.7) that extended about 10 km (10 cm in experiment) outboard. As sediments prograded on top of the allochthonous silicone, downbuilding of the sediments created mini basins that passively moved on top of the silicone until their base welded out.

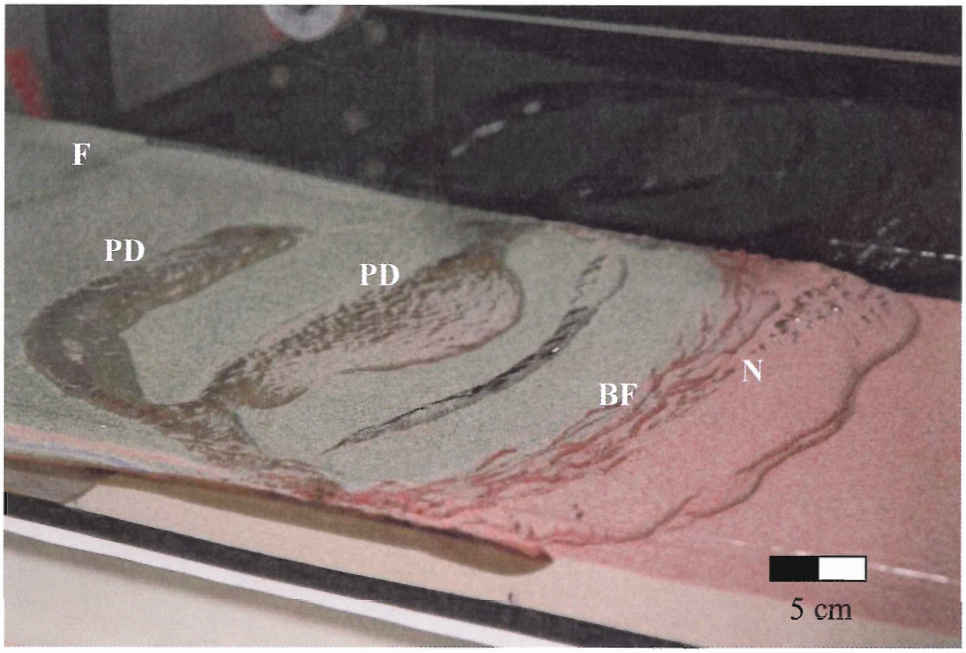

Figure 4.7 Detailed Image of Experiment 5-5 (70 hours) showing faulting to the left, passive diapirs (PD) with basinward (right is basinward) moving overhangs and buckle folding (BF) and a silicone nappe (N) in the deep basin.

4.2.4 Allochthonous System for Experiment 5-6

Exp_5-6 represented a symmetric graben with intermediate horst structure in the center of the syn-rift salt basin (Figure 4.8). Like Exp_5-5, the landward step created by the horst structure, created a buttress which slowed silicone from moving in the basin and trapped much of the silicone within the autochthonous zone. Silicone that was able to flow over the horst quickly extruded into the second sub basin as an expulsion rollover evacuated the salt (ER; Figure 4.8). In mid stage, the salt inflated in the second basin and began to move into the allochthonous zone as a nappe with a 30 km extent (30 cm in experiment).

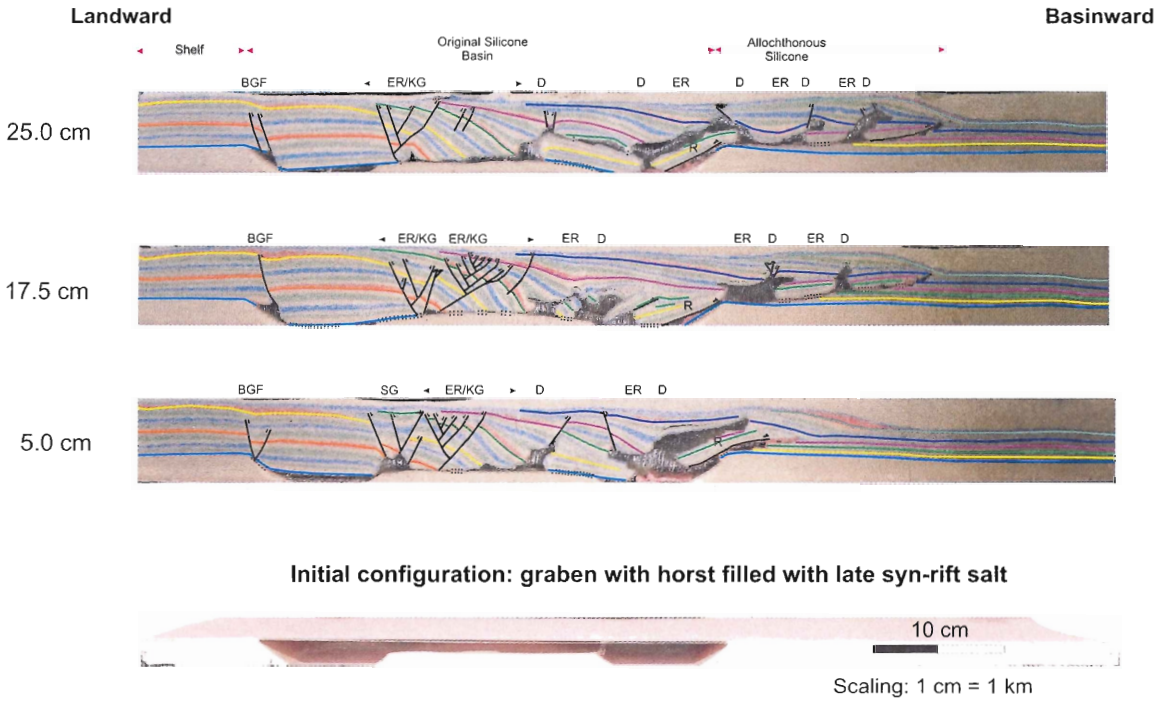

Figure 4.8 Cross-sections of the completed symmetric graben with intermediate horst experiment (Exp_5-6) showing main structures and extent of allochthonous nappe system.

As sediment progradation started (72 hours), a large nappe system developed with a thick silicone sheet moved basinward while downbuilding of sediments over the silicone occurred (Figure 4.9). The salt nappe system extended 14 km (14 cm in the experiment). As with Exp_5-5, a mini basin occurred as sediments descended evacuating silicone (Figure 4.8).

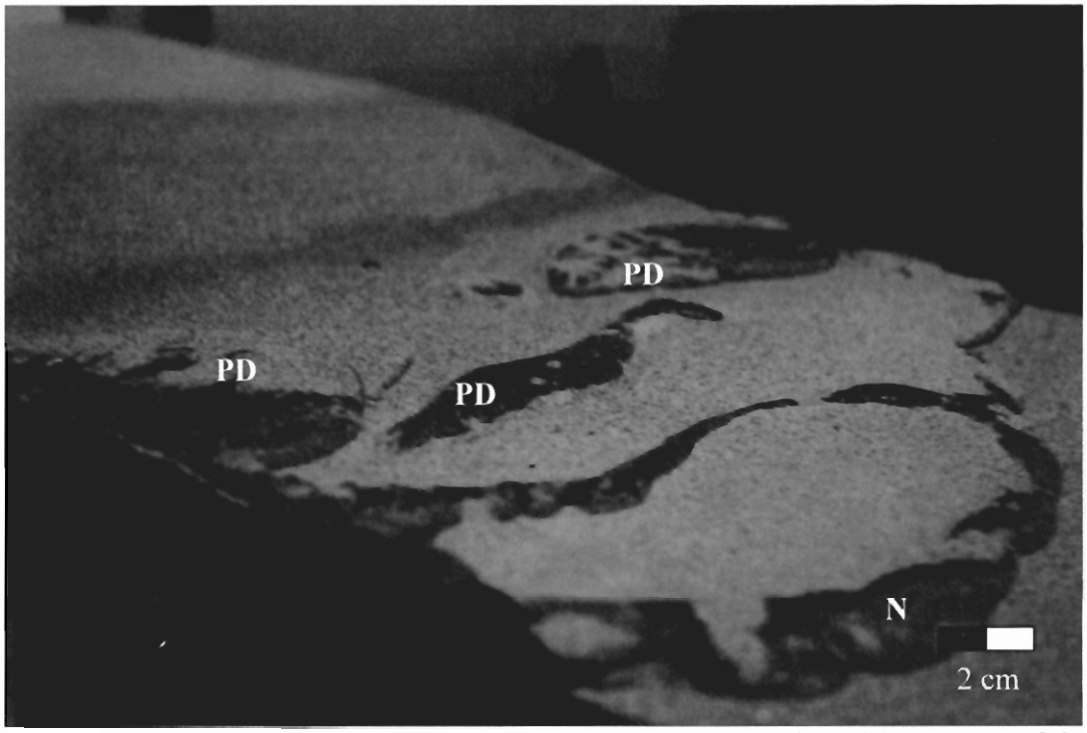

Figure 4.9. Allochthonous silicone nappe (N) with sediment deposition on top of the sheet and passive diapirs (PD).

4.3 Large-scaled Experiment Interpretations

After completion of the pilot experiments, a series of large-scale experiments were completed using PIV strain monitoring. These experiments repeated the same rift basin configurations as the pilot experiments to gain quantitative strain data to analyse the observed tectonic processes and depositional systems. Once completed, each of these experiments was also sectioned in order to analyze their structural evolutions.

4.3.1 Allochthonous System for Experiment 5-7

Exp_5-7 represented a symmetric graben basement morphology, similar to the pilot experiment 5-2. As in Exp_5-2, the early evolution of the silicone basin began with downbuilding of landward deposited sediments creating buckle folding and inflation

of silicone in the deep basin leading to evacuation of silicone into the allochthonous region. Since downbulding was the main mechanism for silicone mobilization, only minor amounts of extension occurred evidenced by the keystone grabens (KG; Figure 4.10) and expulsion rollovers (ER; Figure 4.10) that formed as silicone evacuated out of the initial silicone basin. Unlike Exp 5-2, progradation of sediments continued in the basin to the point most silicone was evacuated out of the depositional basin and continued as the allochthonous nappe system developed. The nappe system advanced as prograding sediments were deposited on top of the nappe generating several downbuilding basins. This experiment succeeded in efficiently evacuating silicone out of the autochthonous initial salt basin (Figure 4.2).

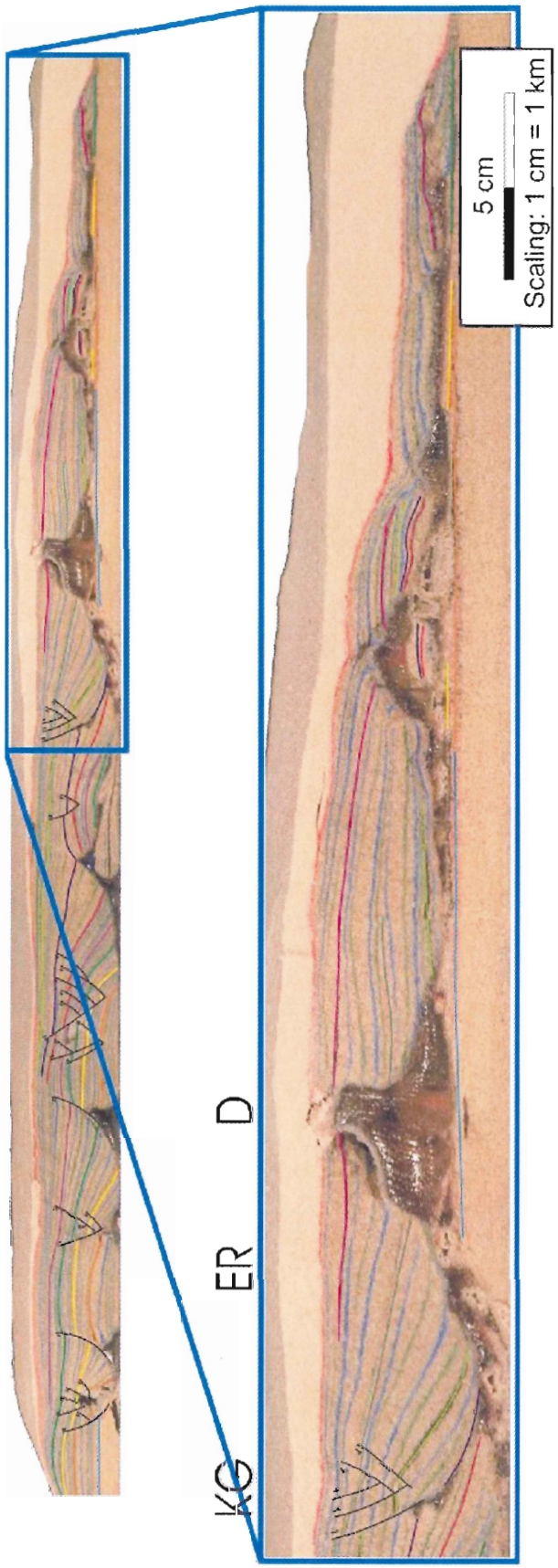

Figure 4.10 Center section from completed large scale symmetric graben experiment (Exp_5-7) showing main structures and extent of all allochthonous salt nappe system.

4.4 Pilot Experiment Restorations

To better understand the evolution of the experiments, structural restorations were completed for center sections of all experiments. This was done by using the relatively undeformed sediments near the glass of the wall of the experiment tank as a regional reference horizon (depositional level of strata before deformation) to correlate how much structural deformation and subsidence took place in the center sections of the experiment. Red horizons were used as markers on every eighth sieve and were used as key marker horizons. The experiments were reconstructed step by step until the experiment was restored back to the initial stage. Bed lengths and cross section area of sediment layers were kept constant during restoration. For purposes of this thesis, the discussion of restoration results will be that of the allochthonous system although it is important to note the complete evolution.

4.4.1 Restoration of Experiment 5-2

Between the end of the early stage and beginning of the late stage of the experiment (67 hours; Figure 4.11), silicone started to extrude into the allochthonous as a nappe in Exp_5-2 as the landward downbuilding of sediments occured. At this time sediments had begun to weld to the basin floor of the rift basin. This occurred as sediments aggrading on top of the basin had subsided down as salt evacuated out of the shallow basin and inflated in the deep basin to a height of 3 cm (Figure 4.11). A raft block had also broke off the wedge and welded to the base of the basin by this time. After 146 hours, subsidence continued and the tongue had flowed out 7 cm into the allochthonous zone as a silicone tongue (ST).

In the late stage, silicone continued to flow into the allochthonous zone as a large silicone tongue (ST) as the depocenter remained in the mid-basin. By 191 hours, further downbuilding of sediments evacuated the silicone out 10 cm (Figure 4.12). By 240 hours, the continuing downbuilding evacuate the silicone 15 cm into the allochthonous zone (Figure 4.12).

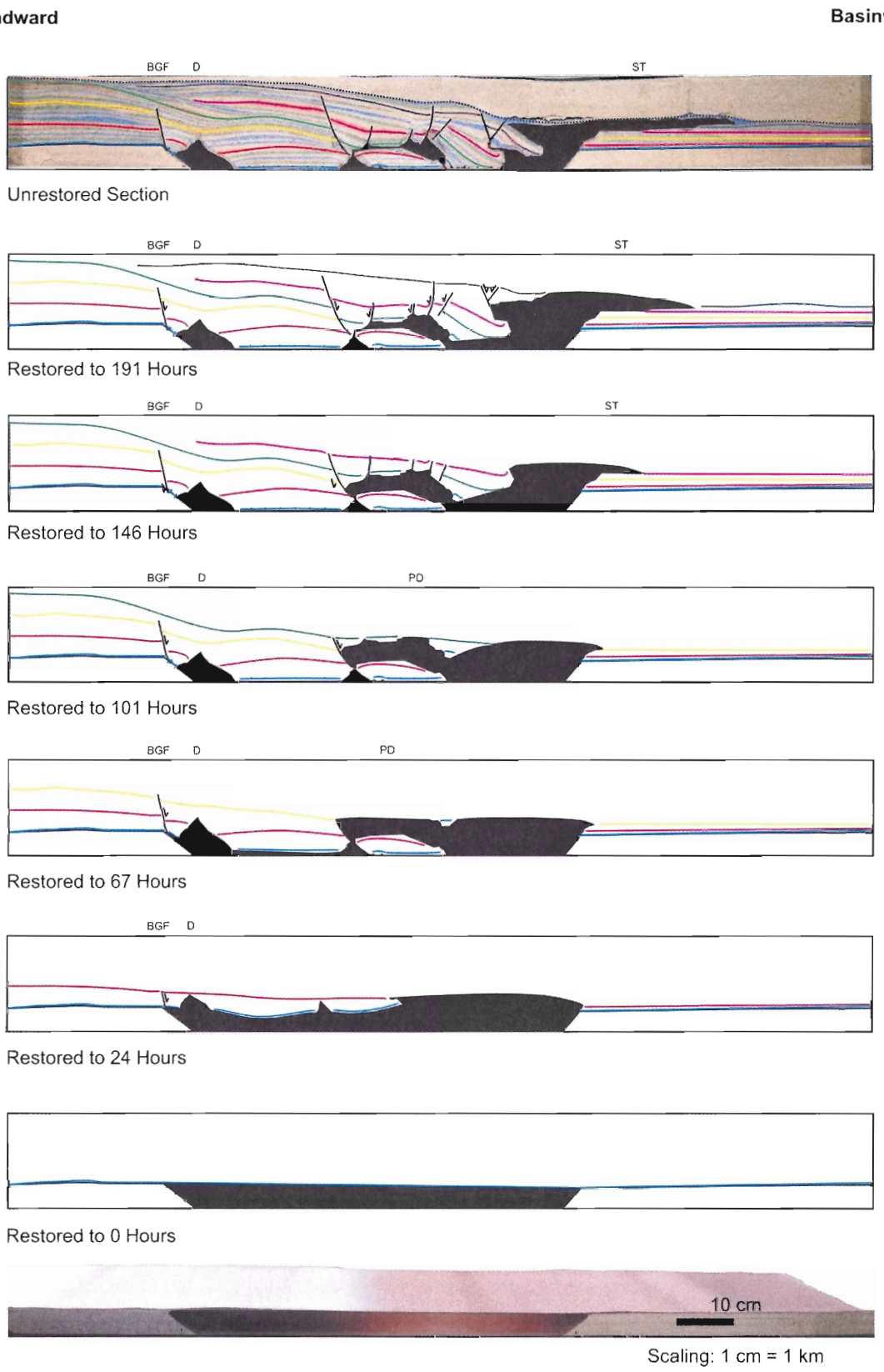

Figure 4.11 Structural restoration of Exp_5-2 showing key structures during its evolution.

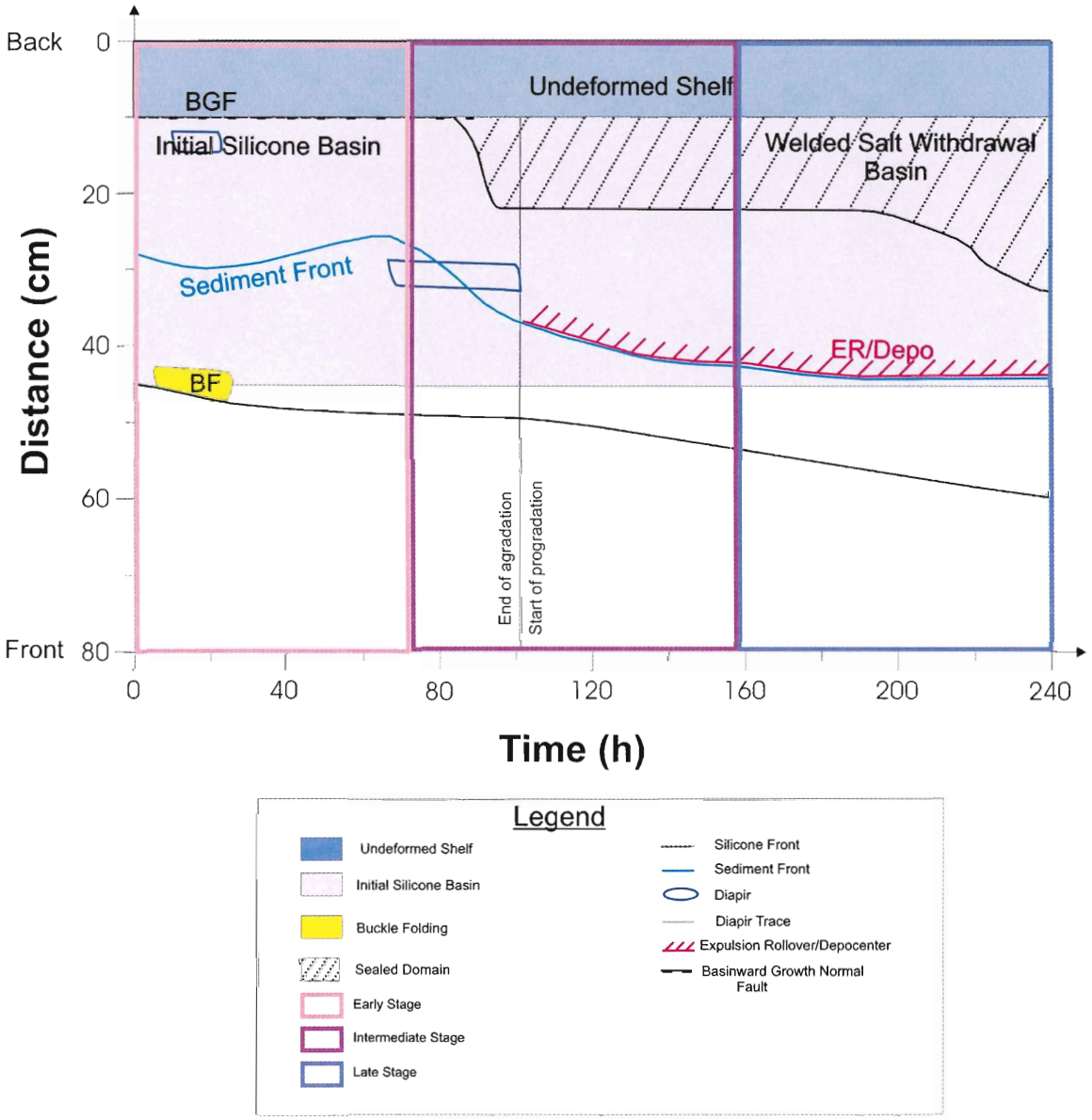

Figure 4.12 Distance vs. Time graph indicating evolution of Exp_5-2 at the center section.

4.4.2 Restoration of Experiment 5-3

In the middle stage of Exp_5-3 (101 hours; Figure 4.13) silicone had begun to be extruded into the allochthonous zone. Before this time in the early stage, basinward dipping growth faulting (BGF) in the landward part of the basin and deformation in the autochthonous zone led to the downbuilding of aggraded sediments which led to subsidence of a thich sediment wedge causing extrusion of salt into the mid basin where silicone inflated to a thickness of 2.5 cm (Figure 4.14). By this time, the silicone nappe had propagated 2 km out of the initial basinward salt basin limit (Figure 4.14). As the raft (R) located in the green layer began to subside at 143 hours, it began to drive silicone out of the system and increased the extent of the salt nappe to 6 km.

In the late stage of the experiment evolution (189 hours; Figure 4.13), the raft had already welded with underlying sediments and a new basinward dipping listric fault (BLS) had formed to further drive the silicone to an extent of 20 km in the allochthonous zone at a rate of 0.2 cm/hr (Figure 4.14). By 218 hours, the silicone had reached a 23 km extent (Figure 4.14) in the allochthonous salt nappe and much of the sediment above the allochthonous silicone forming a weld as silicone evacuated and moved basinward.

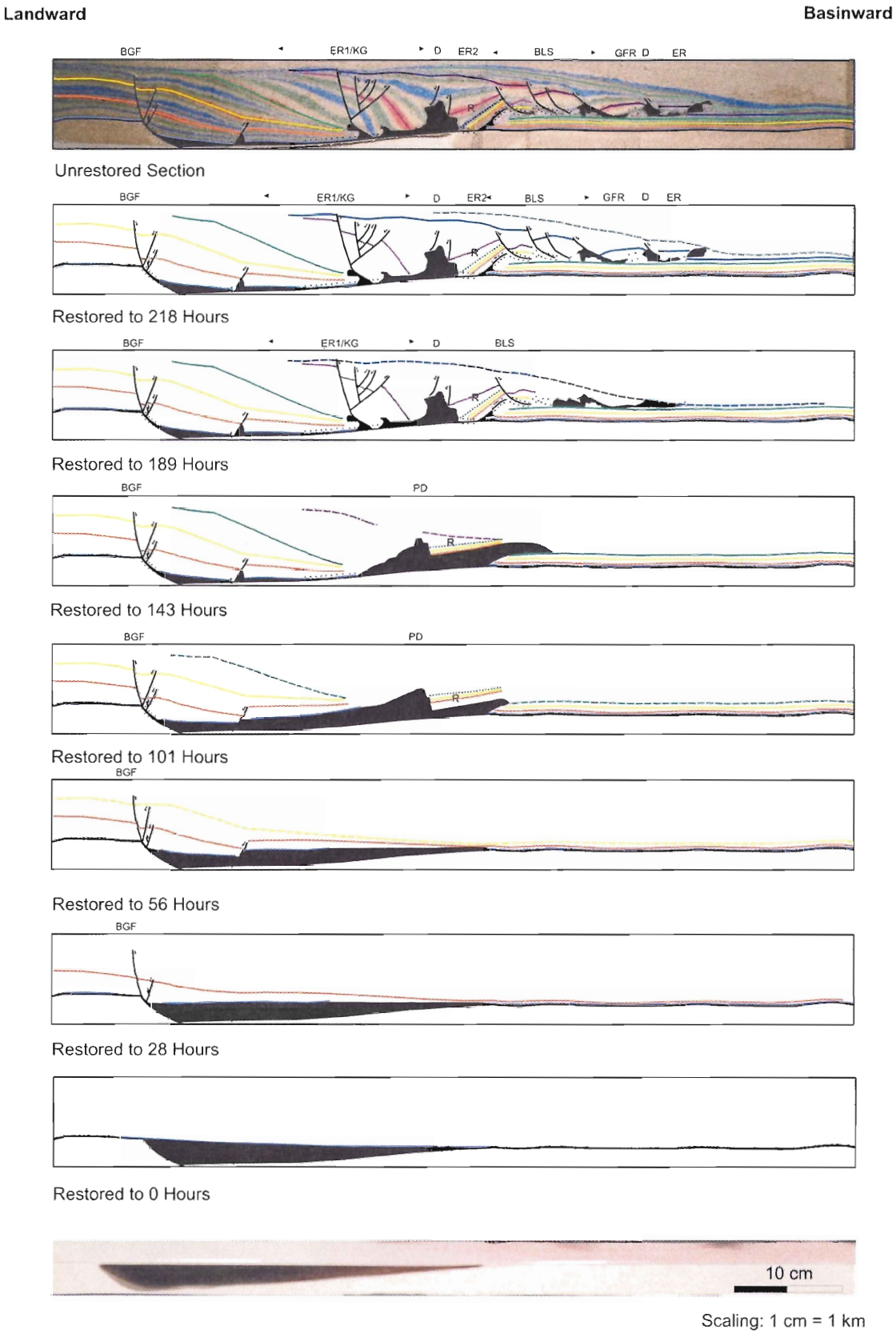

Figure 4.13 Structural restoration of Exp_5-3 showing key structures during its evolution.

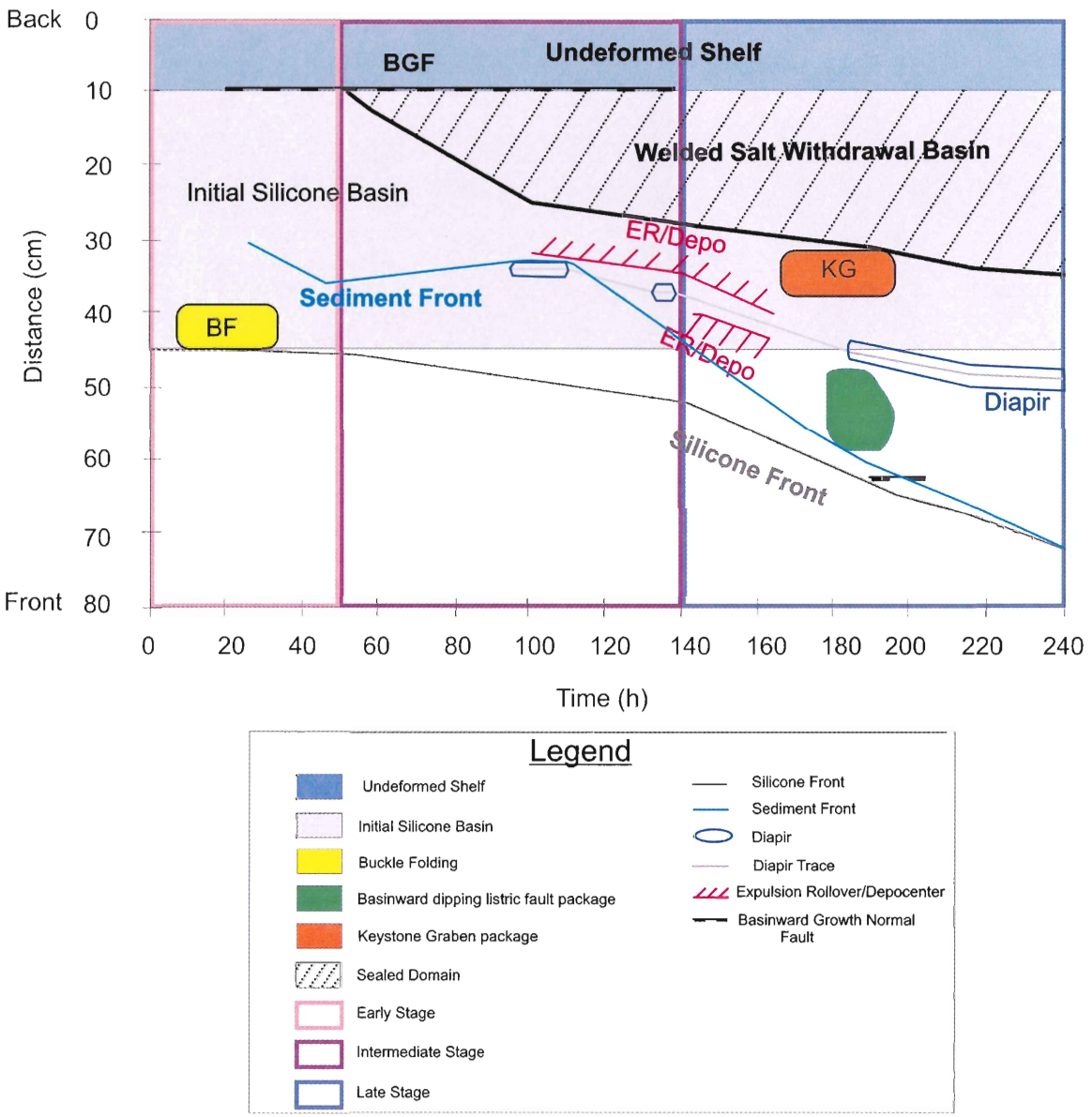

Figure 4.14 Distance vs. Time graph indicating evolution of Exp_5-3 at center section.

4.4.3 Restoration of Experiment 5-5

The beginning of the allochthonous evolution of Exp_5-5 (Figure 4.15) occurred between the end of the early stage and beginning of the mid stage evolution of the basin (72 hours; Figure 4.15). This allochthonous system migrated as a nappe and traveled 5 cm into the allochthonous zone by this time (Figure 4.16). Before this time, the tectonic evolution was limited to the autocthonous zone which included basinward dipping growth (BGF) faulting leading to downbuilding of aggradating sediments at the landward limit of the experiment. At the 28 hour mark, buckle folding and inflation of the silicone above the seaward step of the salt basin (graben) which acted as a buttress to the silicone was occurring. Deformation also included vertical displacement of sediment basins by 28 hours during the early stage (~800 m) and formation of reactive diapirs (D). These diapirs were caused by silicone migrating vertically through differential pressure as space was created by extension and faulting of sediments. Silicone in the landward limit of the basin became sealed due to the thickness of the overburden. Also observed at 28 hours was the beginning of passive diaper overhangs less than 1 km long (PD; Figure 4.15) that were related to sedimentation breaks that occurred in the pilot experiments and correlate with low periods of sedimentation in nature.

In the late stage of the experiment evolution (194 hours; Figure 4.15), the silicone nappe had already traveled 7 cm and continued to flow as a raft block located in the allochthonous zone subsided and evacuated the salt. The process continued until the end of the experiment which saw the block weld to sediments once underlying the silicone. By this time the nappe had traveled 10 cm into the allochthonous region and the passive diaper had risen to a 4 cm height (Figure 4.15).

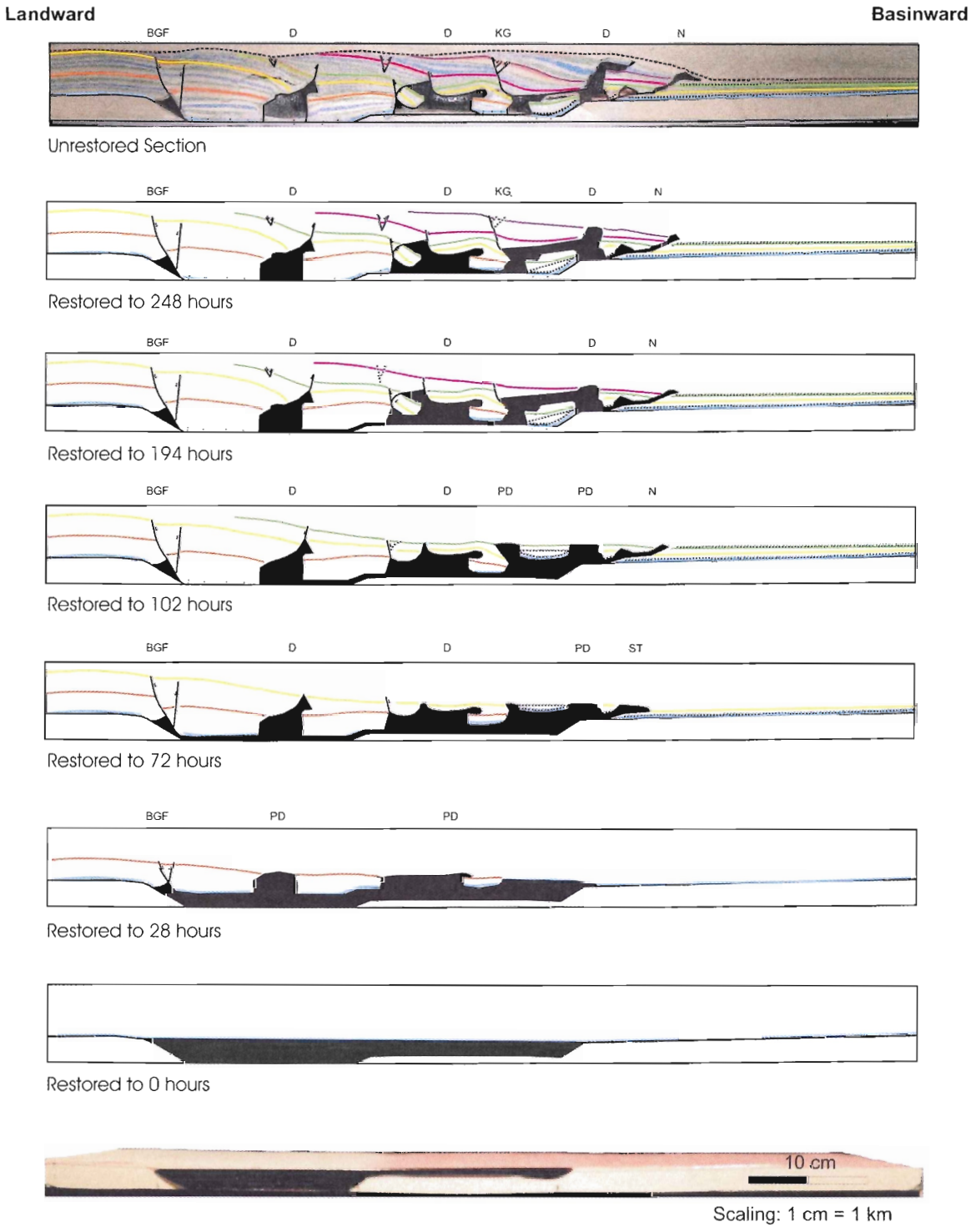

Figure 4.15 Structural restoration of Exp_5-5 showing key structures during its evolution.

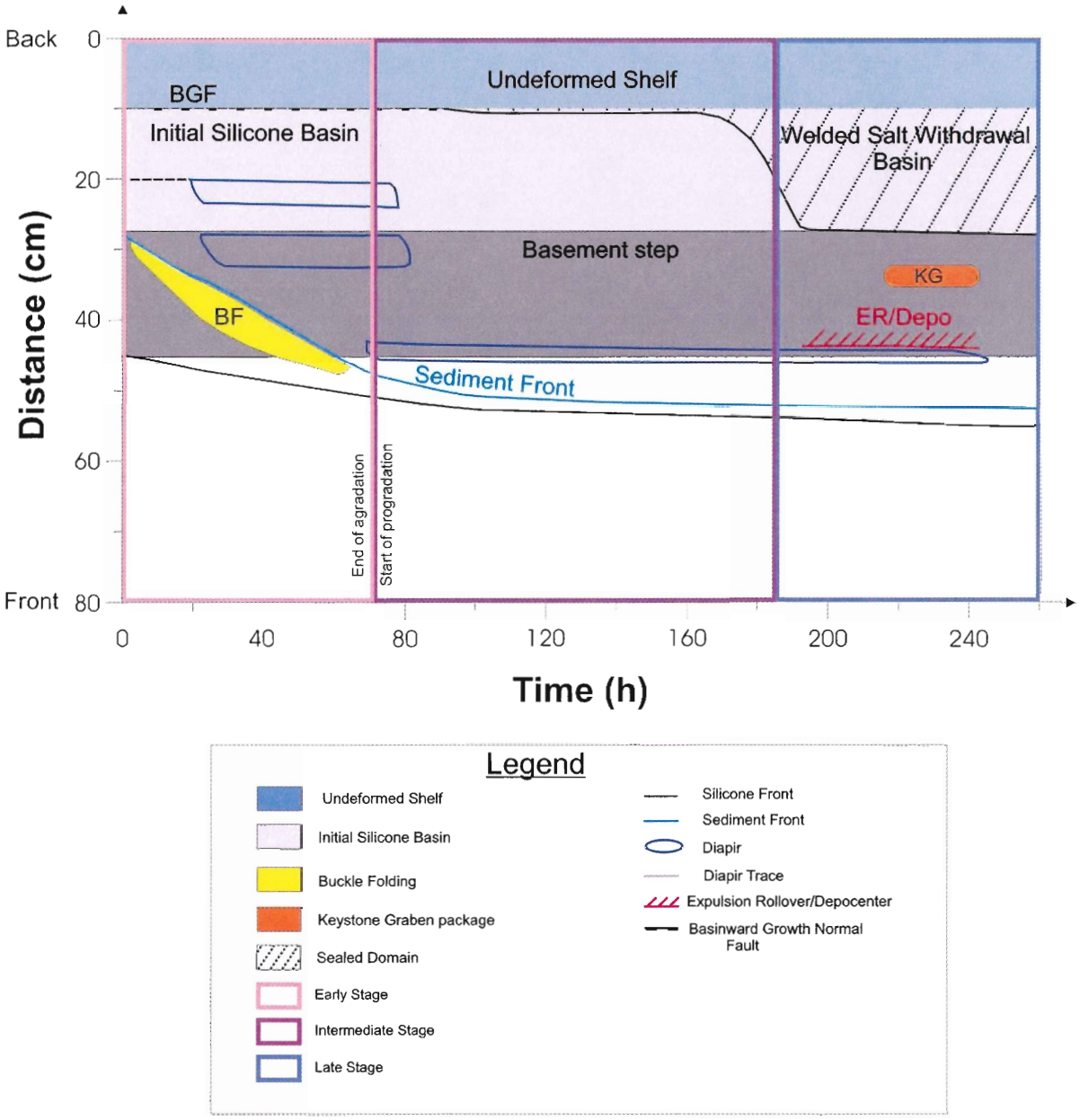

Figure 4.16 Distance vs. Time graph indicating evolution of Exp_5-5 at center section.

4.4.4 Restoration of Experiment 5-6

The development of the allochthonous system for Exp_5-6 began at the transition from the early stage to the mid stage (72 hours; Figure 4.17). Before this time, the tectonic evolution was limited to the autocthonous zone which included basinward dipping growth (BGF) faulting leading to downbuilding of aggradating sediments at the landward limit of the experiment. The intermediate horst served as a obstacle to flow and caused mid basin inflation in early stages. As sediments prograded over the inflated silicone, the silicone was evacuated into the second sub-basin. Expulsion rollovers (ER) continued to evacuate the silicone into the deeper subbasin and caused extensional features in the form of keystone grabens (KG) and rotated fault blocks over the horst. By 102 hours, raft blocks (R) were present as sediments faulted and separated. These rafts subsided and continued to drive silicone into the allochthonous zone to a distance of 7 cm (Figure 4.18).

In the late stage of the experiment evolution (176 hours; 4.17), the allochthonous nappe continued to migrate basinward 7 cm as sediments continued to subside. At this stage, a passive diapir (PD) began to flow basinward creating an overhang to pauses in sedimentation. The allochthonous nappe system continued to migrate 15 cm basinward until the end of the experiment (220 hours; Figure 4.18).

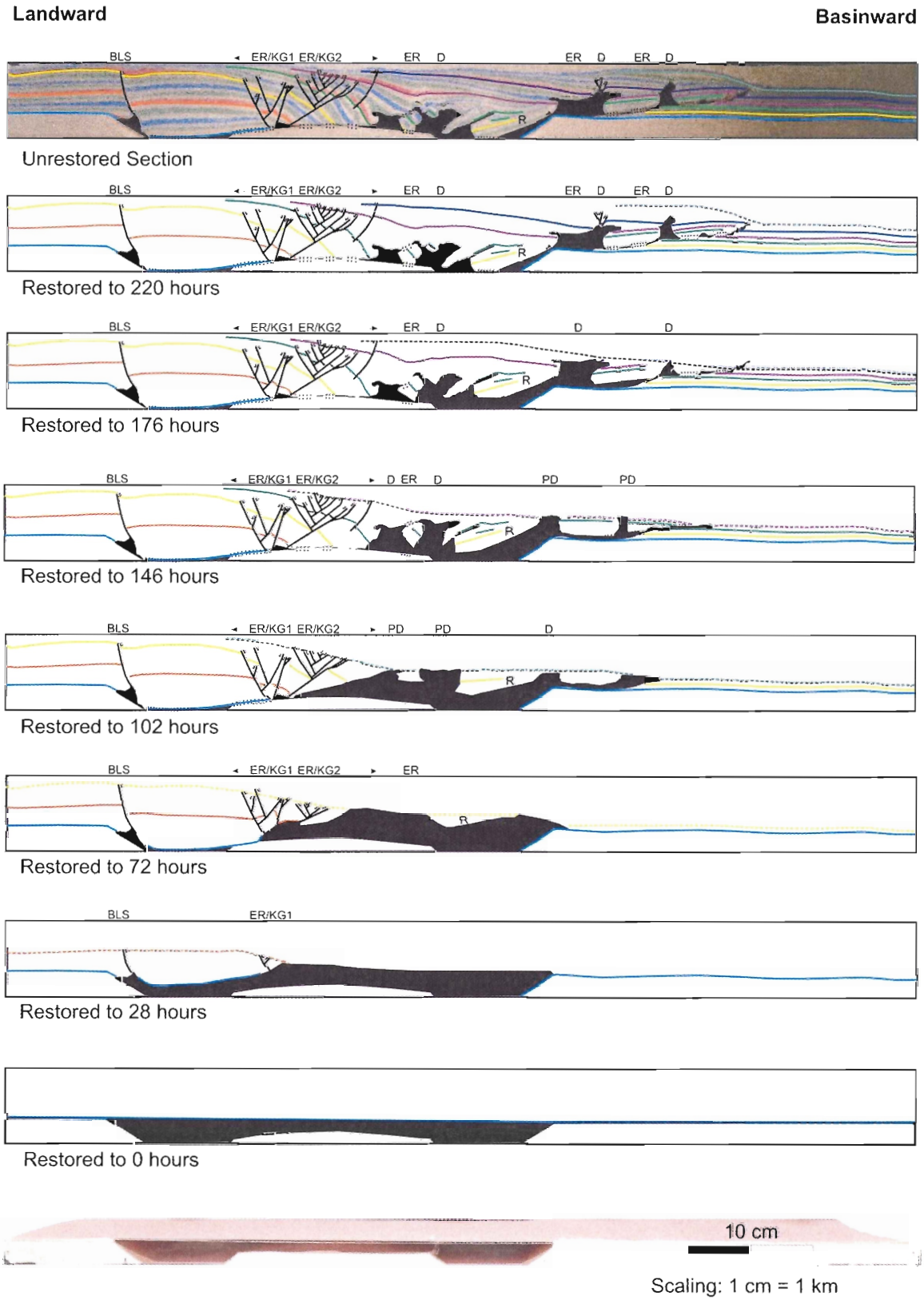

Figure 4.17 Structural restoration of Exp_5-6 showing key structures during its evolution.

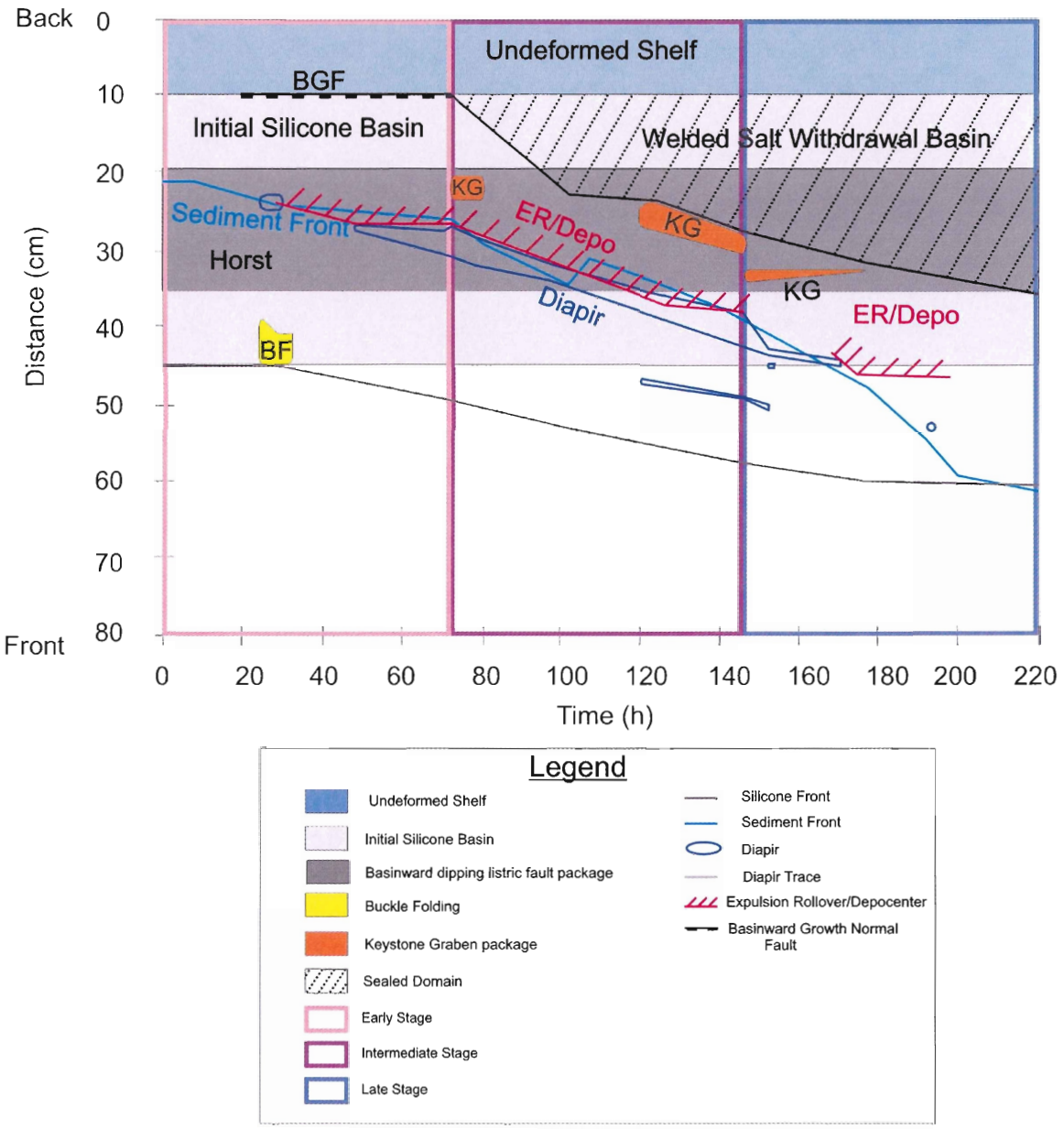

Figure 4.18 Distance vs. Time graph indicating evolution of Exp_5-6 at center section.

CHAPTER 5: CONCLUSIONS AND DISCUSSION

5.1 Conclusions

From the series of analogue experiments (Figure 5.1) an improved understanding could be developed about how the initial salt basin configuration and basement morphology of rift basins affect the early salt mobilization. Also, insight into how basin configuration and basement morphology controls the late evolution of allochthonous salt nappe systems in the deepwater slope, continental passive margins with sedimentation patterns comparable to the Scotian Margin. These concepts include:

1. The dominant mechanism for initial salt mobilization in rift basins with thick salt (≥2 km) is sediment downbuilding causing Poiseuille channel flow.
2. The salt thickness variations controlled by the basement floor morphology, rather than angle and geometry of the basinward rift shoulder, is the controlling factor for early inflation of the basinward autochthonous salt, and later evacuation of salt into the allochthonous canopy or nappe complex.
3. Timing and rate of the allochthonous nappe advancement into the deepwater basin depends on the efficiency of early salt evacuation and progradation of sediments over the inflated autochthonous basinward salt complex.

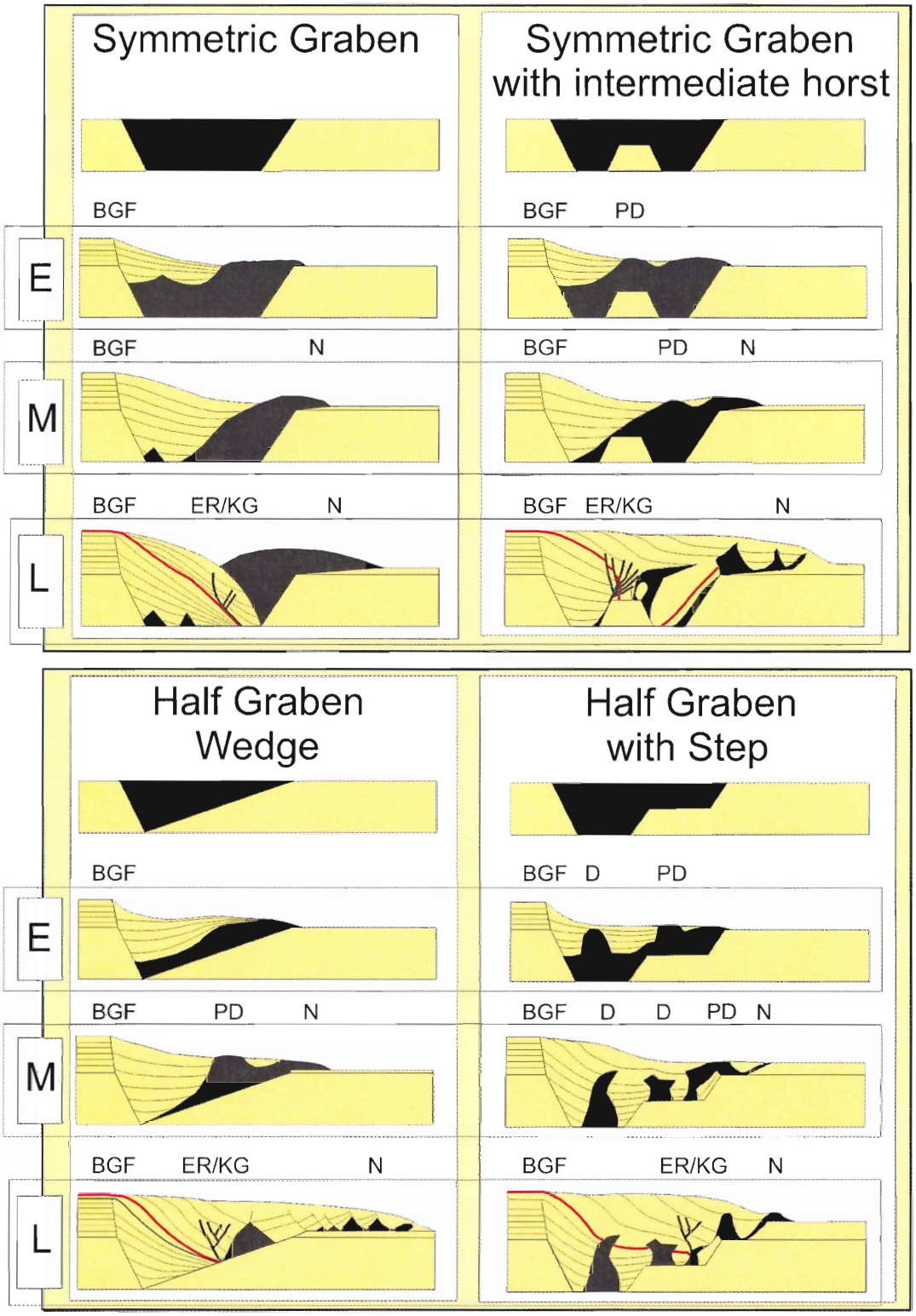

Figure 5.1 Overview of the evolutions of the experiments. E: Early stage, M: Mid stage, L: Late stage. Common structures include basinward dipping growth faults (BGF), expulsion rollovers with associated keystone grabens (ER/KG), passive diapirs (PD), diapirs (D) and nappes (N). The red horizon in late stage depicts the discontinuity created by the transition from aggradation to progradation.

In the landward shelf aggradation stage of each experiment, differential loading caused by the sedimentary wedge results in faulting over the landward border of the salt basin and downbuilding. Early stage evolution (E; Figure 5.1) is caused by early salt mobilization and inflation in the basinward area of the basin. Downbuilding dominates because the thickness of the original salt layer causes Poiseuille channel flow with the highest velocity occurring in the middle of the salt layer. No translation occurred at the base of the sediment overburden. With this overall subsidence, only minor amounts of translation occur as seen by the lack of extensional structures. Progradation begins after sediments have begun to weld to the basin floor in the mid stage (M; Figure 5.1) and expulsion rollover systems push inflated salt into the allochthonous system through channeled flow (Figure 5.2) in the late stage (L; Figure 5.1).

Initial downbuilding of sediments and the position of the basinward inflated salt depends strongly on the configuration of the rift basin. The reason for this dependence is because the various basin floor configurations affect the thickness of the salt and can sequence its flow patterns (Figure 5.2). The experiment results show that in basin areas with thick salt in the basinward area of the salt basin are able to evacuate salt more efficiently into the allochthon nappe, in the presence of a steeper basinward rift shoulder.

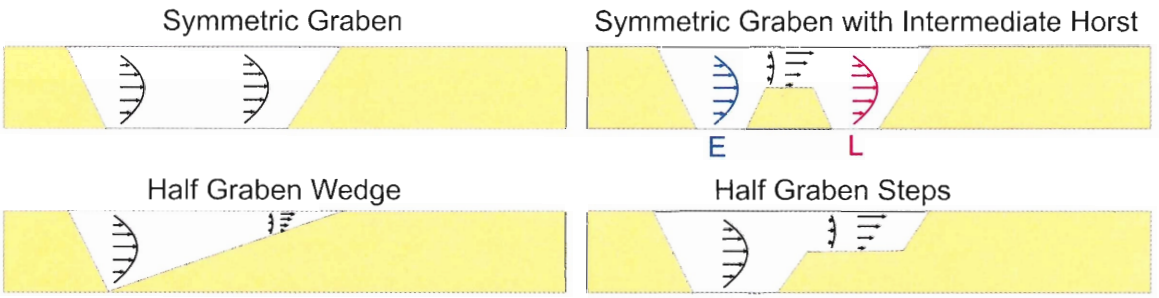

Figure 5.2 Variation of flow regimes for different basement configurations. Initial salt flow in all configurations is associated with poiseuille flow. Low thickness regions of salt basins show lower velocity vectors as well as a combination of Poiseuille with Couette flow.

In both of the symmetric graben setups, early stage salt flow caused by the downbuilding of the large landward salt-withdrawal basin is dominated by Poiseuille flow (channel flow) and yields very efficient salt flow within the ductile layer itself (Figure 5.2). In the symmetric graben setup, the strong Poiseuille flow causes inflation in the basinward limit of the basin in the early stage (E; Figure 5.1). This also occurs in the symmetric graben with intermediate horst setup but is slightly delayed due to the intermediate horst which localizes the inflation of silicone above the horst in the early stage (E; Figure 5.1). This is due to the thinner thickness of salt above the horst which hinders further basinward as exhibited by the slower velocity vectors (Figure 5.2). Once salt is evacuated over this horst and into the basinward subbasin, inflation begins in the basinward limit of the basin much like the symmetric graben setup.

In contrast to the symmetric graben setups, the half graben setups show a distinct evolution caused by the basinward thinning of the salt layer due to the sloping basement topographies (Figure 5.1). This thinning causes flow to decrease drastically towards the basinward margin of the basin, resulting in mid-basin salt inflation, as opposed to basinward inflation that occurs in the symmetric graben setups (E; Figure 5.1). With this style of inflation, larger salt bodies (diapirs) remain in the autochthonous basin longer despite the absence of obstruction in the basinward limit of the basin (M; Figure 5.1).

The timing and rate of the allochthonous nappe advancement into the deep basin shows a high dependence on the efficiency of salt evacuation into the deep basin as a consequence of the progradation of sediments over the inflated salt. As seen complex in the full graben experiments, salt was evacuated and inflated in the deep basin very

quickly. The symmetric graben with horst configuration shows some delay due to the horst impeding flow through the slower velocities experienced in the thinner salt layer. Both half graben setups show a slower initial evacuation of salt into the allochthonous zone (E; Figure 5.1). In the early stages of these setups, minimal salt is evacuated into the allochthonous zone. Once sediments begin to progradate over the basinward autochthonous inflated salt, salt is driven into the allochthonous nappe. In the half graben wedge setup, this progradation causes symmetric expulsion rollovers and a fast movement of the allochthonous nappe system with listric faulting occurring to accommodate extension in the simultaneously deposited sediments to keep up with the fast evacuation of salt through Couette flow (L; Figure 5.1). During the progradation of sediments over the "half graben with step" setup, salt evacuation into the allochthonous zone started mainly in the late mid stage (M; Figure 5.1). Due to the step configuration of the rift basin floor giving a slightly thicker salt inflation than in the wedge setup, Poiseille flow dominated in the late allochthonous evolution, resulting in simple downbuilding of the sediments and little extension taking place (L; Figure 5.1).

5.2 Discussion

Regional interpretations of salt structures observed in public seismic data of the Scotian Basin indicate that thick salt and allochthonous salt nappe systems were affected by similar mechanisms observed in our analogue experiments. In the landward border of the basins in the Scotian Shelf, large basinward dipping growth faults are present as seen in the analogue experiments (Figure 5.3). These resulted from the simple downbuilding of sediments causing a strong Poiseuille channel flow resulting in a very efficient

evacuation of salt into the deep water basin. The presence of diapirs and salt-sediment structures similar to those observed in the experiments may indicate basement structures such as horsts or steps (E; Figure 5.1) that impede flow. Overhangs of some of these diapirs would indicate low sedimentation intervals or periodical sediment stagnation similar to our sedimentation breaks which allow for the passive diapirs to flow basinward on the ocean floor (Figure 5.3).

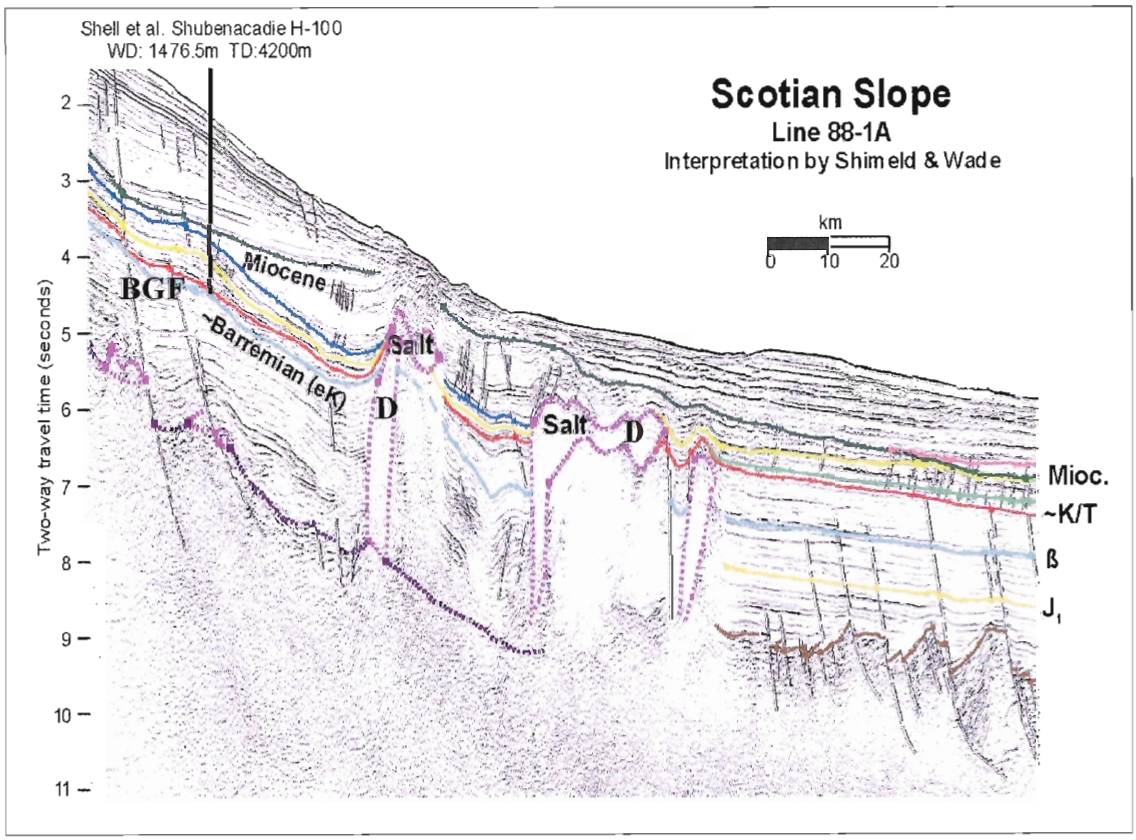

Figure 5.3 Seismic section from the Scotian Margin showing Basinward dipping growth faults (BGF), and diapirs (D) with overhangs from their passive stages (Shimeld, 2006).

As described by Shimeld (2004), the allochthonous systems in Salt Subprovinces III and IV vary even within the subprovinces themselves. This variability can most likely be accounted for by the variations of salt thickness due to basement morphologies, as observed in our analogue experiments and also in gravimetric data of the shelf and slope area. Salt Subprovince IV is defined as having few diapirs located in the original salt basin and a large salt nappe system with an associated basinward listric salt detachement and rollover system associated with the deformation of the brittle overburden (Figure 5.4; Figure 5.5). This evolution may originate from a similar basin structure as simulated in the half wedge experiment which depicts a similar evolution (Figure 5.1).

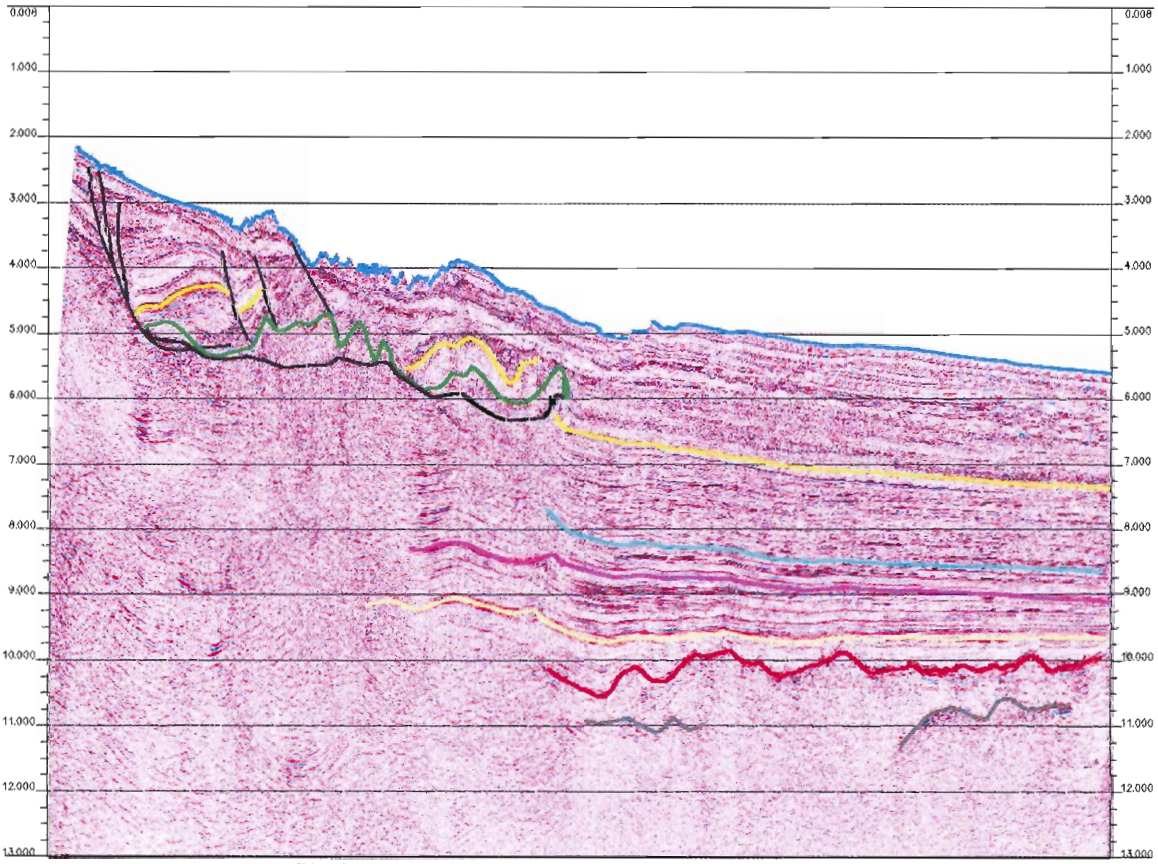

Figure 5.4 Seismic profile from the Scotian Margin showing a large salt nappe system with assocated listric faulting of overburden as salt was evacuated basinward (Kidston et al. 2002).

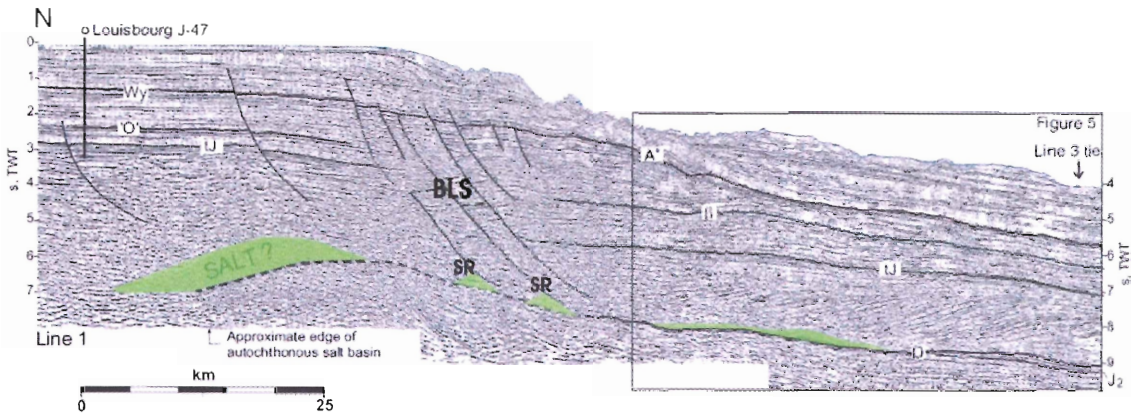

Figure 5.5 Seismic profile from Salt Subprovince IV depicting allochthonous nappe system with basinward dipping listric growth faulting as salt was evacuated basinward (after Ings and Shimeld, 2006)

The purpose of these experiments was to study the first order control factors and salt deformation mechanisms to better understand the role of basement configurations based on structures observed in the Scotian Margin. With further seismic interpretation and processing of PIV strain data for the large scaled experiment, a more quantitative analysis will be achieved. This analysis will lead to a better understanding the complexity of salt tectonic evolution in the Scotian Basin and its petroleum system. Future research will be completed by the Dalhousie Salt Dynamics Group to achieve these more quantitative results and aid in understanding the complexity of this passive margin and salt tectonics affecting the area.

REFERENCES

Adam, J., Shimeld, J., Krezsek, C., Grujic, D., 2006. How Sedimentation Controls Structural Evolution and Reservoir Distribution in Salt Basins. Nova Scotia's Energy Research and Development Forum, May 24-25, 2006, Antigonish, Canada (on CD).

Adam, J., Urai, J.L., Wieneke, B., Oncken, O., Pfeiffer, K., Kukowski, N., Lohrmann, J., Hoth, S., Van der Zee, W., Schmatz, J., 2005. Shear localisation and strain distribution during tectonic faulting--new insights from granular-flow experiments and high-resolution optical image correlation techniques. *Journal of Structural Geology* **27**, 283–301.

Bally, A.W., 1981. Thoughts on the tectonics of folded belts., in McClay, K.R., and Price., N.J. eds., Thrusting and Nappe Tectonics. *Spec. Publs geol. Soc. Lond. 9:*13-32.

Costa, E., Vendeville, B.C. 2002. Experimental insights on the geometry and kinematics of fold-and-thrust belts above weak, viscous evaporitic decollement. *Journal of Struc. Geol.* **24**, 1729-1739.

Enachescu, M. and G. Wach (2005). Exploration Offshore Nova Scotia: Quo Vadis? *ocean-resources: 23-35.*

Ge, H., Jackson, M.P.A., and Vendeville, B.C., 1997. Kinematics and dynamics of salt tectonics driven by progradation. *AAPG Bulletin 81*(3), 398-423.

Gemmer, L., C. Beaumont, et al. (2005). Dynamic modelling of passive margin salt tectonics: effects of water loading, sediment properties and sedimentation patterns. *Basin Research 17: 382-402, doi: 10.1111/j.1365-2117.2005.00274.x.*

Haq, B.U., Hardenbol, J. and Vail, P.R., 1987. Chronology of Fluctuating Sea Levels Since the Triassic. *Science*, Vol.235, p.1156-1167.

Hubbert, M.K., 1937. Theory of scale models as applied to the study of geologic structures *Geological Society of America Bulletin* **48**(10), 1459-1519.

Ings ,S.J., and Shimeld, J.W., 2006. Structural evolution of a regional salt detachment on the northeast Scotian Margin, offshore eastern Canada: A new conceptual model.

Jackson, M.P.A., 1995. Retrospective salt tectonics, in M.P.A. Jackson, Roberts, D.G., and Snelson, S. eds., Salt Tectonics: a global perspective. *AAPG Memoir 65:* 1-28.

Jackson, M. P. A. and B. C. Vendeville (1994). Regional extension as a geologic trigger for diapirism; with Suppl. Data 9401. *Geological Society of America Bulletin* **106**(1): 57-73.

Jackson, M. P. A., B. C. Vendeville, et al. (1994). Structural dynamics of salt systems. *Annual Review of Earth and Planetary Sciences* **22**: 93-117.

Jackson, M.P.A. and Talbot, C.J. 1991. A Glossary of salt tectonics: The University of Texas at Austin, Bureau of Economic Geology Geological Circular, No. 91-4, p. 44

Jackson, M. P. A., and C. Cramez (1989). Seismic recognition of salt welds in salt tectonics regimes. SEPM Gulf Coast Section Tenth Annual Research Conference Program and Abstracts, Houston, Texas, p. 66–71.

Jansa, L.F., Wade, J.A., 1975. Geology of the continental margin off Nova Scotia and Newfoundland. In: W.J.M. van der Linden, J.A. Wade (eds.): *Offshore geology of Eastern Canada*, Vol. 2, Regional geology: Geological Survey of Canada, Paper 74-30, 51-106.

Kidston, A.G., Brown, D.E., Altheim B., Smith B.M., 2002. Hydrocarbon Potential of the Deep-water Scotian Slope, Canada-Nova Scotia Offshore Petroleum Board, Open Report, 111 p.

Lohrmann, J., Kukowski, N., Adam, J., and Oncken, O., 2003. The impact of analogue material parameters on the geometry, kinematics, and dynamics of convergent sand wedges. *J. Struc. Geol.* **25**(10), 1691-1711.

Palmer, A.R. and Geissman, J., 1999.1999 Geologic Time Scale. Geological Society of America Website: http://www.geosociety.org/science/timescale/timescl.htm

Rowan, M.G., 2005. Salt Tectonics and Sedimentation: A Structual and Sedimentary Framework for Petroleum Systems in Salt Basins.

Rowan, M. G., F. J. Peel, et al. (2004). Gravity-driven fold belts on passive margins. *AAPG Memoir, vol.82.* K. R. McClay**:** 157-182.

Shimeld, J., 2004. A comparison of salt tectonic sub-provinces beneath the Scotian Slope and Laurentian Fan. In: P.J. Post, D.L. Olson, K.T. Lyons, S.L. Palmes, P.F. Harrison, N.C. Rosen (eds.): *Salt-sediment interactions and hydrocarbon prospectivity: Concepts, applications and case studies for the 21st century*, 24th Annual GCSSEPM Foundation Bob F. Perkins Research Conference proceedings, 291-306. (On CD Rom - ISSN: 1544-2462).

Stonely, R., 1981. Petroleum: the sedimentary basin. Economic Geology and Geotectonics. p. 51-71

Vendeville, B.C., and Jackson, M.P.A., 1993. Rates of extension and deposition determine whether growth faults or salt diapirs form, in Armentrout, J.M., Bloch, R., Olson, H.C., and Perkins, B.F., eds. Rates of Geological Processes: Fourteenth Annual Research Conference, Gulf Coast Section, SEPM Foundation, Program with Papers, p. 263-268

Vendeville, B.C., Jackson, M.P.A., 1992. The fall of diapirs during thin-skinned extension. *Marine and Petroleum Geology* **9**(4), 354-371.

Vendeville, B.C and Cobbold, P.R., 1988. How normal faulting and sedimentation interact to produce listric fault profiles and stratigraphic wedges. *J. Struc. Geol.* **10**, 649-659.

Wade, J.A., MacLean, B.C.& Williams, G.L.; 1995. Mesozoic and Cenozoic stratigraphy, eastern Scotian Shelf: new interpretations. *Canadian Journal of Earth Sciences*, Vol.32, No.9, p.1462-1473.

Wade, J. A. and B. C. MacLean (1990). The geology of the southeastern margin of Canada. *Geology of the Continental Margin of Eastern Canada*. M. J. Keen and G. L. Williams. **2:** 167-238.

Weijermars, R., Jackson, M.P.A., Vendeville, B., 1993. Rheological and tectonic modeling of salt provinces. *Tectonophysics* **217**(1-2), 143-174.

Wu, S., A. W. Bally, et al. (1990). Allochthonous salt, structure and stratigraphy of the north-eastern Gulf of Mexico. Part II: Structure. *Marine and Petroleum Geology* **7**(4): 334-340.

APPENDIX A- INTERPRETATIONS OF EXPERIMENTS

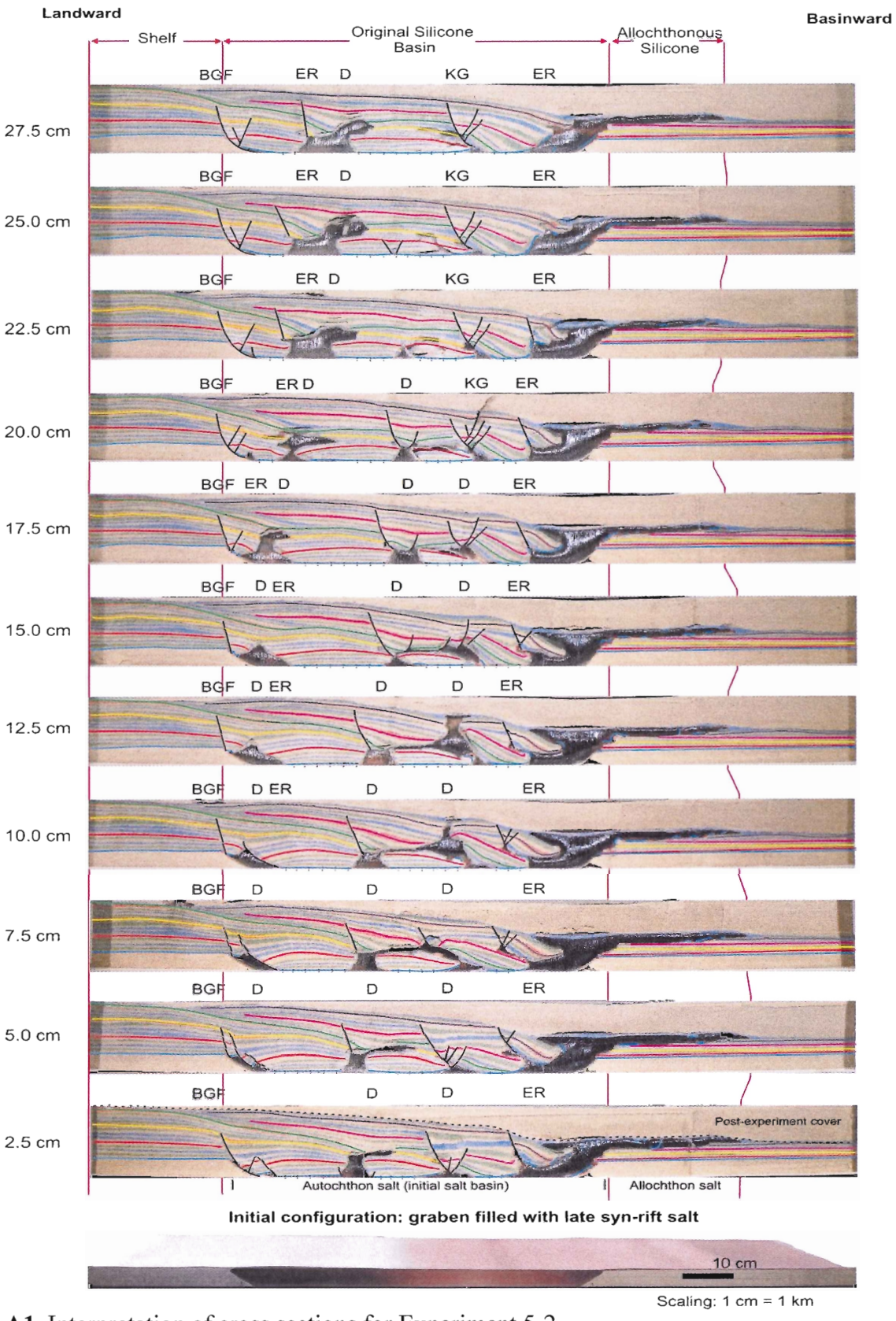

A1. Interpretation of cross sections for Experiment 5-2

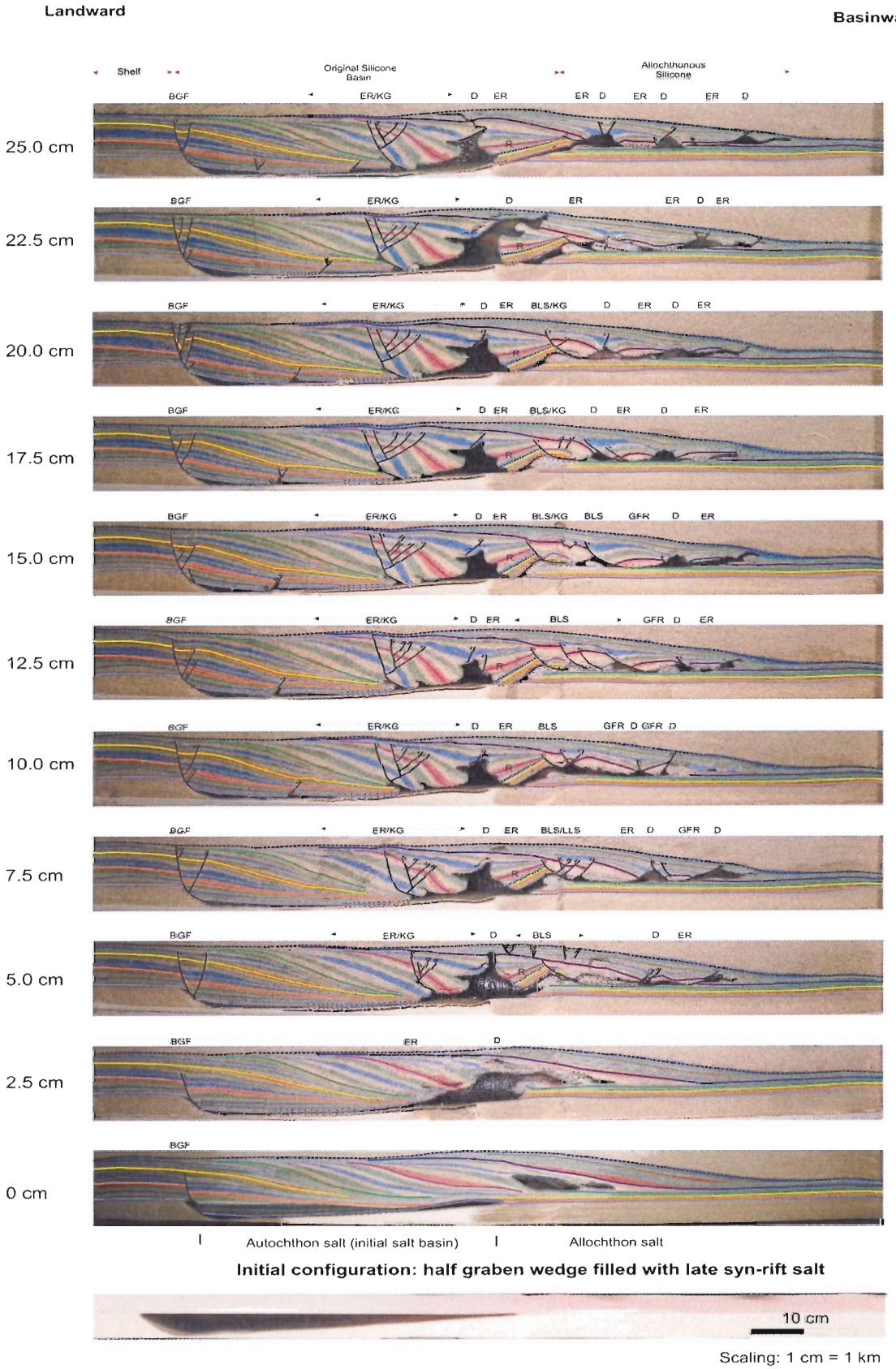

A2. Interpretation of cross sections for Experiment 5-3.

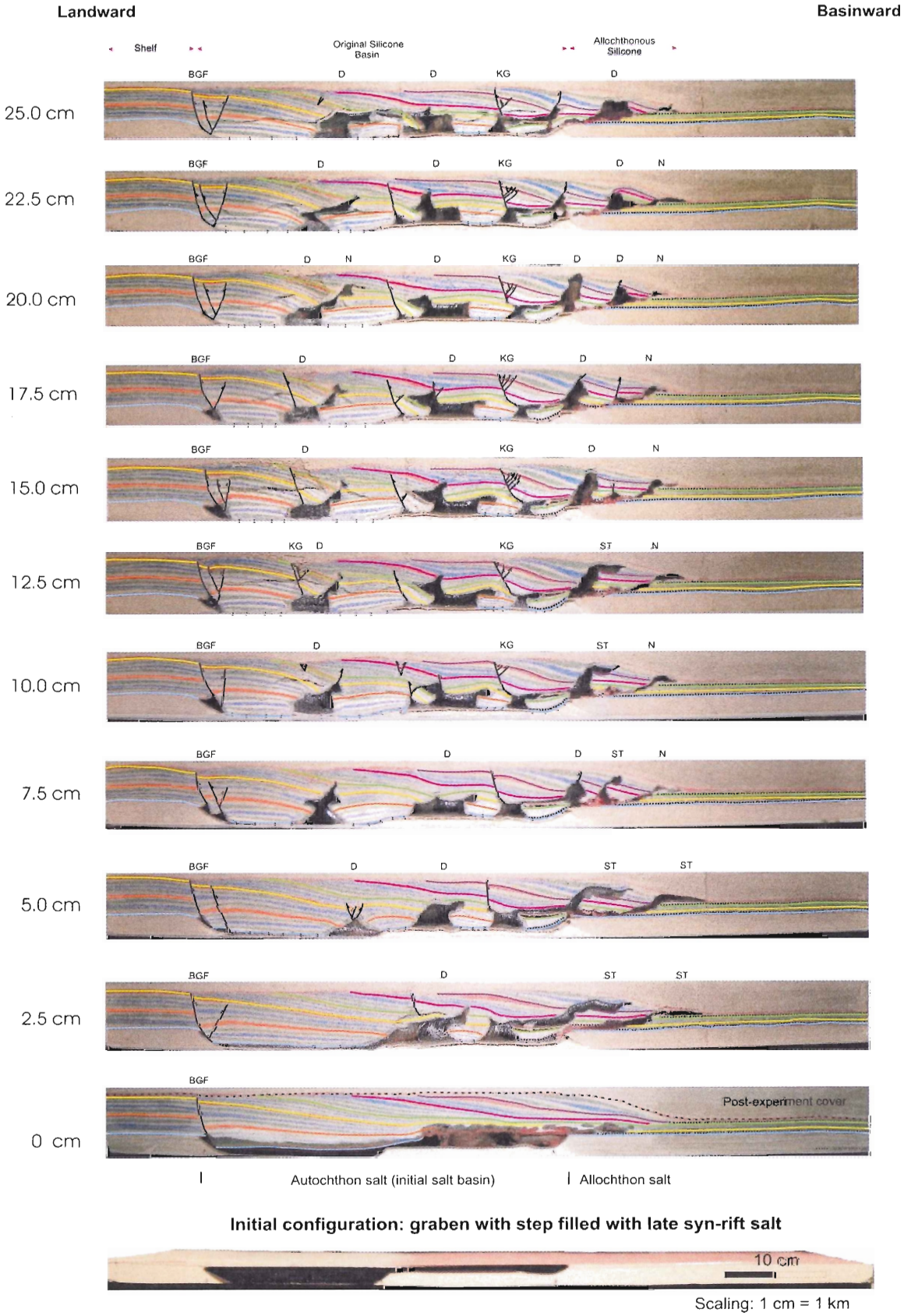

A3. Interpretation of cross sections for Experiment 5-5

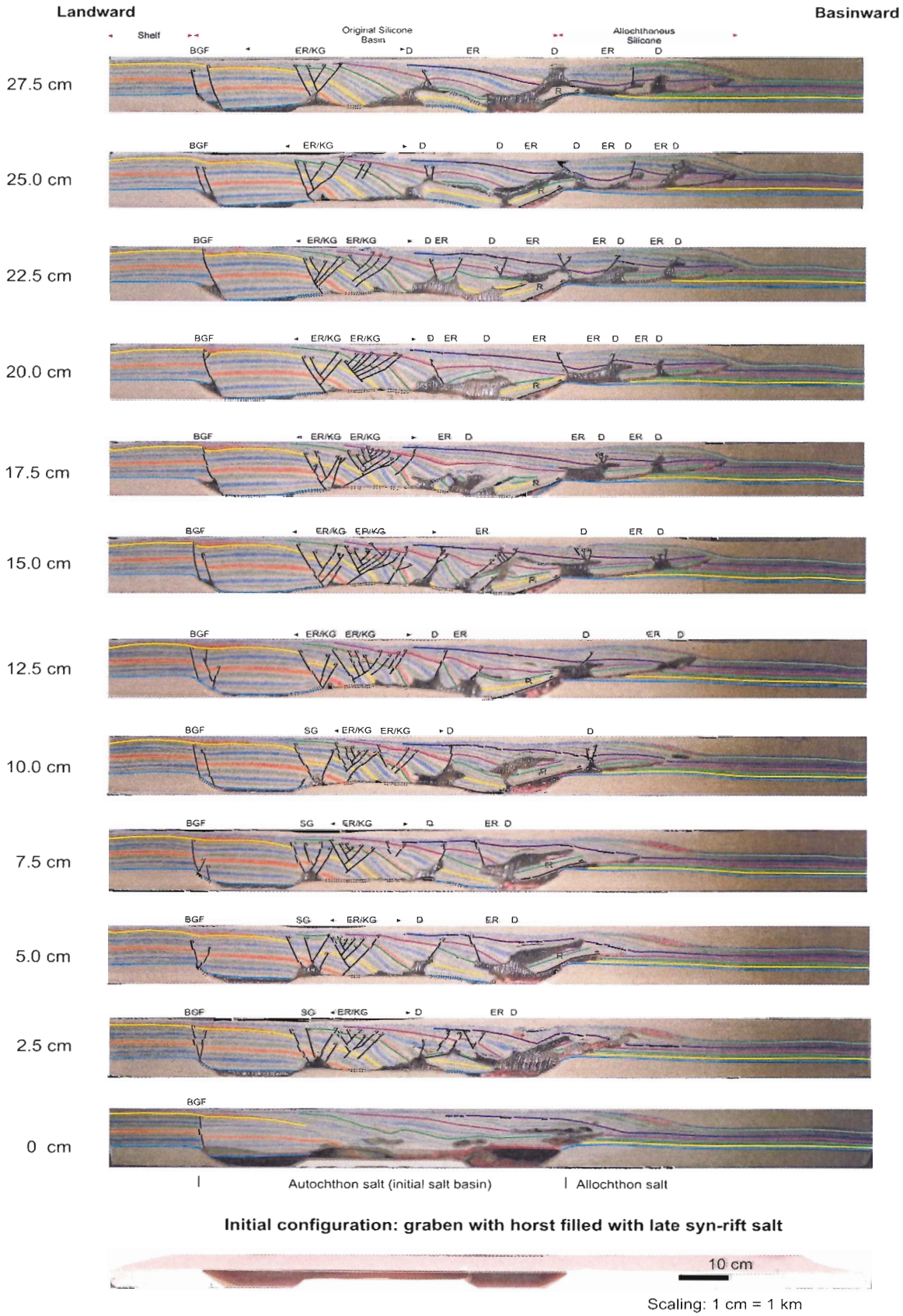

A4. Interpretation of cross sections for Experiment 5-6.

APPENDIX B- TIME SERIES IMAGES OF EXPERIMENTS

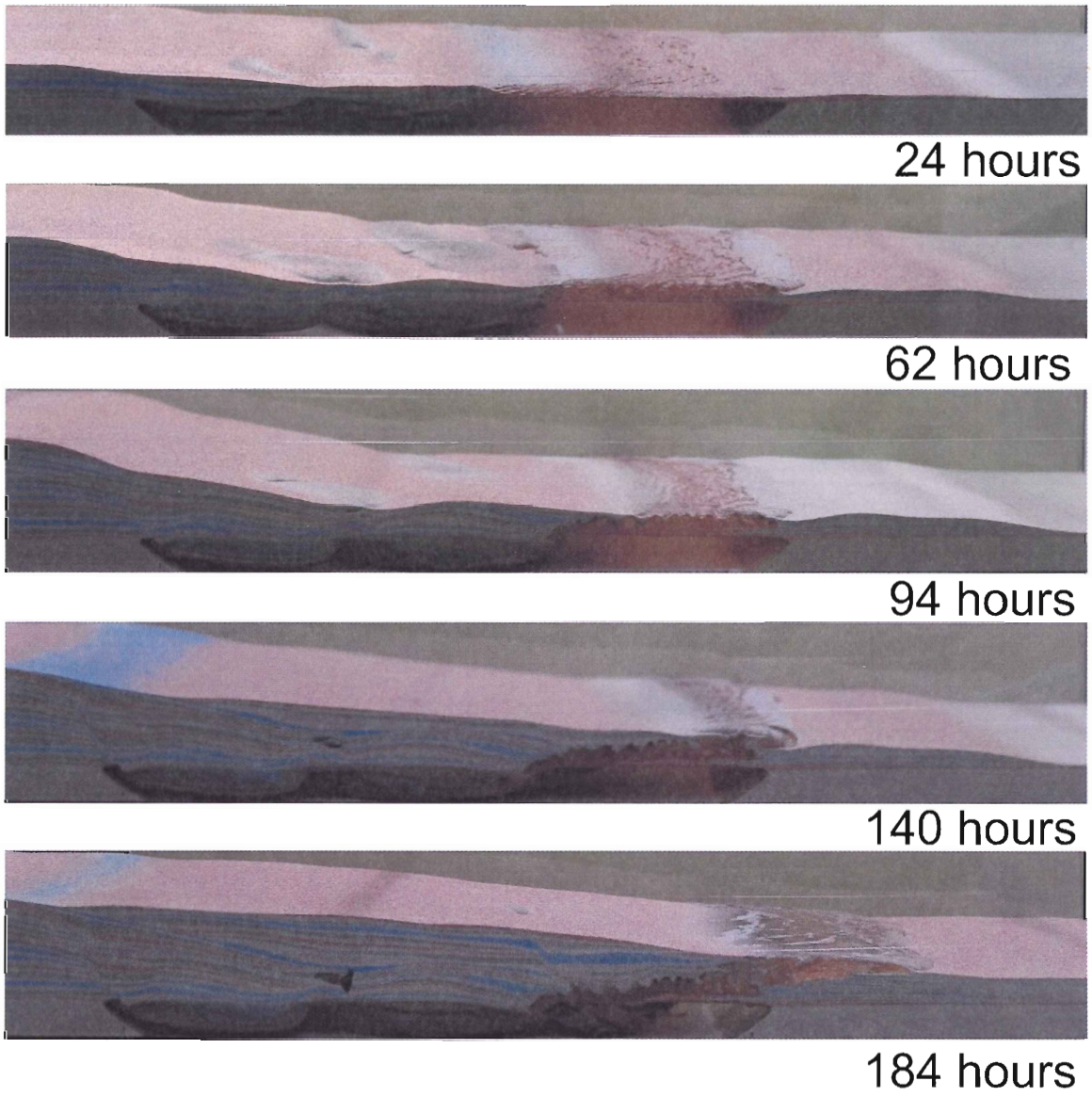

B1. Time series images for Exp_5-2 which represents a symmetric graben basin configuration.

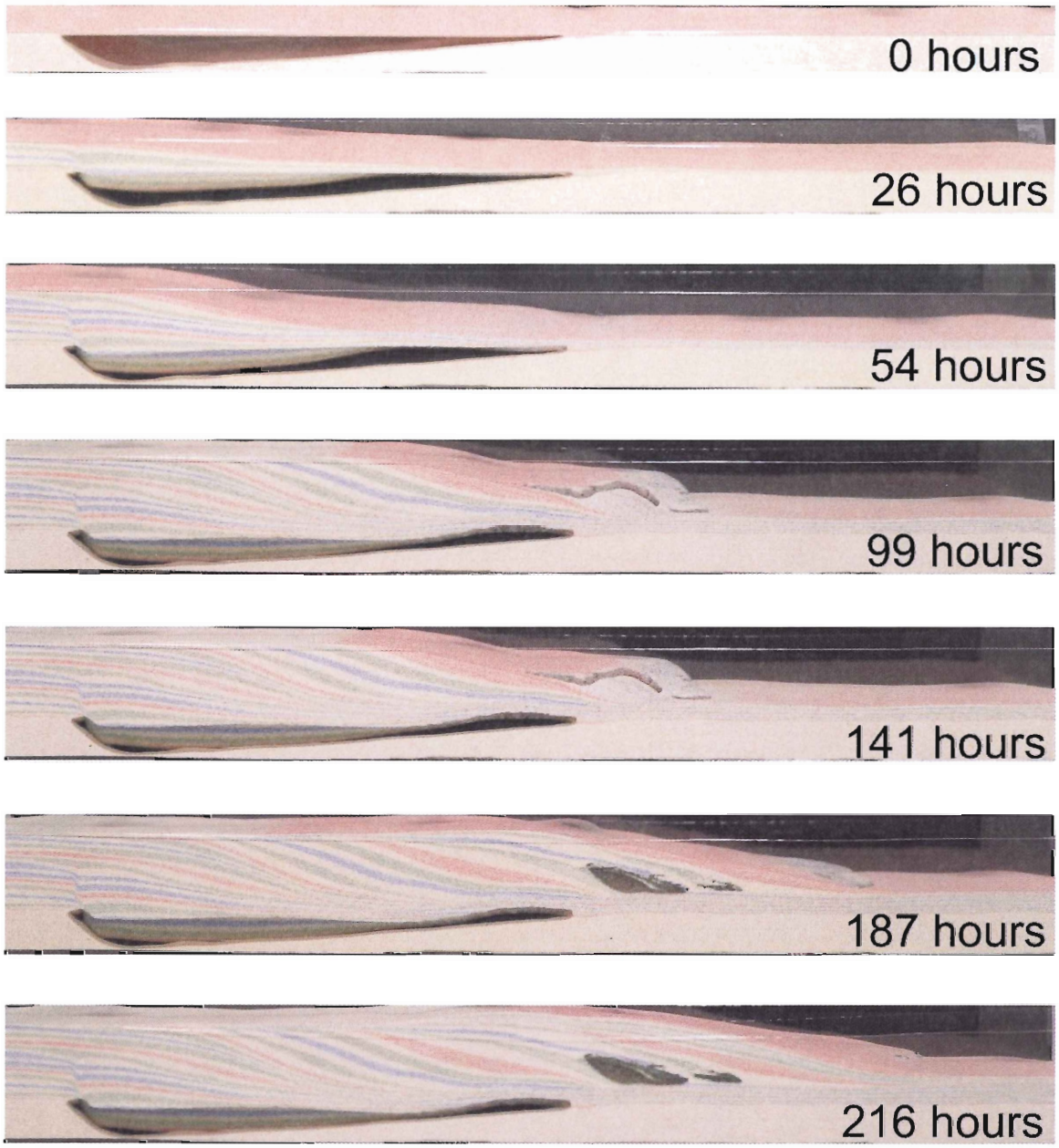

B2. Time series images for Exp_5-3, a half graben wedge basin configuration.

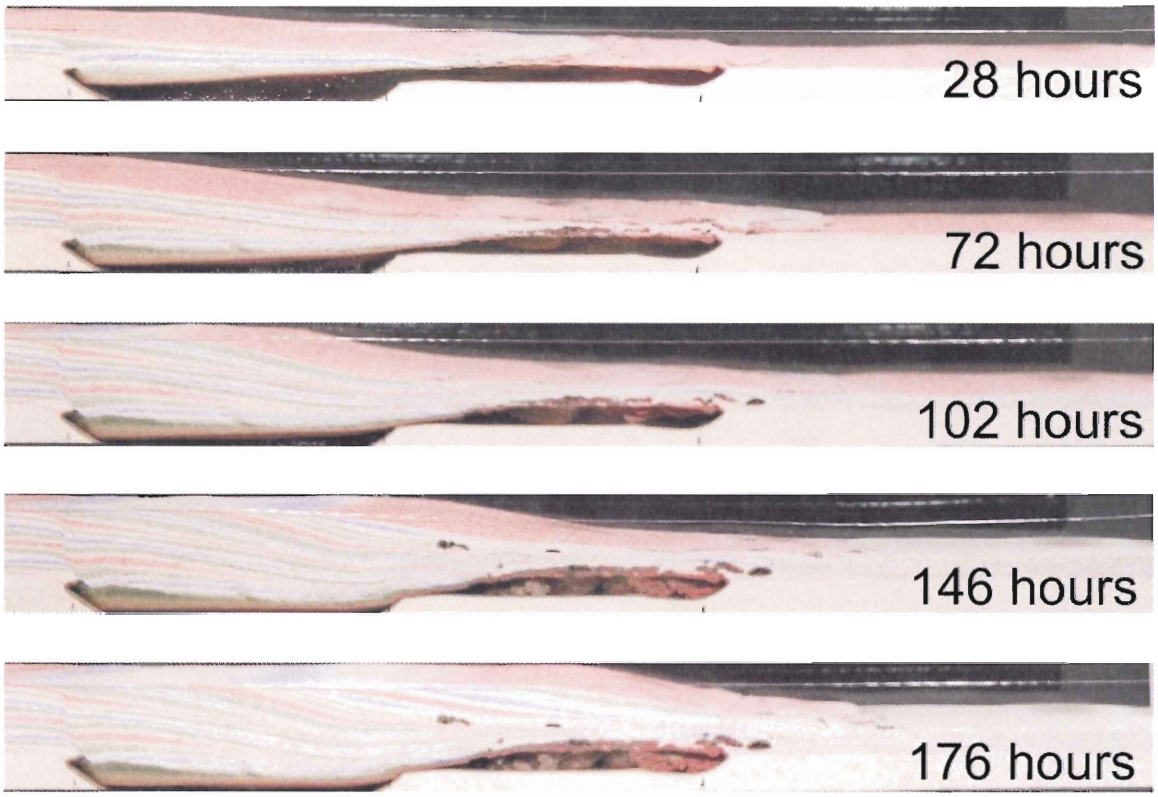

B3. Time series images for Exp_5-5, a half graben with step initial basin configuration.

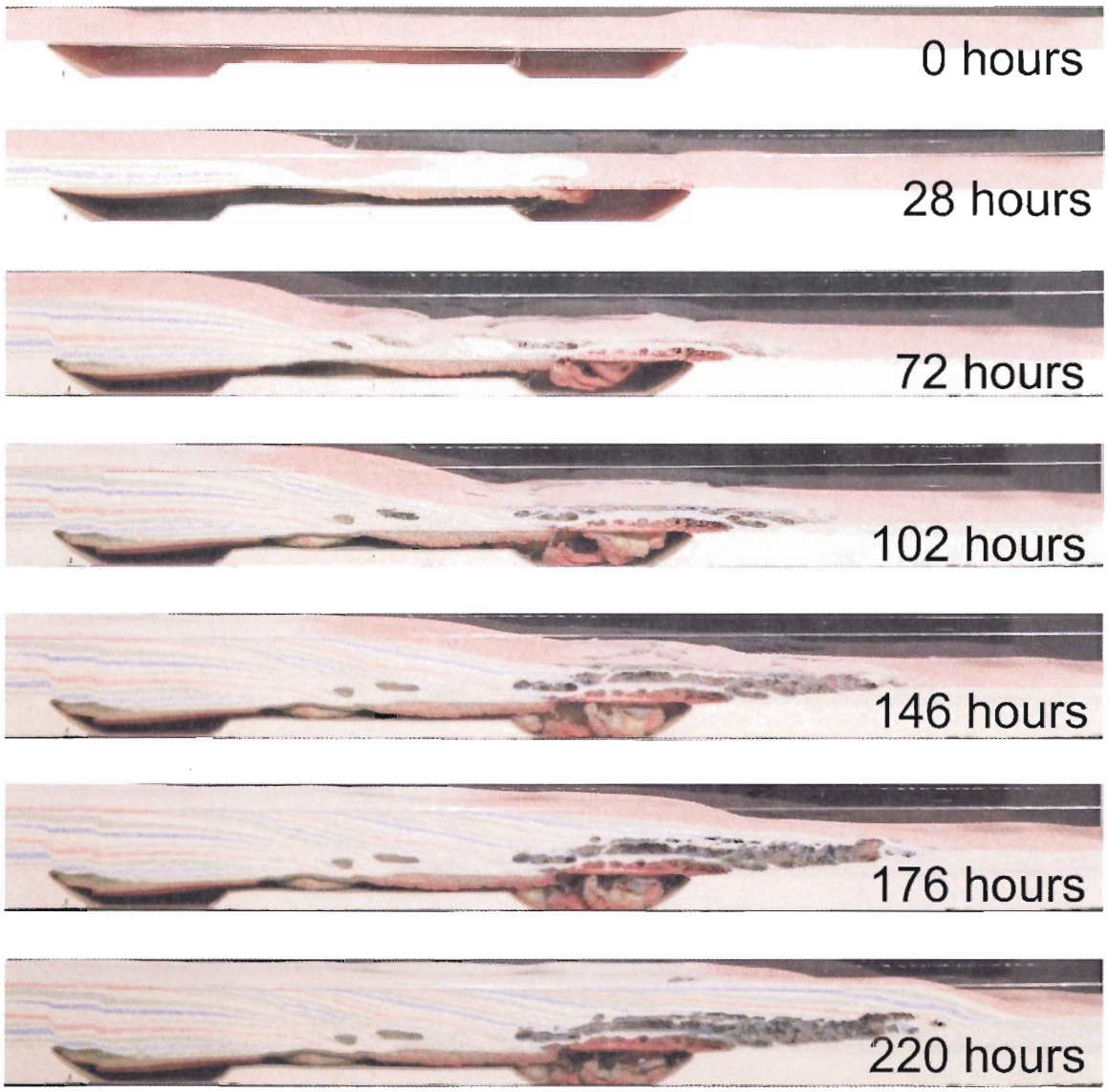

B4. Time series images for Exp_5-6, a symmetric graben with intermediate horst initial basin configuration.

APPENDIX C- SAMPLE PIV DATA

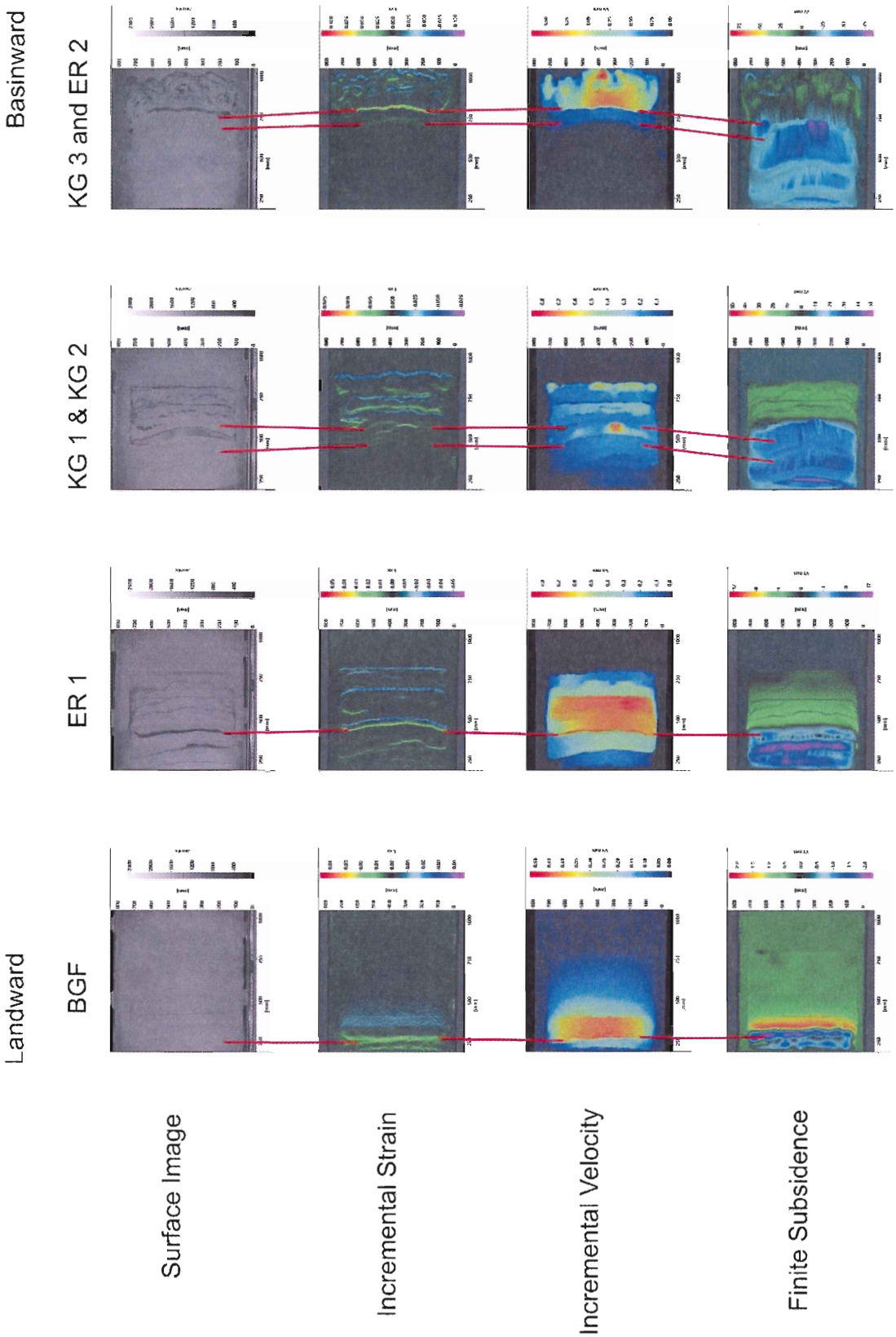

C1: Sample of PIV data obtained for Exp_5-7, a symmetric graben initial basin configuration.